INCREMENTAL PLASTIC STRESS WAVES IN ALUMINUM AND COPPER RODS UNDER AXIAL QUASISTATIC PRELOADING

By

CHANG-SHENG TING

A DISSERTATION PRESENTED TO THE GRADUATE COUNCIL OF
THE UNIVERSITY OF FLORIDA
IN PARTIAL FULFILLMENT OF THE REQUIREMENTS FOR THE
DEGREE OF DOCTOR OF PHILOSOPHY

UNIVERSITY OF FLORIDA

1975

ACKNOWLEDGMENTS

I wish to express my sincere appreciation to Dr. Lawrence E. Malvern who initiated this problem. I shall always be grateful for his invaluable guidance and efficient counsel throughout this research.

Thanks are also given to Dr. M. A. Eisenberg, Dr. E. K. Walsh, Dr, R. E. Reed-Hill, Dr. C. S. Hartley and Dr. S. Y. Lu for their services on my supervisory committee. Appreciation is also expressed to Dr. N. Cristescu for his classroom lectures in the course of Dynamic Plasticity.

A special word of thanks is due to my friend Dr. C. G. Langner who built most of the test apparatuses and ingeniously designed the velocity transducer used in this work.

I would also like to thank Mr. H. E. Stroud, Mr. J. D. McMillan, Jr., and Mr. J. C. Van Leer for their help in the machine shop.

All the computer time used in this research was granted by the Computing Center at the University of Florida.

I wish to thank my beloved Sheu-Ling Lee who helped me to put things together in the final week just after she had studied a long time for her own qualifying examination.

TABLE OF CONTENTS

TABLE OF CONTENTS (Continued)

LIST OF FIGURES

LIST OF FIGURES (Continued)

LIST OF FIGURES (Continued)

LIST OF FIGURES (Continued)

Abstract of Dissertation
Presented to the Graduate Council of the University
of Florida in Partial Fulfillment of the Requirements for
the Degree of Doctor of Philosophy

INCREMENTAL PLASTIC STRESS WAVES IN ALUMINUM AND COPPER RODS UNDER AXIAL QUASISTATIC PRELOADING

By

Chang-Sheng Ting

August, 1975

Chairman: Lawrence E. Malvern
Major Department: Engineering Sciences

A series of tests of incremental stress waves of small amplitude were performed on annealed aluminum 1100-F rods and copper rods under axial quasistatic preloading beyond the elastic limit. Particle velocity records of the incremental waves were obtained at four gage stations along the rod. The strain rates of the quasistatic preloading were in the range of 10^{-6} to 10^{-4} sec^{-1}, while the strain rates of the order of 1.0 sec^{-1} were achieved in the incremental plastic waves with maximum particle velocity around 50 cm/sec and duration of around 500 μsec.

Test results indicated that except near the plateau in the records for aluminum any given level of incremental particle velocity propagates along the rod with a constant speed, not affected by the strain rate within the small range of the incremental wave strain rates encountered.

However, the obtained propagation speed function for each incremental wave was found dependent on both prestrain and prestrain-rate values. A precondition parameter composed of prestrain and prestrain rate was proposed to give a quantitative description of this phenomenon. This discovery revealed another physical property of metal under incremental loading in addition to the well-known phenomenon of the leading edge propagating at the elastic bar-wave speed.

Both strain-rate-independent and strain-rate-dependent theories were used to interpret the experimental results. By applying the simple-wave solution of a modified rate-independent theory, incremental stress-strain curves were calculated from the wave-propagation-speed function for both cases of aluminum and copper. Quasilinear and semi-linear rate-type constitutive models with linearized terms were proposed. Numerical computer solutions were obtained for incremental waves at various prestrain levels of both aluminum and copper specimens. Results show that the proposed quasilinear constitutive equation is adequate for copper and the semilinear constitutive equation is qualitatively adequate for aluminum. Results for copper showed that matching the particle velocity records by adjusting the parameters in the quasilinear constitutive equation does not guarantee a reasonable solution in incremental stress and strain, when it was compared with the incremental

stress-strain curve of rate-independent theory. Therefore a strong inequality was proposed for determining the parameter in the instantaneous response term of the quasilinear equation. This proved to be an efficient aid in the parameter identification since only one parameter was left, which can be determined from matching the velocity records. Results show that the parameters in the rate-type constitutive equation in both materials depend on the proposed precondition parameter.

CHAPTER 1

INTRODUCTION

1.1 Background

Dynamic plasticity is the branch of the mechanics of solids in which rapid deformation of solid bodies beyond the elastic limit is studied without neglecting inertia effects. The transient spreading out of the deformation from the loaded part of a body subjected to impact loading is referred to as plastic wave propagation. When inertia effects are included, the analysis of the deformation of a rapidly loaded body requires the consideration of plastic wave propagation except for very small specimens in which the assumption of uniform stress and strain may be a satisfactory approximation for practical purposes. The analysis of plastic wave propagation is relatively new, with a history of about 35 years. There was some study of the subject before 1940; the first important paper was by Donnell (1930).

Two basic assumptions about the constitutive law of the material behavior under dynamic plastic loading were proposed in the 1940's. A strain-rate-independent theory was proposed independently by Taylor (1940) in England, von Karman (1942) in America, and Rakhmatulin in the Soviet

Union. They analyzed the problem of longitudinal impact of thin rods and assumed that radial inertia effects were negligible. A single-valued stress-strain relation, independent of strain rate was used in these analyses. The partial differential equation of motion was derived and a simple wave solution for continued impact on a semiinfinite bar was obtained.

Experiments were carried out shortly after the development of this theory. A summary paper by Duwez and Clark (1947) presented the major results of the experimental work in the preceding few years. In general, the prediction of the formation of a strain plateau near the impact end in a constant-velocity impact and the relation between the impact velocity and the maximum plastic strain reached were fairly well verified by the experiments. Some systematic discrepancies in the magnitude of the residual strain and in the stress-time history at the fixed end opposite the impact end were observed. In the tension impact tests the maximum residual strain was smaller than predicted by the theory, and the observed stress time variation at the fixed end during impact showed the stress there was greater than the theory predicted. It was suggested that this might be attributable to strain-rate effects in the material under impact loading.

The strain-rate-dependent theory was proposed by Sokolovsky (1948) and by Malvern (1949) independently of each other. They considered the plastic flow stress as a

function of strain rate as well as the level of strain. Both Sokolovsky and Malvern proposed semilinear constitutive laws and used them to analyze examples of longitudinal impact on bars. Malvern (1949) also suggested a more general quasilinear law and showed how it could be used to study wave propagation by the method of characteristics. Sokolovsky (1948) assumed perfect plasticity, while Malvern (1949) considered work hardening. The constitutive law proposed by Malvern was of the elastic-visco-plastic form given by

$$E\dot{\varepsilon} = \dot{\sigma} + g(\sigma,\varepsilon) \qquad (1.1)$$

where $g(\sigma,\varepsilon)$ is an arbitrary function expressing the strain-rate dependence. An idealized form of the constitutive law (1.1) was used in which $g(\sigma,\varepsilon) = k[\sigma - f(\varepsilon)]$, where $[\sigma - f(\varepsilon)]$ was called the "overstress", that is, the excess of dynamic stress over the static yield stress. A numerical example was given using the idealized linear overstress form, and it was concluded that the assumed constitutive law could account for discrepancies observed in the stress-time variation at the fixed end of an impact specimen. However, this type of flow law failed to predict a strain plateau near the impact end of constant-velocity impact specimens in the short time for which the calculations were made.

The question concerning the possibility of the existence of a strain plateau in the solution of a Malvern-type theory was considered by several authors. Rubin (1954)

obtained a solution by using Laplace transformation for the problem of the small increment with linearized quasistatic curve. An asymptotic plateau was proved to exist from the closed form solution. However, no example was given; how fast the asymptotic plateau was approached still remained a question. Later Bianchi (1963), Efron (1964) and Wood and Phillips (1967) showed directly the asymptotic plateau in their numerical computer solutions. A recent theoretical work by Suliciu, Malvern and Cristescu (1972) has placed restrictions on the form of the constitutive equations under which a plateau can occur and has shown that with the usual form of the Malvern type semilinear modèls only an asymptotic plateau is possible.

Concerning the apparent increase in the yield stress at high velocity impact, Malvern theory predicts such an increase in the value of initial yield stress at infinitely high strain rates because plastic strain does not occur instantaneously but takes time in which to become appreciable. At high finite rates the dynamic curves rise near the elastic line, but any increase in the yield stress would have to be made an explicit assumption. Regarding this point, the experiments of Campbell (1954) on steel, Tietz and Dorn (1949) on aluminum, and Taylor (1957) on steel all show that the dynamic yield stress increases with the rate of strain.

Rubin (1954) also showed that according to the linearized Malvern theory the leading edge of an incremental plastic wave would travel at the elastic wave speed instead of at the plastic wave speed predicted by the rate-independent theories. Experiments by Bell (1951) on steel bars and Sternglass and Stuart (1953) with copper strips involved the propagation of incremental impact loads superimposed upon static dead loads in excess of the elastic limit. The wave fronts were found to propagate at the elastic wave speed. Later results of incremental loading waves in dynamically prestressed bars were obtained by Alter and Curtis (1956) for lead and by Bell and Stein (1962) for aluminum. These results also showed that the leading incremental wave edge propagates at the elastic bar-wave speed. Similar results were also reported by Papirno and Gerard (1961) on annealed aluminum 1100-H, and by Bianchi (1963) on copper strip.

This phenomenon of incremental wave was widely interpreted as evidence of strain-rate effect as predicted by the Malvern strain-rate-dependent theory. However, Bell and Stein (1962) disagreed with this idea and stated that such an interpretation is inconsistent for annealed aluminum, annealed copper, and pure lead, in that, large amplitude wave propagation has been shown to be in very close agreement with the strain-rate-independent finite amplitude theory [see Bell (1956), (1960a), (1961a,b,c), (1968)]. They explained

the phenomenon by a trigger mechanism which has the property of reinaugurating plastic deformation for the incremental wave when it occurs after the dynamic prestressed wave has reached a maximum value.

Bell and his coworkers have obtained many valuable experimental results in finite amplitude stress wave propagation. By using the diffraction grating technique, Bell (1960b) has shown that the dynamic overstress is determinable from a consideration of the three dimensional development of the plastic wave in the first diameter. Also, by means of diffraction grating measurements of strain in the free flight impact of identical specimens of varying diameter, the geometric character of the wave development given in Bell (1961a) was shown to be consistent. Thus, dynamic overstress was seen to depend upon the diameter and not upon the distance from the impact face as would be expected if the phenomenon were associated with strain rate behavior. However, Bell maintains that the dynamic stress-strain relation is not necessarily the same as the quasistatic relation. Similar results were also given by Kolsky and Douch (1962) for copper and aluminum.

By examining various forms of $g(\sigma,\varepsilon)$ in equation (1.1), Ripperger and Watson (1968) concluded that wave-propagation experiments with long initially unstressed specimens in compression were of little value in deciding whether dynamic material behavior obeys the rate-independent or the

rate-dependent theory. Results for titanium obtained by Lawson and Nicholas (1972) in torsion also support this finding. Recently from results of an experiment which could measure simultaneously tensile and compressive wave profiles in the specimen, Khan (1973) demonstrated the strain-rate-independent theory is also applicable for propagation of tensile waves in annealed aluminum 1100-F. The dynamic stress-strain curve was found to be the same in tension and compression.

On the side of theoretical development, a general quasilinear constitutive equation, which includes both the rate-independent theory and the Malvern semilinear theory, as special cases, was proposed by Cristescu (1963) and Lubliner (1964). It has the form

$$\dot{\varepsilon} = \phi(\sigma,\varepsilon)\dot{\sigma} + \psi(\sigma,\varepsilon) \qquad (1.2)$$

with the implication that a certain part of the plastic strain is also developed instantaneously. Working with Bell's experimental data, Cristescu (1972) has shown that the above constitutive equation, with special forms for the functions ϕ and ψ, can fit reasonably well data of the problem of longitudinal impact between two thin rods. Lubliner and Valathur (1969) studied wave propagation in constant velocity impact by applying a similar constitutive equation with ϕ derived from a Ramberg-Osgood curve. A more recent theoretical work by Suliciu, Malvern and Cristescu (1974)

has proposed some restrictions on the quasilinear material function. It was shown that the incremental wave behavior implies that at least one continuous transition from the quasilinear equation to a semilinear equation occurs in the neighborhood of the relaxation boundary, under the assumption of certain continuity properties of ϕ and ψ for both increasing and decreasing stress.

The split Hopkinson pressure bar introduced by Kolsky (1949) has been widely used as a practical method in obtaining the dynamic flow properties of materials, including strain rate effects [see Hauser, Simmons and Dorn (1961) and Lindholm (1964)]. This technique has been criticized because of the lateral bulging in the short specimen during compression and on other grounds [see De Vault (1965) and Bell (1966)].

Experiments in torsional waves were sought to eliminate any complicating effect due to the radial inertia that arises in longitudinal impact. Baker and Yew (1966) developed a torsional split Hopkinson bar and compared their experimental shear strain time records both with rate-independent theory, using the quasistatic stress-strain curve, and with a linear overstress rate-dependent theory as used by Malvern. The conclusion was that the rate-dependent theory gave better agreement qualitatively.

Convery and Pugh (1968) studied the propagation speed of torsional plastic waves in metals pretwisted statically

into the plastic range. A new method was developed in which a tubular test specimen together with a concentric bar of a brittle material was twisted slowly such that at some time after the specimen was stressed beyond its yield the brittle bar broke suddenly and transmitted a plastic torsional stress increment along the specimen. It was found that the velocity of propagation both in copper and in mild steel was the same as the elastic shear wave velocity.

Since then, experimental results of this kind have appeared frequently in the literature. Data obtained at higher rates of strain can generally be classified as results of one among two different methods of testing. In the first, specimens are exclusively deformed at a dynamic rate during the test, while the second method involves preloading the specimen beyond its elastic limit at a chosen rate before subjecting it to an incremental disturbance. In both methods, a long specimen can be used along which the propagation of the stress pulse is measured and analyzed; alternatively, with a short specimen, the complete history of the flow stress, as related to the strain-rate history involved, can be obtained.

Reports concerning the torsional wave propagation [see Baker and Yew (1966), Yew and Richardson (1969), Lawson and Nicholas (1972), Banerjee and Malvern (1975)] have shown that theoretical predictions of experiments involving plastic wave propagation and interaction in metals are not very

sensitive to changes in the rate-dependent constitutive equation. The fact that most of the plastic deformation in the experiments took place within a narrow band of strain rates explains the insensitivity of the results to the form of the constitutive equation, as long as the stress in this narrow band of strain rates does not vary greatly with strain rate.

Therefore most experiments seeking to determine rate effects were performed by using the short specimen on the torsional split Hopkinson bar, where a wider range of strain rates can be obtained. These experiments can be divided into two categories: (1) approximately constant strain-rate test over a broad range of strain rates and (2) tests with the specimen prestressed at a quasistatic or dynamic strain rate and then subjected to an incremental disturbance. Results of the second type of experiment show an initial elastic responce to the incremental loading followed by strain hardening with increasing deformation.

An example of such an incremental stress-strain curve is given here, after Frantz and Duffy (1972). Figure 1.1 shows the constant rate curves together with a curve obtained by suddenly changing from the lower rate to the higher rate. Klepaczko et al. (1974) interpreted this kind of stress-strain behavior by including a strain-rate-history effect. It was suggested that the influence of strain rate on the flow stress can be divided into two parts. The initial part is due to the existing work-hardened structure at

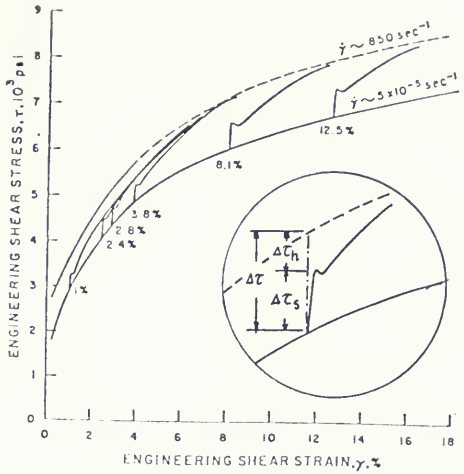

Figure 1.1 Torsional Split Hopkinson Bar Records in Aluminum [after Frantz and Duffy (1972)].

the strain level, while the second is associated with the formation history of that structure. The total stress difference $\Delta\tau$ between the two stress-strain curves, each obtained at a constant strain-rate, can be divided into two parts. The first, denoted by $\Delta\tau_s$, is probably developed by a single thermally activated dislocation mechanism. The second part, denoted by $\Delta\tau_h$, is related to the two different structures at the same value of strain. The difference between these two structures is probably due to a dynamic recovery process which occurred to a greater degree in the preceding deformation at the lower strain rate.

Reports of similar experiments on copper and titanium were given by Eleiche and Campbell (1974). Smooth incremental stress-strain curves were obtained for the material considered, without the knee reminiscent of an upper yield point found by Frantz and Duffy. Eleiche and Campbell used a fading memory to explain the strain-rate history effect. Santosham and Ramsey (1970) made an incremental wave test on annealed copper axially prestressed by dead loading. Incremental stress-strain curves were calculated at various prestrain levels by applying a modified strain-rate-independent theory.

1.2 Outline of the Present Study

To find the nature of strain-rate effects in materials under dynamic loading has been the major concern in the past history of dynamic plasticity. As the results from the torsional split Hopkinson bar confirmed the old results in axial impact loading, there has been fairly general agreement that:

(a) Strain-rate effect plays an important role in the incremental waves.

(b) A strictly one-dimensional plastic stress wave, with most of the deformation occurring within a narrow band of strain rates as in most of the cases considered, can be predicted well either by

the strain-rate-independent theory with a single dynamic stress-strain curve or by a strain-rate-dependent theory with a suitable choice of constitutive equations.

The study reported in this thesis contains:

(a) Experimental results of incremental wave tests on annealed copper and aluminum rods under quasistatic preloading. Incremental waves were recorded by measurements of particle velocity at four stations along the rod. It was found that an exponential function of two parameters can fit well the computed wave-propagation speed function. The major parameter of the wave-propagation speed function was found to be dependent on both prestrain and prestrain rate. This discovery provided direct evidence that the incremental waves are both prestrain and prestrain-rate, or strain-rate-history, dependent.

(b) Interpretation of the experimental results by using both strain-rate-independent and strain-rate-dependent theories. Incremental stress-strain curves were obtained from the fitted function of wave-propagation speed by applying a modified rate-independent theory similar to that of Santosham and Ramsey (1970). Numerical computer solutions were performed for the rate-dependent theories of

Malvern and Cristescu. The velocity record of the first gage station was used as the boundary condition to predict the velocity versus time at the other three gage stations. A new criterion was suggested for determining adequate parameter values to get a good solution.

Chapter 2 describes the experiment. Experimental results are given in Chapter 3, and an exponential function is fitted to the wave speed data. Chapter 4 gives theoretical analysis and numerical solutions, and Chapter 5 presents discussion and conclusions.

CHAPTER 2

THE EXPERIMENT

2.1 General Description

A 3-meter-high steel frame, with a hydraulic jack at the bottom and a load cell at the top was built for the purpose of studying incremental stress waves in a prestressed rod. A series of tests were performed on several aluminum and copper rods of 0.95 cm nominal diameter.

A schematic diagram of the test system is shown in Figure 2.1. Uniaxial tensile loading was achieved by using compressed hydraulic fluid in order to avoid bringing any kind of mechanical vibration to the system. While the specimen rod was being continuously prestrained into plastic deformation up to 0.05 nominal strain, a series of incremental waves was recorded at 4 locations along the rod by using electromagnetic velocity transducers. The transducers are described in Section 2.3.

The incremental particle-velocity wave generated in an elastic material was found to be approximately a square pulse with amplitude around 100 cm/sec and rise time 20 μsec.

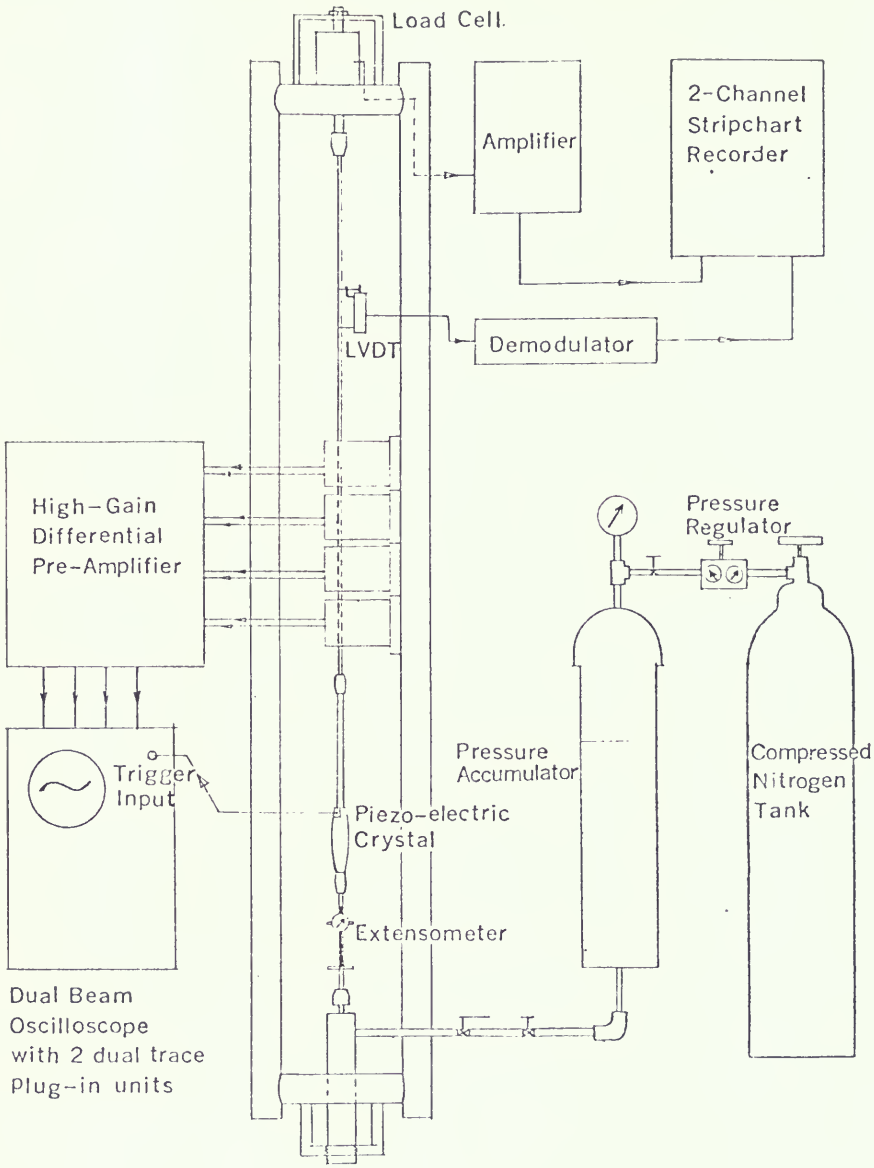

Figure 2.1 Schematic Diagram of Test Set Up.

Unloading occurs when the first compressive wave front reflected from the bottom reaches the first velocity transducer station. The loading durations of the incremental waves were about 300 μsec and 400 μsec for aluminum and copper specimens, respectively.

2.2 Specimens

Commercially pure copper rods and aluminum 1100-F rods were chosen as specimen materials. Both rods were manufactured by cold extruding with a nominal diameter 0.95 cm and 3.66 m original length. The specimens of 2.05 m length were cut down from them. Four holes each 12.7 cm apart were drilled at the velocity transducer locations by using a high speed drilling machine with Whitman & Barnes No. 72 drill (0.0250 inch diameter).

Another 0.45-meter-long rod was also cut down from the remaining 1.61 m length of rod. Both long and short rods were then annealed simultaneously and furnace cooled in a 3-meter-long electrical furnace which was built in the laboratory [see Figure 2.2]. Temperatures and times used for annealing were 345±4°C, 0.5 hr for aluminum and 370±4°C, 2.0 hr for copper. The densities of the two kinds of material used were found as

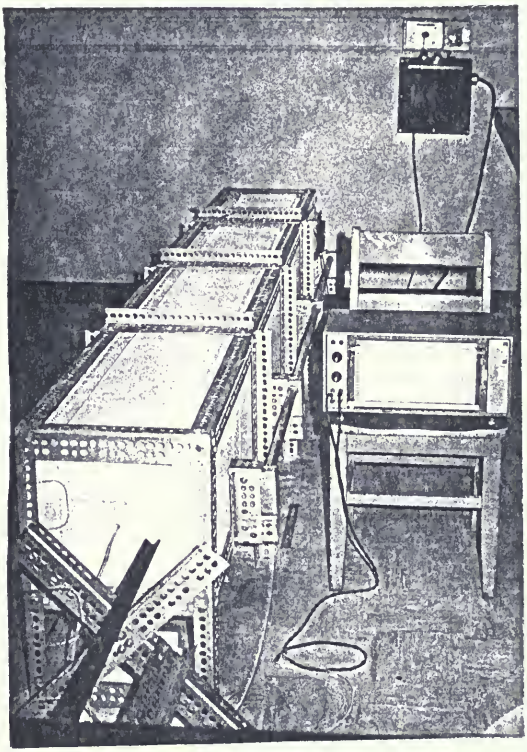

Figure 2.2 Three-Meter-Long Electric Furnace with a High Power Proportional Solid State Temperature Controller.

$$\rho_{aluminum} = 2.67 \pm 0.004 \text{ gm/cm}^3$$

$$\rho_{copper} = 8.89 \pm 0.003 \text{ gm/cm}^3$$

2.3 Velocity Transducer

The velocity transducer measures the voltage produced in a transverse conductor attached to a rod of nonmagnetic material as the rod moves axially in a magnetic field. See, for example, Ripperger and Yeakley (1963) and Efron and Malvern (1969). The transducer is based on the Faraday Principle of Electromagnetism, which can be expressed as

$$e_v = - \int \vec{B} \times \vec{v} \cdot d\vec{l} \qquad (2.1)$$

where $\vec{B}$ is the magnetic field intensity vector, $\vec{v}$ is the velocity of the conductor relative to the magnetic field, and $\vec{l}$ is the vector representation of length measured along the conductor. The units in the SI system are

e_v : volts
$\vec{B}$: weber/m^2 (or 10^4 Gauss)
$\vec{v}$: m/s
$\vec{l}$: m

From the arrangement shown in Figure 2.1, it can be seen that the longitudinal displacement of each velocity transducer conductor varies as much as 4.5 to 6.5 cm as the

rod is carried to 0.05 nominal tensile prestrain. Therefore two requirements must be fulfilled in order to have good velocity transducers. They are (1) a long magnetic field is required for each transducer, and (2) the velocity transducer must be able to move along with the rod.

Four pairs of permanent horseshoe magnets were obtained from surplus. The original area of each magnetic pole was 2.2 cm x 6.0 cm and the distance between north and south poles was 2.8 cm. The area of each magnetic pole was enlarged to 4 cm x 12 cm by adding to it pieces machined from soft magnetic iron. This makes the magnetic field more uniform and thus reduces the errors from possible deviations in position measurement of the velocity transducer. Figure 2.3 shows an example of the difference in the magnetic field intensity before and after the enlargement of the pole area.

Figure 2.4 shows a schematic diagram of the velocity transducer which was designed and built to meet the above mentioned second requirement after several other kinds of unsuccessful attempts. The transducer is made by passing a No. 25 gauge enamel-coated wire through a hole drilled along the diameter of the rod cross-section. The wires came out at points A' and D' from holes on the brass holder. It is by the inertia effect of the brass holder that during the passing of the stress wave only the movement of section BC is detected. The total displacement of section BC is 0.4 mm for a square wave of 100 cm/sec amplitude and 400 μsec

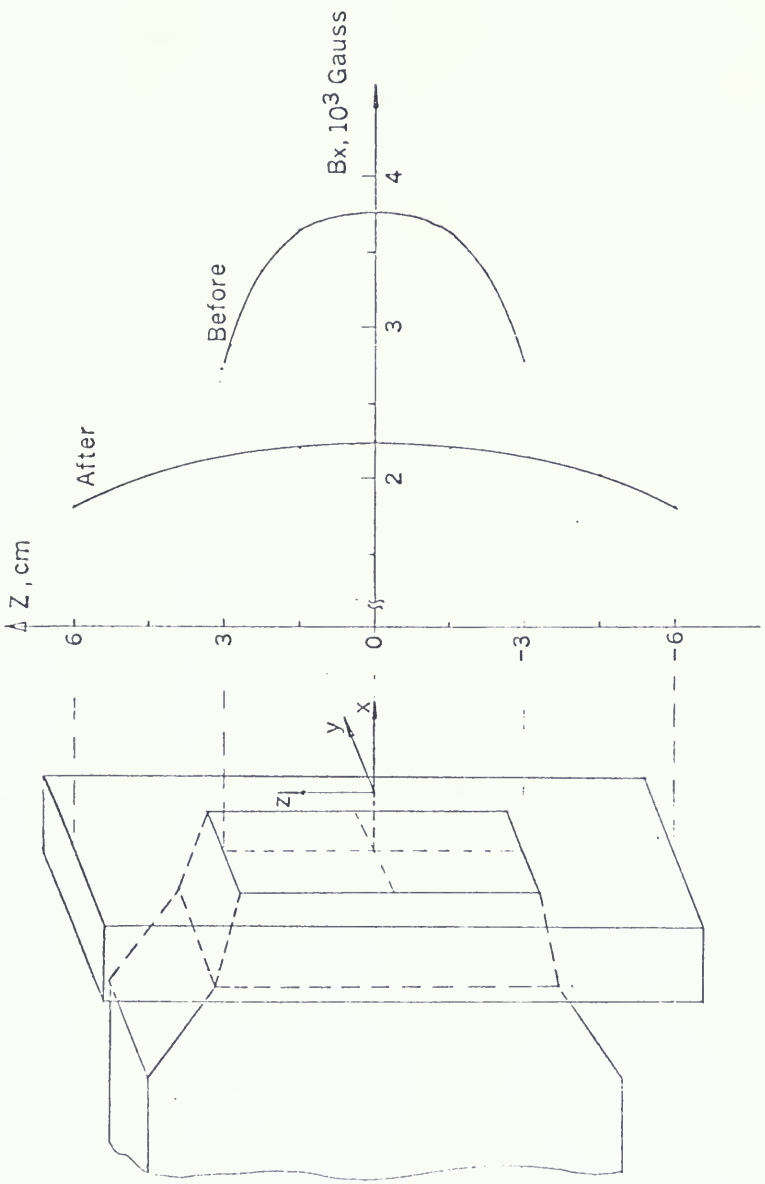

Figure 2.3 Enlargement of Magnet Pole and Effect on the Intensity Distribution.

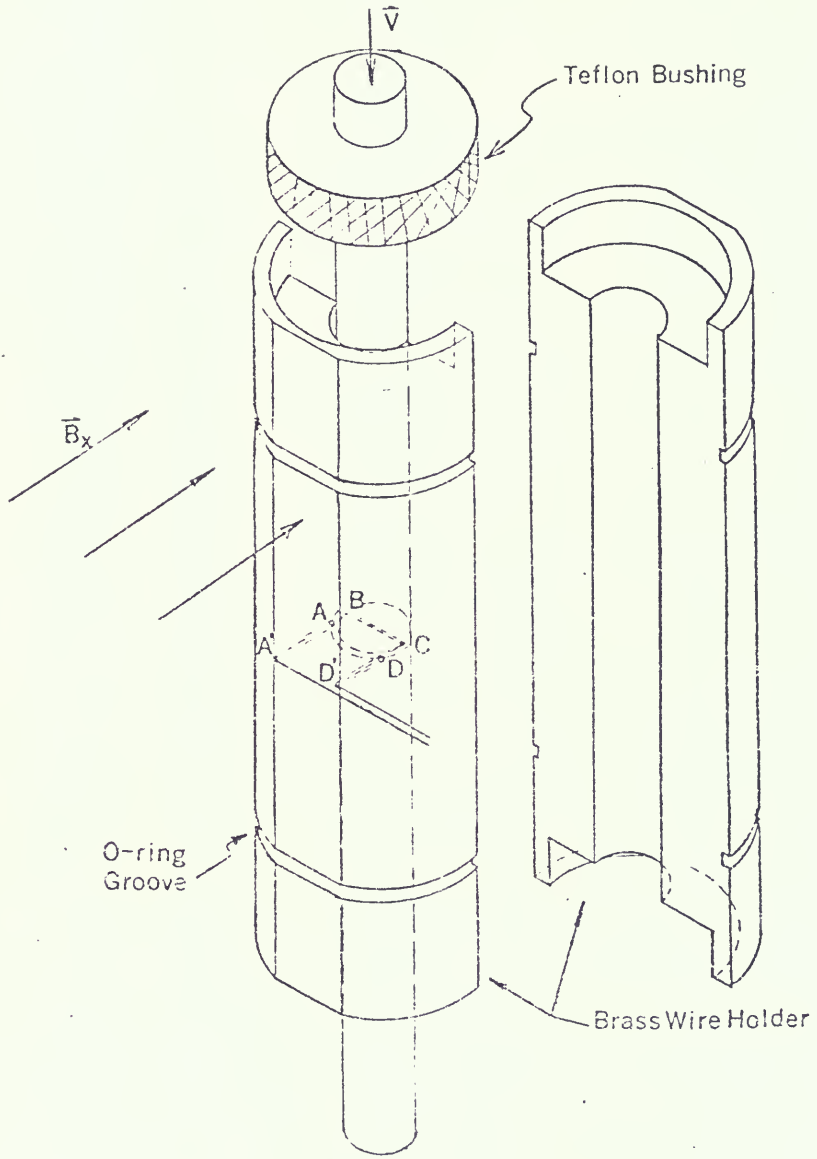

Figure 2.4 Incremental Particle Velocity Transducer.

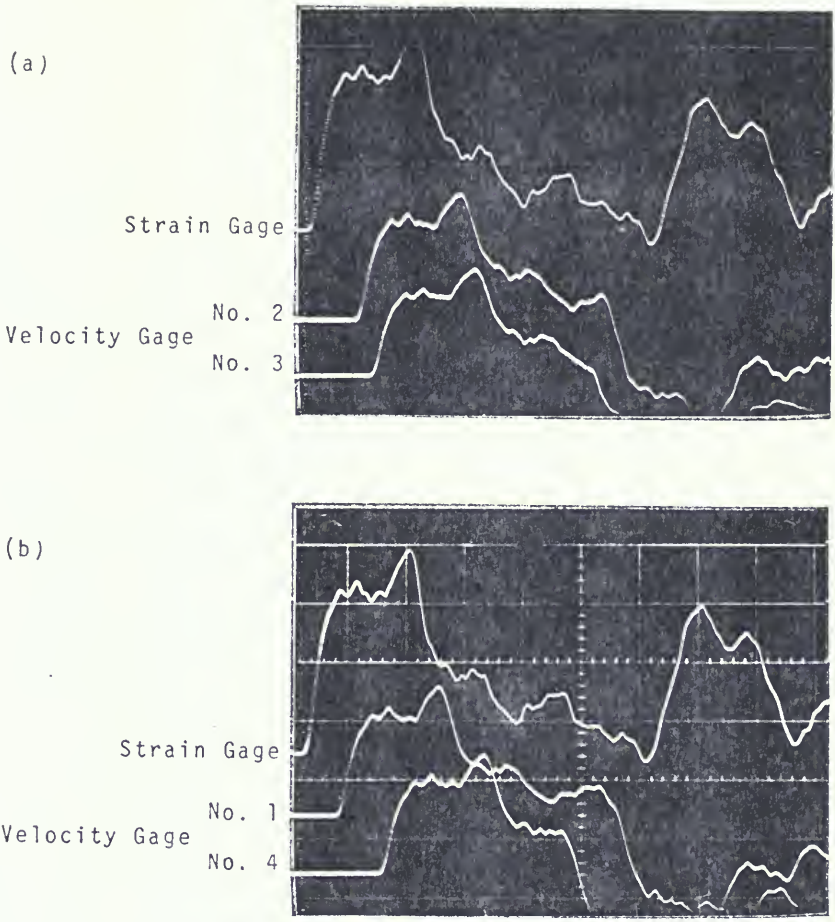

Vertical Scale: Strain Gage: 0.51 mv/cm
Velocity Gage: 0.89 mv/cm (upper)
1.05 mv/cm (lower)

Horizontal Scale: 100 μsec/cm

Figure 2.5 Trace Records for Outputs of Strain Gage and Velocity Transducer.

duration. For the incremental waves in this experiment the displacement is much less than 0.4 mm. This means that the angle of rotation of wire AB or CD with respect to point A or D is less than 0.08 radian or 4.6 degrees. Four pairs of such brass holders were made.

The validity of the velocity transducer was also checked by obtaining a signal simultaneously from a surface strain gage on an aluminum rod for an elastic wave. Resistance strain gages of Micro-Measurement Type ED-DY-250 BF-500 with gage factor 3.31 were selected for the test. Because the amplitude of the elastic wave in strain is only about 0.0001, this type of gage with a resistance of 500 ohms was selected in order to give better resolution. The gages were mounted in pairs, diametrically opposed to cancel any effects due to bending, at a position 30 cm below the lowest velocity transducer station. The gages were connected in series and installed as one arm of a Wheatstone bridge. The results are shown in Figure 2.5. The upper curve is the strain gage output, the lower curves are velocity transducer outputs. It is obvious that the shapes of these two kinds of signal agree well. The magnitude of each signal was also checked. The results are

Station No.	Velocity (cm/sec)	Strain	c_o = velocity/strain
2	71.5	142×10^{-6}	$5.03 \times 10^{+5}$ cm/sec
3	71.3		
1	71.8	146×10^{-6}	$4.92 \times 10^{+5}$ cm/sec
4	71.9		

The average of these two values of c_0 is about 3% below the value of elastic bar wave speed obtained in Section 3.3.

2.4 Velocity Transducer Calibration

An aluminum frame of length 0.5 m which can span all the four magnets was made and mounted as shown in Figure 2.6. Since the positions of velocity transducers varied as the rod was being prestrained and the magnetic field was not uniform, the calibration of the velocity transducer was required to give a relation between the effective magnetic field intensity at the conductor wire and the conductor position expressed in a coordinate system. The aluminum frame functioned essentially as a reference coordinate frame, on which the magnetic field was mapped and with which, later in each series of incremental wave tests, the initial and final positions of the transducer conductor were measured.

An O. S. Walker Company type MG-1 Gaussmeter with Hall-effect flat probe was used to map the magnetic field. The coordinate system was chosen so that the origin was close to the center of rod. Field intensity, denoted by B_x, was measured at fifteen points on an x-y plane for every 0.5 cm increment of z-coordinate. In practice, (x,y) was fixed first, and the probe moved along z-axis, stopping for a few seconds at every 0.5 cm interval. The output from the

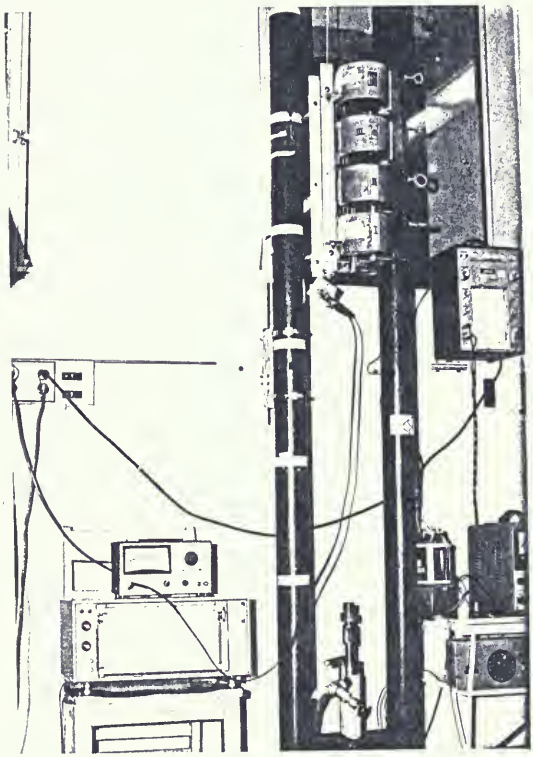

Figure 2.6 Magnetic Field Mapping.

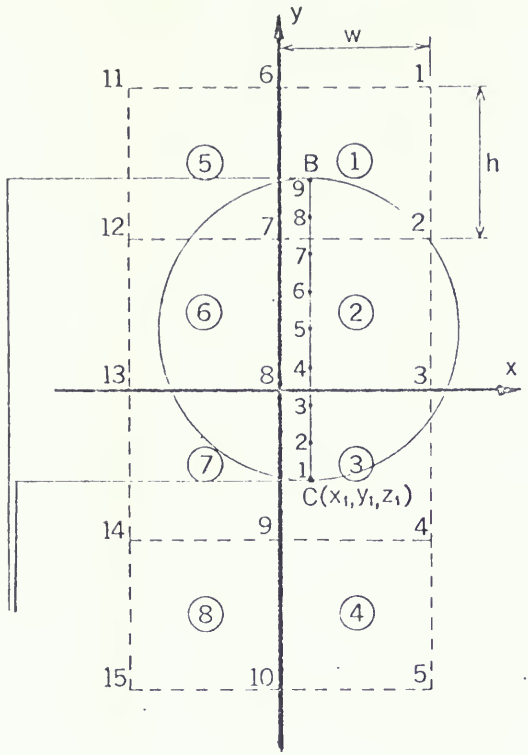

(a)

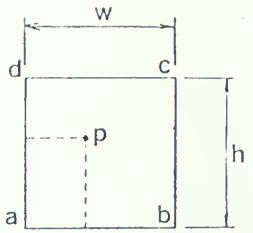

(b)

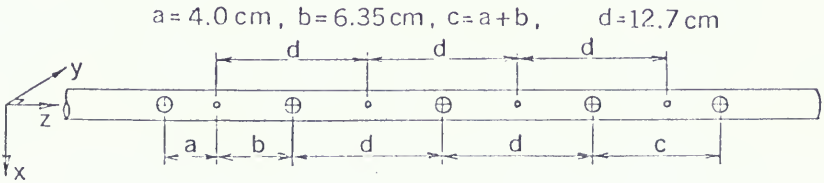

(c)

Figure 2.7 Interpolation Grids and Transducer Positions.

Gaussmeter was recorded by a Honeywell Electronik-194 strip-chart recorder with 10 inch pen movement. Each stop at a 0.5 cm interval showed on the records as a flat step. All the data were read and punched as input data cards for the Velocity Data-Processing Computer Program [see Section 3.3].

Because the transducer wires were enclosed by the brass holders, so that their positions could not be observed during the test, five reference marks were made on the rod at known positions relative to the wire holes before the brass holder was mounted [see Figure 2.7(c)]. During the incremental wave test, the (x,y,z) coordinate values of these five marked points were measured at two or three pre-strain levels, usually the beginning and end of each dynamic incremental loading. Thus, for any value of prestrain, the (x,y,z) coordinate values of the transducers could be obtained by interpolation. Once a transducer's coordinates are determined, denoted by (x_1, y_1, z_1), the effective magnetic field intensity for this velocity transducer can be obtained by a subroutine contained in the velocity data processing computer program. This routine essentially contains the following procedures:

(a) Determine the values of B_x at the 15 points on the $z = z_1$ plane by using linear interpolation from the two adjacent z-planes where values of B_x were known [see Figure 2.7(a)].

(b) Assuming that the conductor wire BC is perfectly parallel with y-axis, evaluate B_x at 9 points on line BC. Successive points are 0.125 cm apart. A subroutine automatically determines the element number to which the points belong. The equation of interpolation for a generic point shown in Figure 2.7b is simply:

$$B_p = B_a + r\cdot(B_b-B_a) + t\cdot(B_d-B_a) + r\cdot t\cdot(B_a-B_b+B_c-B_d) \qquad (2.2)$$

where

$$r = \frac{x_p - x_a}{w} \qquad t = \frac{y_p - y_a}{h} \qquad (2.2a,b)$$

(c) By applying the trapezoidal rule, the calibration factor for converting voltage to velocity is obtained as:

$$g = \int_C^B B_x dl = \frac{1}{2(n-1)} [B_1 + B_n + 2(B_2 + ... + B_{n-1})]\cdot\overline{BC} \qquad (2.3)$$

where n = 9 in this case.

From equation (2.1), it is obvious that

$$v = e_v/g \qquad (2.4)$$

2.5 Quasistatic Uniaxial Tension Test

The purpose of this research was to study the incremental wave on the quasistatically prestrained rod. Therefore

a complete and accurate record of the quasistatic stress-strain relation was needed. Since prestrain had to be measured at some other location apart from the velocity transducers, the uniformity of the long rod had to be checked at first. The major factor that influences the uniformity is the annealing temperature distribution along the rod. The long furnace was made by joining three cores. It was found that the temperature was lower near the junctions. The position of the rod in the furnace was arranged as shown in Figure 2.8. The effect of annealing temperature on the specimen rod was determined by checking the stress-strain curve for the 5 sections A, B, C, D, E, cut down from a 7-ft aluminum rod after annealing. The results show that there are hardly any differences in stress-strain relation among A, C, and E or between B and D. However, the stress-strain curve for B and D consistently lies above that of A, C, and E with a difference in stress value varying monotonically from 1 MN/m^2 for small strain to 0.3 MN/m^2 for $e_o = 0.05$. Therefore the prestrain value obtained from the extensometer located in section A should represent very well the local strain at the velocity transducers, which were located in section C.

The load cell on the main test frame was calibrated by adding step by step ten 10-lb weights before and after each set of incremental wave tests. The aluminum specimens

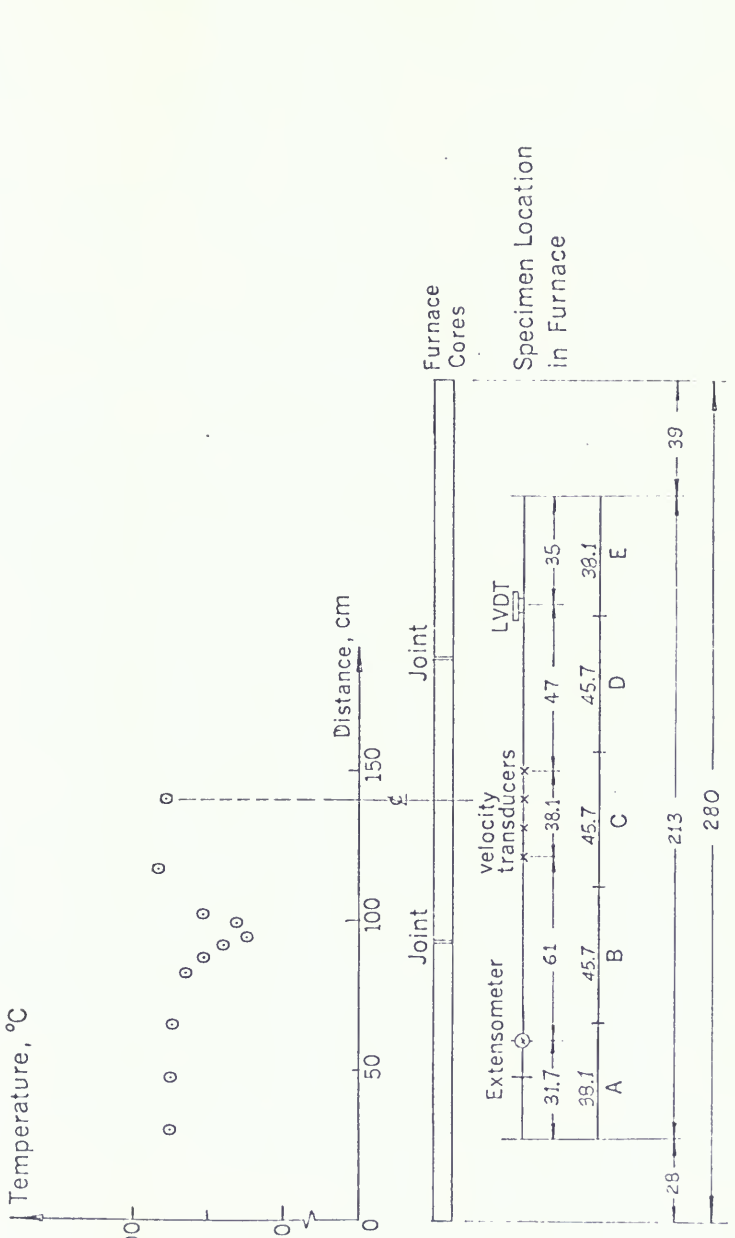

Figure 2.8 Location of Specimen Rod in Furnace and Temperature Distribution.

need a 1000 lb force to load up to 0.05 nominal strain, while the copper specimens need a 1700 lb force to do the same thing. The force was supplied from an AIRCO Nitrogen tank with full pressure 2200 psi. It was found that in order to obtain a 1000 lb force the pressure needed was 1150 psi. The force obtained is proportional to the pressure.

Prestrain records for incremental wave test were obtained by using a 5-inch gage length extensometer and also a 2-inch gage length LVDT (Linear Variable Differential Transformer) which was a part of the recording equipment of the Tinius Olsen U-Celtronic testing machine. The LVDT was calibrated by comparison with the reading from the extensometer, when both instruments were mounted on a short rod loaded on the Tinius Olsen Machine. The LVDT was mounted inside the 5 inch range of extensometer's gage length. The result of the calibration showed that an initial nonlinear relation exists until strain larger than 0.006, after which the output from the LVDT is a linear function of strain.

A 6-volt lantern battery was used to drive the Wheatstone bridge circuit of the load cell. Output from it was first amplified by a Hewlett-Packard HP-425A DC Micro-Volt-Ammeter, then fed into one channel of a Gould Brush 220 2-channel stripchart recorder. Output from the LVDT was fed into the other channel. Strains from the reading of the extensometer gage dial were also recorded on the

Brush 220 by a remote push-button event marker. The resolution of the strain reading by the extensometer is 0.0001. During the incremental wave test, the Brush 220 chart speed was set at 25 mm/min. and sensitivity was set at 10 mv/div for both channels, which had 50 divisions full range.

2.6 Incremental Wave Test and Wave Recording Equipment

From the results of some preliminary tests, it was found that the characters of the incremental waves are substantially different among three kinds of loading states, which are: (1) constant prestressed state, which is the case that the force exerted on the jack piston, by the pressured hydraulic fluid, is in equilibrium with the resistance force in the rod, (2) constant prestrained state which is the case that the manual control valve was closed, and (3) continuous quasistatic loading state. Since creep and relaxation phenomena were involved in the constant prestressed and prestrained states, respectively, and their influences on material structure are not well known, no further incremental wave tests were done on these two preloading states.

The incremental wave was generated by striking a steel tubular hammer on a collar attached on the bottom end of the hard aluminum transmitter tube. The top end of the transmitter tube was attached to the specimen rod by a

4-piece grip collar. This collar was located 15 cm below the lowest velocity gage station [see Figure 2.1]. The steel hammer has a mass of 345 gm. The dropping height is 15.6 cm. This resulted in a free-fall striking velocity of 174 cm/sec. This striking velocity was increased by connecting the steel hammer and bottom collar with 3 soft tension springs. The spring constant was found to be 7.74×10^4 dyne/cm. This arrangement increased the striking velocity to 351 cm/sec.

Some examples of the velocity pulses generated by this kind of hammer mechanism on elastic rods are shown in Figure 2.9. It was found that the transmitted velocity in the rod depends on the tightness condition of the grip.

For the reasons cited in the first paragraph of this section, a compressed nitrogen tank with an output pressure regulator is a necessary arrangement. By slowly turning up the output pressure on the regulator, the specimen rod can be further prestrained continuously. This avoids the relaxation of the specimen in the usual procedure of closing the manual valve first and increasing the pressure in the accumulator to a higher value, then opening the valve and reloading. Figure 2.10 is a general view of the physical set up of testing equipment.

Outputs from the four velocity transducers were fed into four Tektronix 1A7A high-gain differential amplifiers in rack-mounted Tektronix 127 pre-amplifier power supplies.

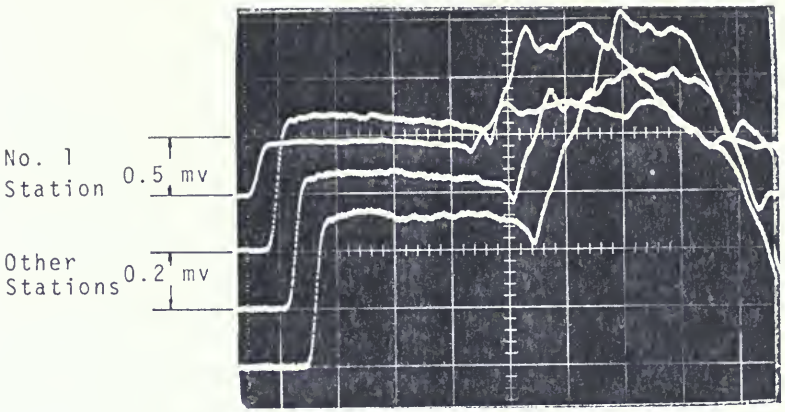

(a)

Initial State, e_o = 0.00

Average v = 22.5 ± 0.5 cm/sec

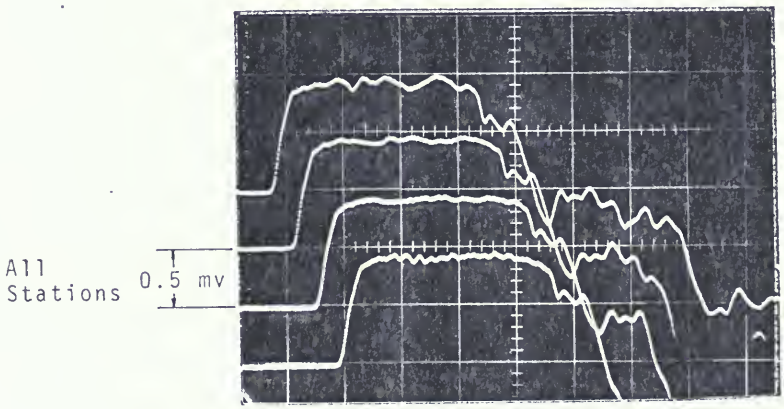

(b)

Residual Strain = 0.0488

Average v = 47.6 ± 0.4 cm/sec

Figure 2.9 Incremental Elastic Waves (From Copper Specimen No. 4).

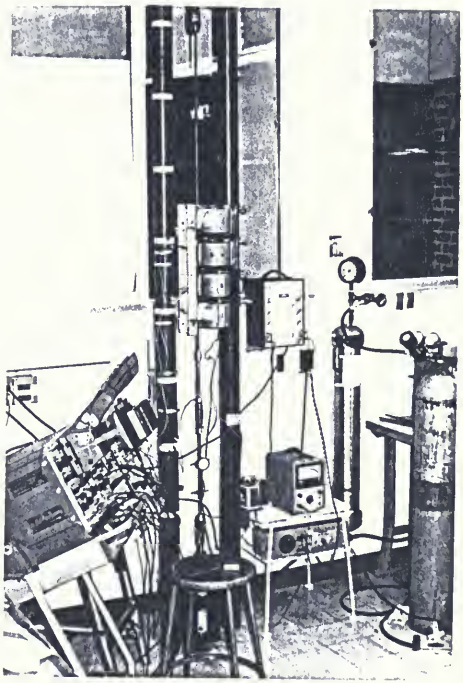

Figure 2.10 General View - Load Frames, Electronics and Recording Equipment.

The high and low frequency -3dB points were set at 1 MHZ and DC, respectively. The outputs from the 1A7A units, which were approximately 0.25 volts for an input of 1 mv when 1A7A input setting was 1 mv/cm, were then connected to the inputs of two Tektronix 1A1 dual-trace plug-in units on a Tektronix Type 556 dual beam oscilloscope. All four channels of the two 1A1 plug-in units were set at 0.2 v/cm. The whole recording system was calibrated by inputting a square wave signal into one 1A7A differential amplifier at a time. The magnitude of the square wave signal was set equal to the value of the scale variable setting on the 1A7A. The gain adjustment on the 1A7A was then adjusted to make the square wave trace appeared on the oscilloscope to have a 1 cm height. This was checked once again after each set of incremental wave tests. The gain in voltage of the system is 50 dB (400 times) for input setting on 1A7A at 0.5 mv/cm and 60 dB (1000 times) for 0.2 mv/cm.

The time base on the oscilloscope was calibrated by inputting a sine wave from a Wavetek Model 112 wave generator simultaneously into each channel and a Monsanto Model 100A Counter-timer. The exact frequency of the sine wave was obtained from the counter. The display on the oscilloscope screen was recorded by using a Polaroid camera. The results of the time base calibration for the 100 μsec/cm and 50 μsec/cm ranges on the oscilloscope are obtained as shown:

100 μsec/cm range:

upper beam : 102.51 μsec/cm

lower beam : 100.00 μsec/cm

50 μsec/cm range:

upper beam : 50.80 μsec/cm

lower beam : 49.78 μsec/cm

A Polaroid camera was used to make a permanent record of each single-sweep trace on the oscilloscope. The shutter speed was set at 1 sec and a remote control push-button was used to open the shutter just before dropping the hammer. The oscilloscope was set at single sweep and external trigger. The trigger was provided by a piezo-electric crystal element mounted on the top of the steel hammer. This arrangement allows for the delay in the scope sweep mechanism.

CHAPTER 3

EXPERIMENTAL RESULTS AND DATA REDUCTION

3.1 Quasistatic Stress-Strain Curves and Their Slopes

The quasistatic stress-strain curves were obtained from load-time and strain-time histories recorded during the prestraining of each specimen rod in the incremental wave tests. The results for 7 annealed aluminum specimens and 4 annealed copper specimens are shown in Figures 3.1 and 3.2, respectively.

It can be seen from Figure 3.1 that the maxumum variation in stresses among different aluminum specimens is about 6 MN/m^2 which is around 25% of the yield stress value. Results for copper specimens shown in Figure 3.2 appear to be more uniform among different specimens.

The large variation in stresses among the aluminum specimens is believed to be caused by the unequal amounts of previous work hardening of the specimens during the extrusion process of manufacturing. The annealing process used in this experiment can only recover about 75% of previous work hardening. No attempt was made to average these curves, since each curve should describe the best stress-strain relation for the individual specimen.

The slope of the stress-strain curve, dS/de, versus strain, e, was obtained numerically for each individual stress-strain curve. The stress value corresponding to each Δe strain increment was first obtained by interval-by-interval cubic Lagrange interpolation. The value of dS/de at $e = e_i$ was then obtained by calculating $(S_{i+1} - S_{i-1})/(2\ \Delta e)$. The results for aluminum and copper specimens are shown as the lower curves in Figures 3.1 and 3.2, respectively. $\Delta e = 0.00025$ was used in these calculations.

It will be shown later in Section 3.3 that the wave-propagation speed as a function of incremental particle velocity, denoted by c(v), is affected by both prestrain and prestrain rate. The prestrain rate was determined by two approaches and the average value of them was adopted. The first way was to measure the slope directly from e-t record. In practice the angle of slope is in the range of 0.5 degree to 10 degrees. The error in reading the angles is large in those angles less than 5 degrees. The second way was to measure dS/dt from load-time record first, then to obtain de/dt from de/dt = (dS/dt)/(dS/de). Some typical examples of the values of de/dt are tabulated together with some other results in Tables 3.1 and 3.2.

In the numerical computation the slope, $d\sigma/d\varepsilon$, of the true stress-strain curve will be needed. Therefore the value of dS/de will be converted to $d\sigma/d\varepsilon$ by the relation:

$$d\sigma/d\varepsilon = (1 + e)^2\ dS/de + (1 + e)S \qquad (3.1)$$

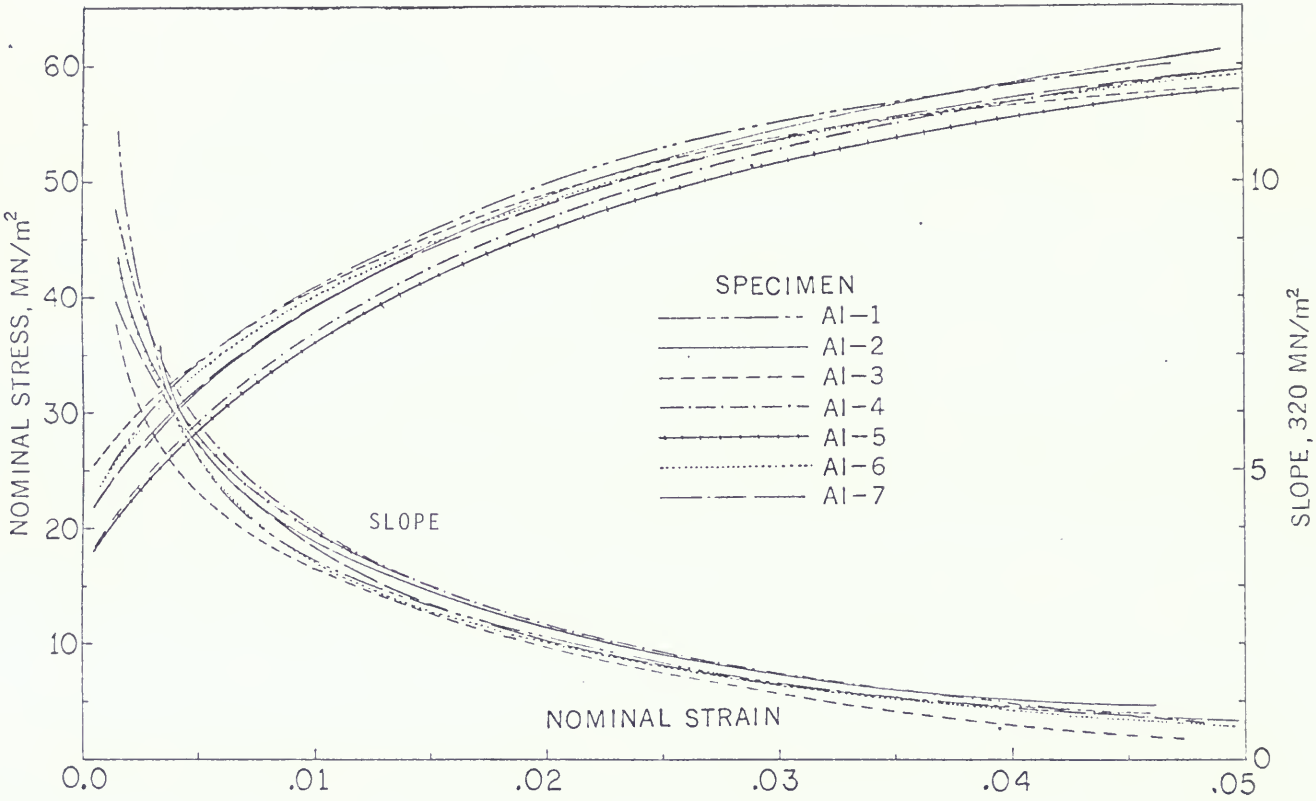

Figure 3.1 Stress-Strain Curves and Their Slopes (Annealed Aluminum).

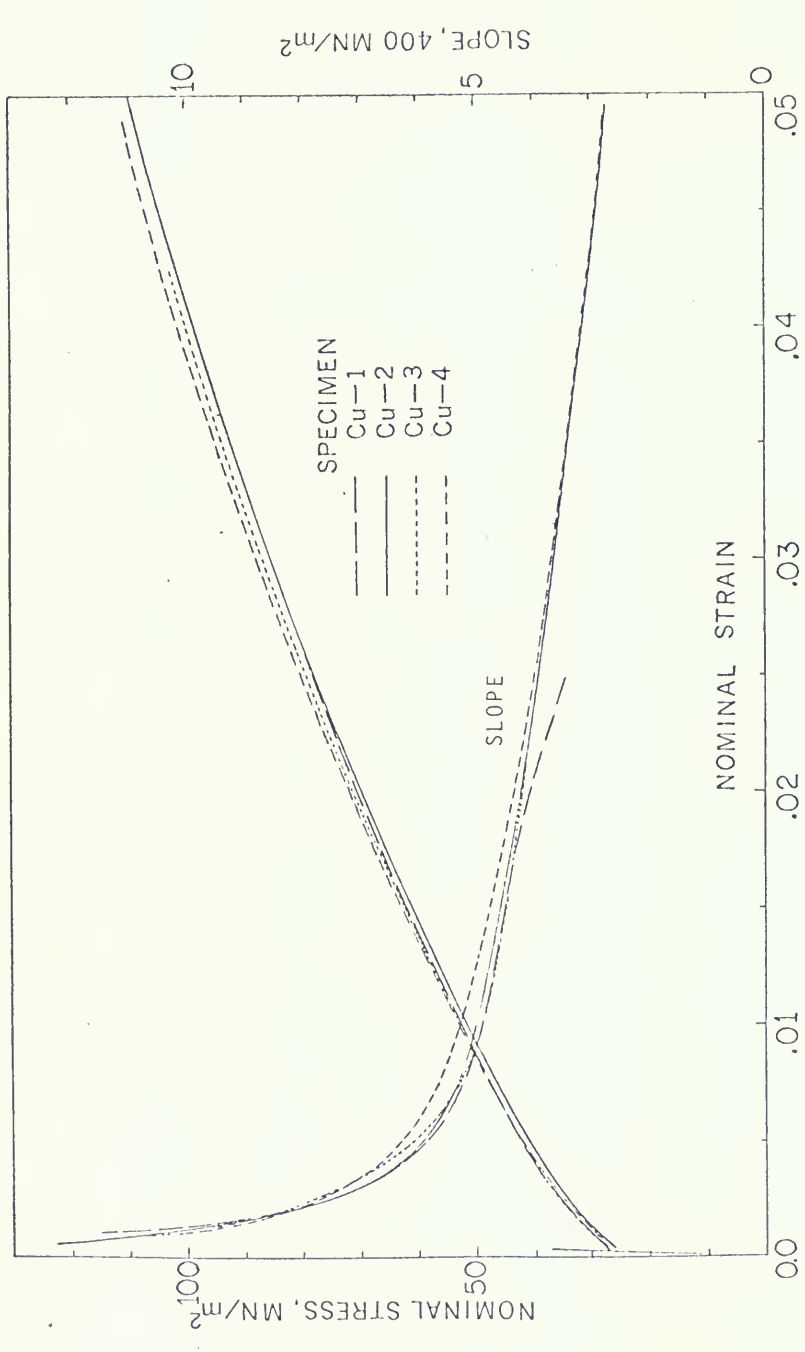

Figure 3.2 Stress-Strain Curves and Their Slopes (Annealed Copper).

3.2 Incremental Wave Test Results-Oscilloscope Photographs

The incremental wave test for each specimen contains about 20 runs at increasing prestrain levels during the quasistatic loading in plastic deformation. All the velocity profile traces on the oscilloscope screen were recorded by Polaroid pictures. In this section, some typical examples of oscilloscope trace photographs will be shown. Since the amount of data for 7 aluminum and 4 copper specimens is around 170 pictures, data reduction was done by using a computer program, which will be described in the next section. The dependence of the incremental wave behavior on both prestrain and prestrain rate will be discussed in Section 3.4.

Figures 3.3 and 3.4 show examples of oscilloscope traces of incremental particle velocity for an aluminum specimen. It can be seen in the case of small prestrain values, like those in Figure 3.3(a) and (b), that the velocity profile shows an initial step, which propagates with very little attenuation and is followed by a more slowly rising part that attenuates rapidly along the gage stations. For the cases with prestrain larger than 0.006, the rising part was flattened out even in the trace for the first gage station.

Figures 3.5 and 3.6 show examples of oscilloscope traces for incremental particle velocity in copper specimens. In these pictures, it can be seen that the shape of the velocity profile varies gradually from concave upward and

Prestrain

$e_o = 0.0015$

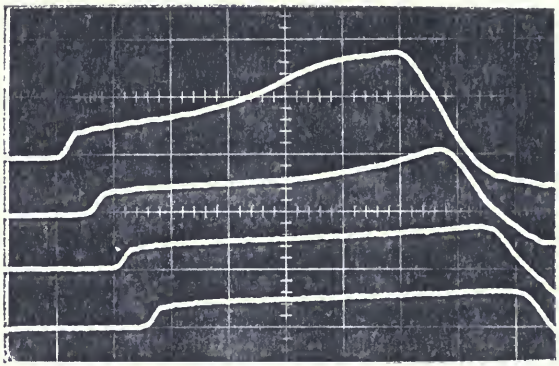

$e_o = 0.0060$

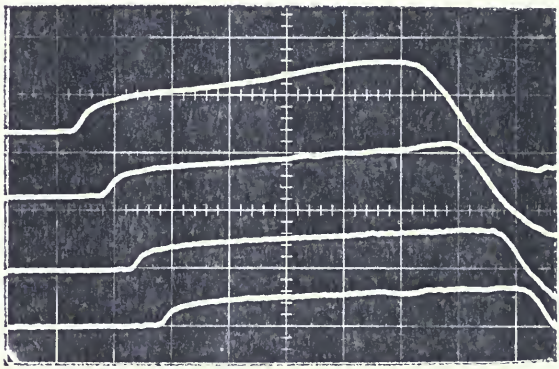

$e_o = 0.0100$

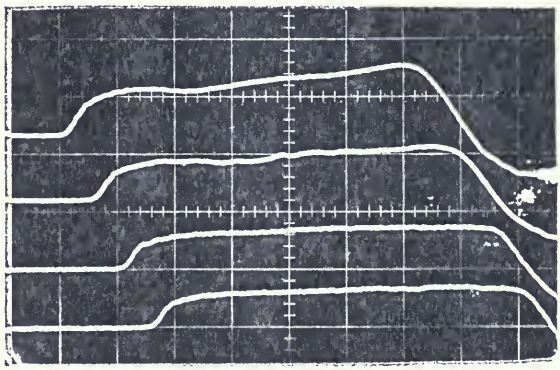

Vertical scale: 0.5 mv/cm, Time scale (Nominally): 50 μsec/cm

Figure 3.3 Oscilloscope Trace Records (Aluminum Specimen No.4)

Prestrain

e_o = 0.0200

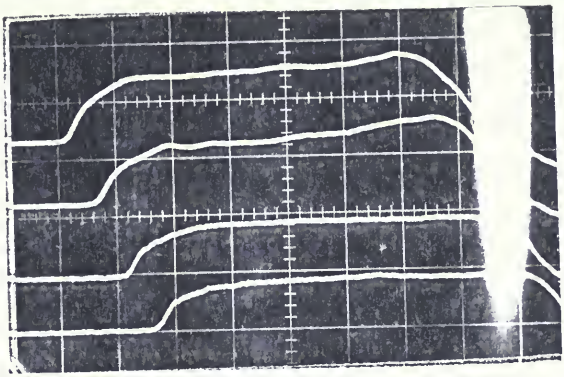

e_o = 0.0342

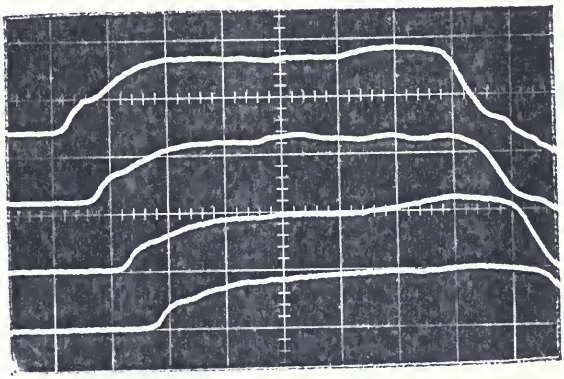

e_o = 0.0460

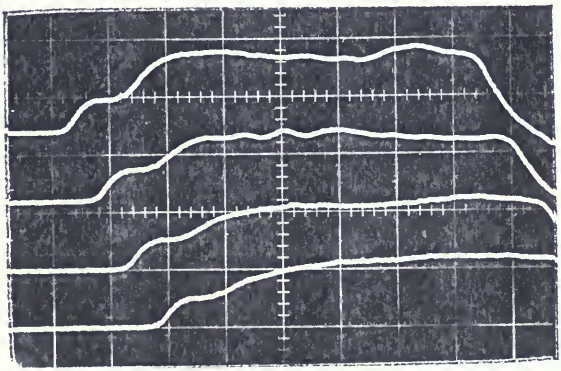

Vertical Scale: 0.5 mv/cm, Time Scale (Nominally): 50 μsec/cm

Figure 3.4 Oscilloscope Trace Records (Aluminum Specimen No.4)

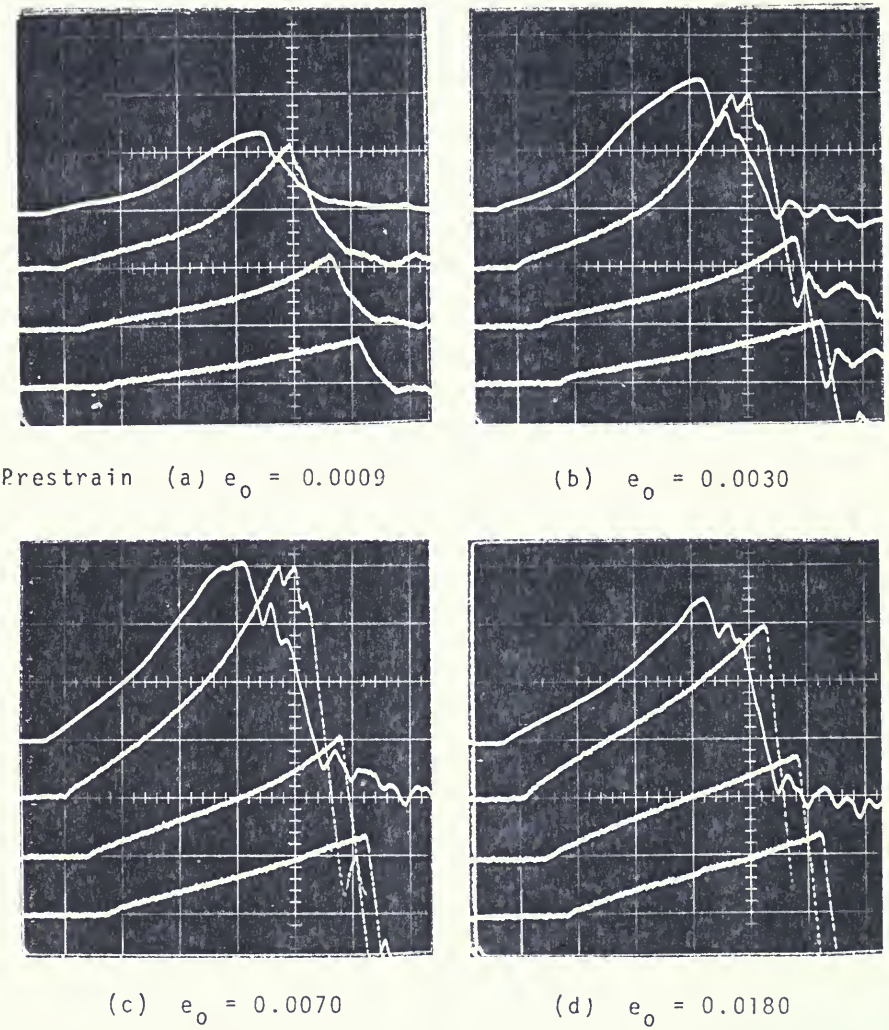

Prestrain (a) e_o = 0.0009 (b) e_o = 0.0030

(c) e_o = 0.0070 (d) e_o = 0.0180

Vertical Scale : Station No. 1 is 0.5 mv/cm

Others are 0.2 mv/cm

Time Scale : (Nominally) 100 μsec/cm

Figure 3.5 Oscilloscope Trace Records (Copper Specimen No. 4).

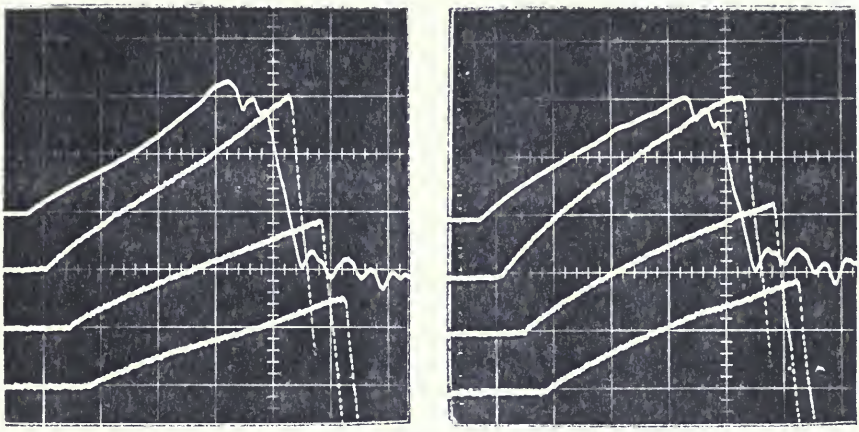

Prestrain (a) e_o = 0.0220 (b) e_o = 0.0330

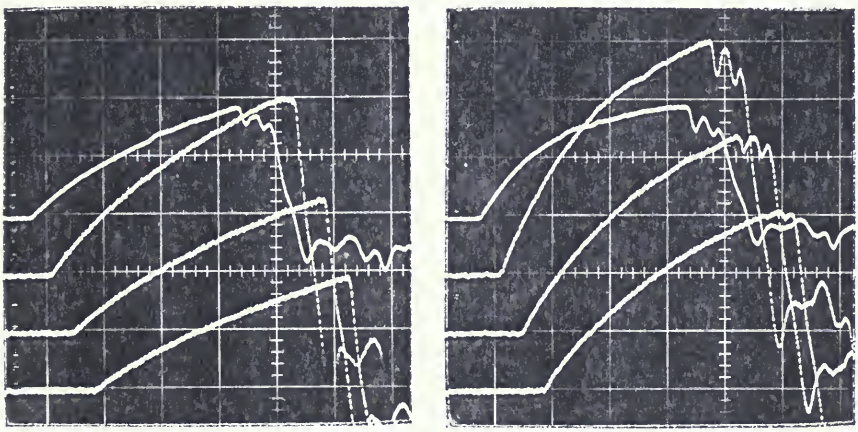

(c) e_o = 0.0400 (d) e_o = 0.0488

Vertical Scale : Station No. 1 is 0.5 mv/cm

Others are 0.2 mv/cm

Time Scale : (Nominally) 100 μsec/cm

Figure 3.6 Oscilloscope Trace Records (Copper Specimen No.4).

attenuating fast to concave downward and attenuating slower as the value of prestrain increases.

From a rough examination it was found that this kind of shape changing in the velocity profile will give a family of wave-propagation speed functions. In order to get a quantitative result, the wave speed functions for all the 200 incremental tests were obtained numerically by the computer program.

3.3 Velocity Data Reduction and Wave Speed Function

A Fortran program was written to reduce the large amount of incremental wave test results and obtain wave speed functions by numerical computations. The program is given in Appendix A - 1. Only some basic procedures are explained briefly in the following.

(a) Data reading and conversion into velocity units.
Coordinates of about 15 points of each velocity trace on the oscilloscope photograph were read and converted into values in velocity units by using the velocity transducer calibration factors obtained from a subroutine [see Section 2.4].

(b) Interpolation.
By applying an interval-by-interval cubic Lagrange interpolation subroutine, the values of velocity at much smaller time intervals, Δt, were obtained.

Δt was chosen to be 4 μsec for aluminum results and 6 μsec for copper results.

(c) Computing wave-propagation speed function. From the result of (b), each velocity profile is actually composed of discrete points each with Δt time interval. These data points are expressed by two corresponding arrays, say V(I) and T(I). To obtain wave-propagation speed of velocity level $v_k = k\ \Delta v$, a routine will locate the interval in which v_k lies, and then use linear interpolation between the two adjacent points to obtain the corresponding time t_k and store it in another array Q(k). Wave-propagation speed computed between gage 1 and 2 can then be obtained from

$$c(v_k) = \text{distance}/[Q_2(k) - Q_1(k)] \qquad (3.2)$$

In this manner, wave-propagation speeds were calculated between velocity stations 1 and 2, 2 and 3, 3 and 4, and 1 and 4. Δv used in the computation is equal to 0.4 cm/sec.

(d) The results of particle velocity and wave-propagation speed are printed. They are plotted to give a better impression.

Some typical examples of resulting velocity-time profiles of an incremental wave plotted by computer are given in Figures 3.7 to 3.21. In these figures are shown also

results from the theoretical computation of Chapter 4.

Figures 3.7 to 3.13 are selected from specimen No. 4 of copper. Figures 3.14 to 3.21 are selected from the results of aluminum specimen No. 4. Most of the original oscilloscope traces for these results have already been shown in Figures 3.3 to 3.6.

It can be seen from these figures that most of the results were good except that the gage station No. 2 of the aluminum case shows a discrepancy consistently. In general the discrepancy may be caused by the following possible sources of error: (1) error in reading traces on the photograph, (2) error in magnetic field mapping, (3) error in locating the transducer's position in the magnetic field during the wave test, (4) error in the calibration of the oscilloscope vertical scale, (5) noise signal caused by the random movement of wire in the velocity transducer's hole, which was drilled a little too large. For the case just mentioned it was No. (5) that caused the error.

The elastic bar-wave propagation speed c_0 was obtained by measuring the time interval between leading edges of incremental velocity profiles. The resolution in determining the position of the leading edge is very poor in general. It can be seen from Figures 3.3 to 3.6 that the distance between two adjacent leading edges on the picture is around 5 mm. A 0.5-mm error will produce about 10% error in wave-propagation speed. No systematic variation of the

value of c_o among different prestrain levels was found. The result of c_o is the averaged values of 76 cases for copper and 100 cases for aluminum. Young's modulus was calculated from $E = \rho c_o^2$.

Aluminum: $c_o = 5.13 \times 10^5$ cm/sec, $E = 0.71 \times 10^{12}$ dyne/cm^2

Copper: $c_o = 3.67 \times 10^5$ cm/sec, $E = 1.20 \times 10^{12}$ dyne/cm^2

By checking all the computer output of wave-propagation speed functions, it was noted that the variations among the curves computed from gage stations 1-2, 2-3, 3-4 and 1-4 were insignificant and random. Therefore it was concluded that the propagation speed of a given level of incremental velocity was independent of propagation distance. The wave speed function computed from gage stations 1-2 hence was used to express the wave speed function.

From the computer outputs it was also noticed that wave-propagation speed functions were different for incremental waves generated at different prestrain levels. Figures 3.22 and 3.23 show the typical examples of these results for copper and aluminum, respectively. It was apparent from these figures that the value of wave speed at a certain velocity level is usually larger for larger prestrain values. But there are some exceptions like curve No. 5 in Figure 3.22 and No. 7 in Figure 3.23. These are not the only exceptions, since many curves have not been plotted in the figure to avoid curves mingling together.

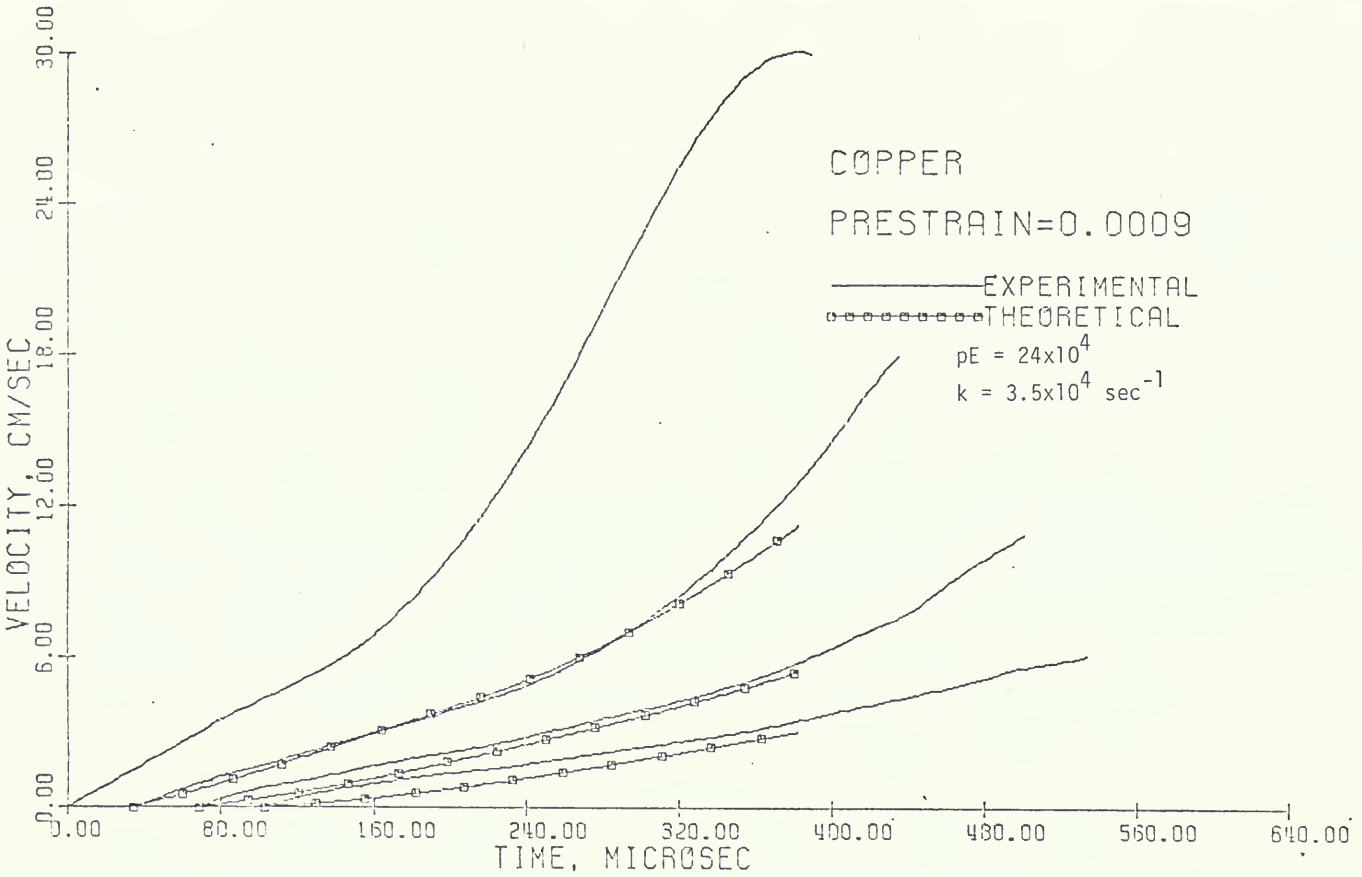

Figure 3.7 Particle Velocity Records (Copper Specimen No. 4, Prestrain 0.0009).

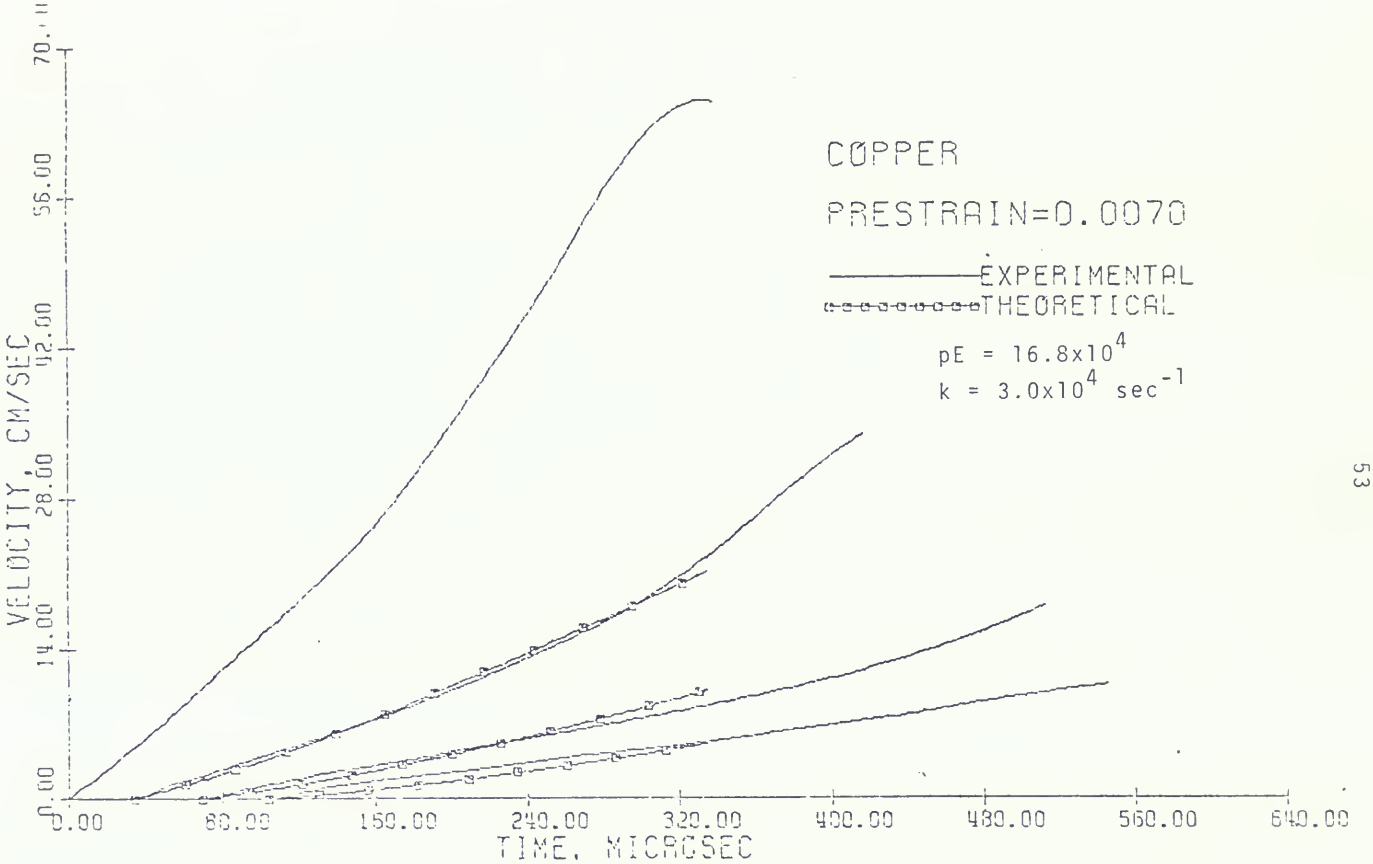

Figure 3.8 Particle Velocity Records (Copper Specimen No. 4, Prestrain 0.0070).

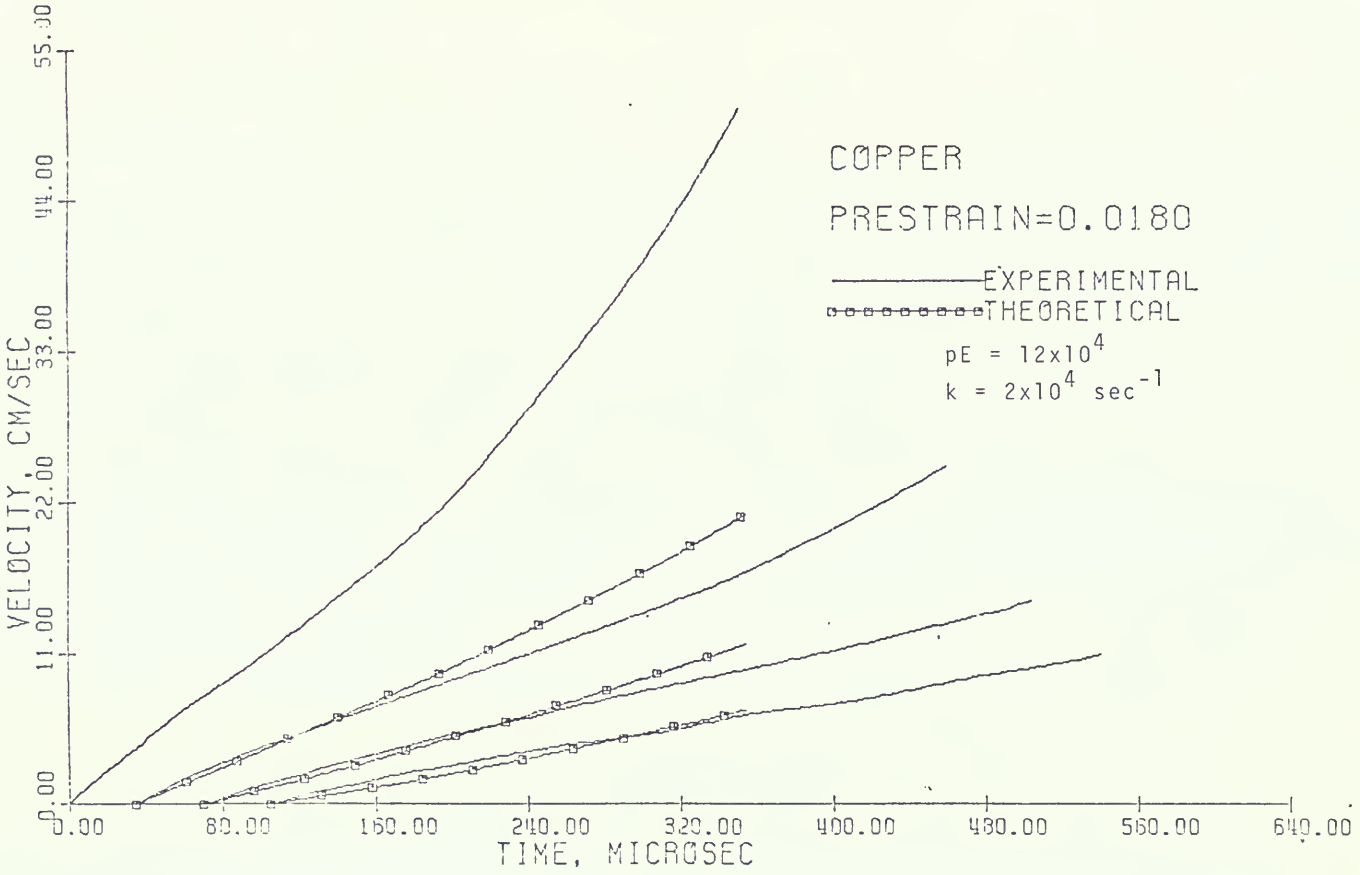

Figure 3.9 Particle Velocity Records (Copper Specimen No. 4, Prestrain 0.0180).

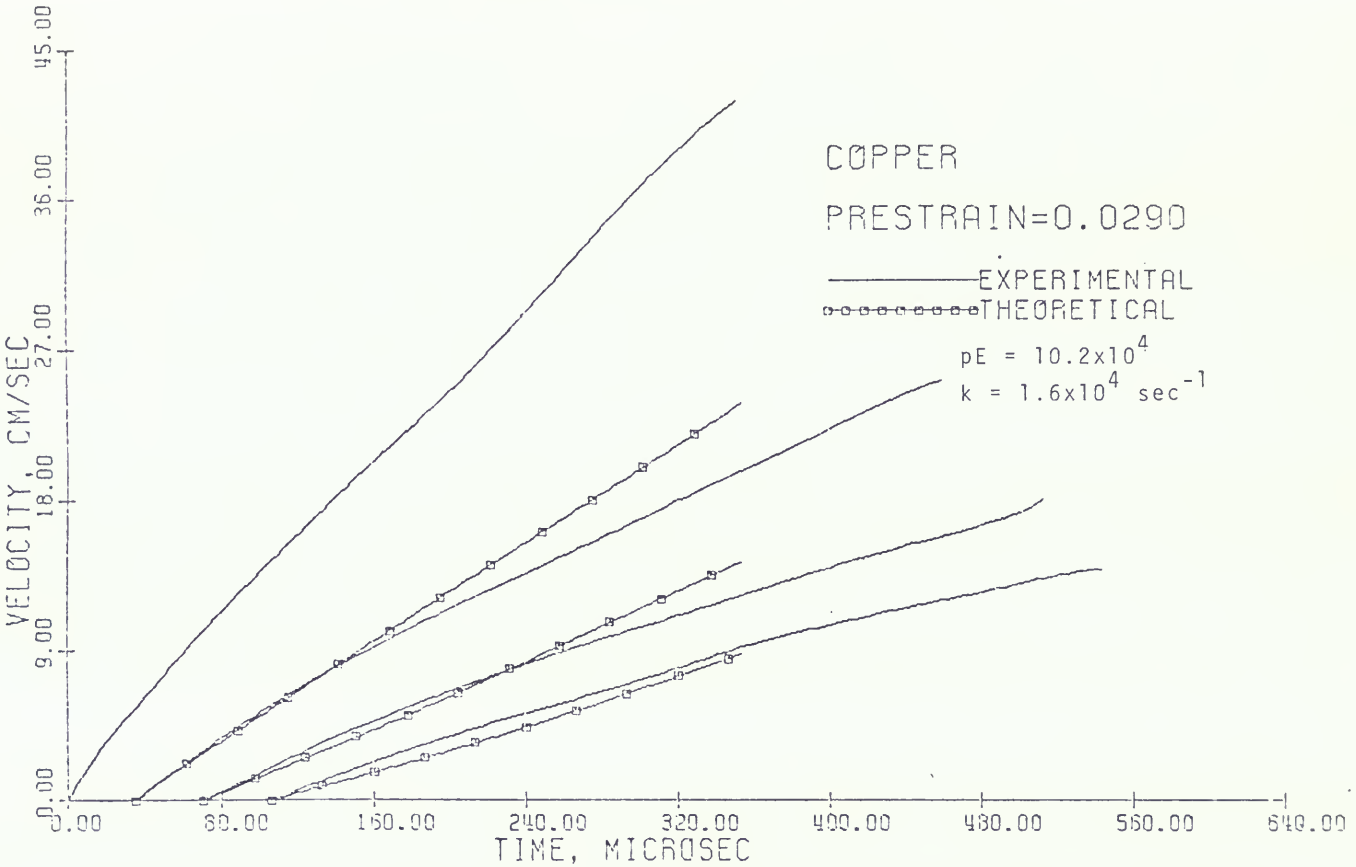

Figure 3.10 Particle Velocity Records (Copper Specimen No. 4, Prestrain 0.0290).

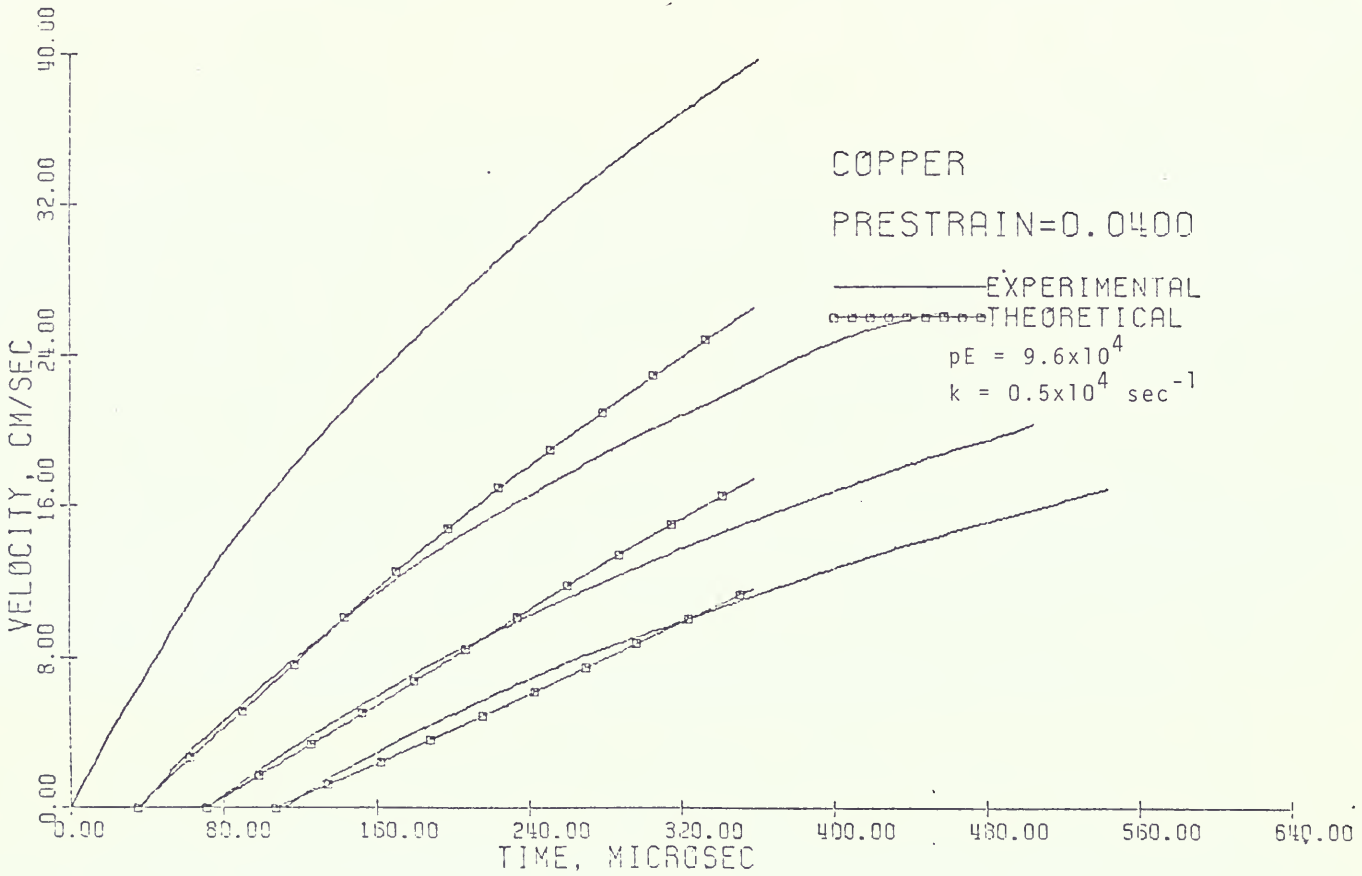

Figure 3.11 Particle Velocity Records (Copper Specimen No. 4, Prestrain 0.0400).

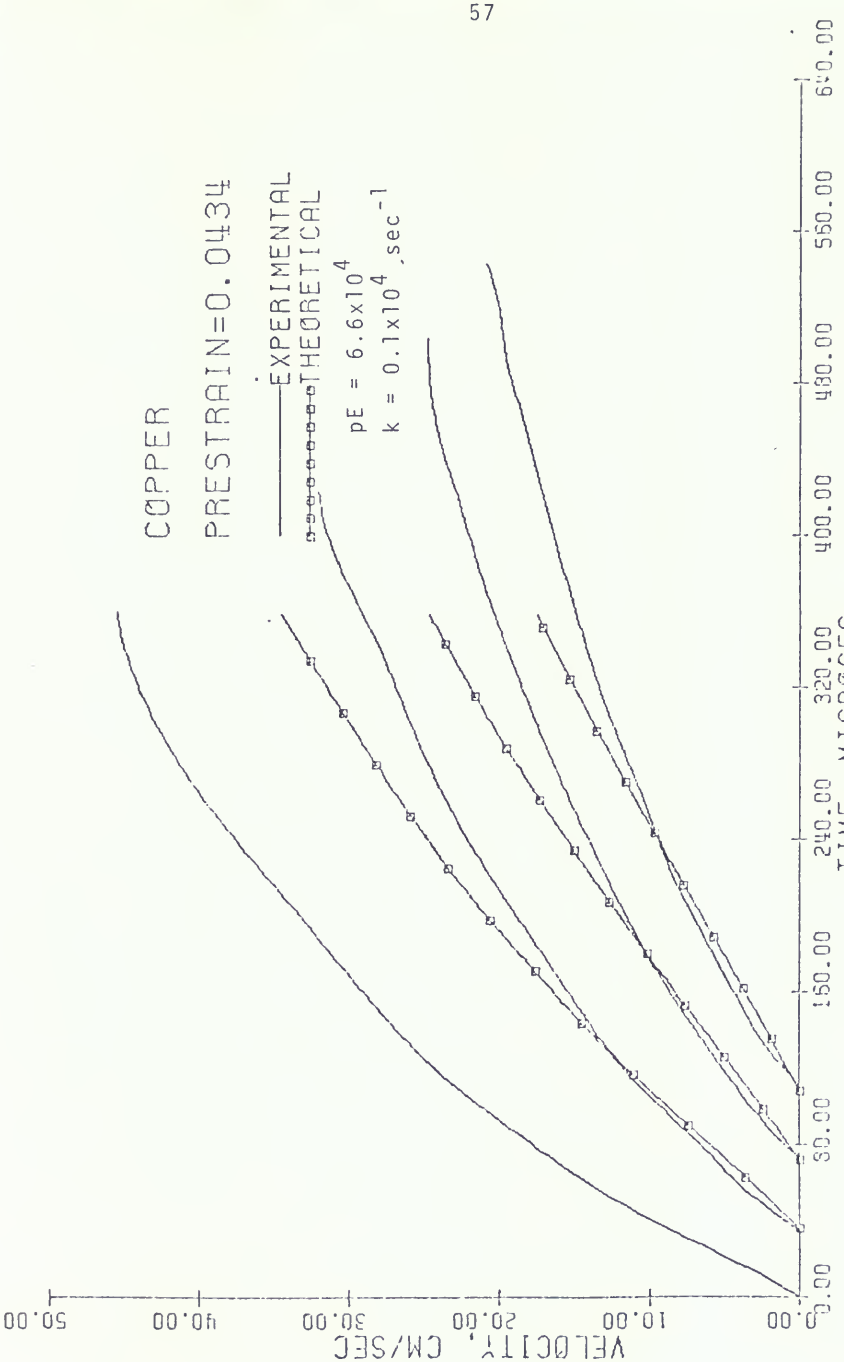

Figure 3.12 Particle Velocity Records (Copper Specimen No. 4, Prestrain 0.0434).

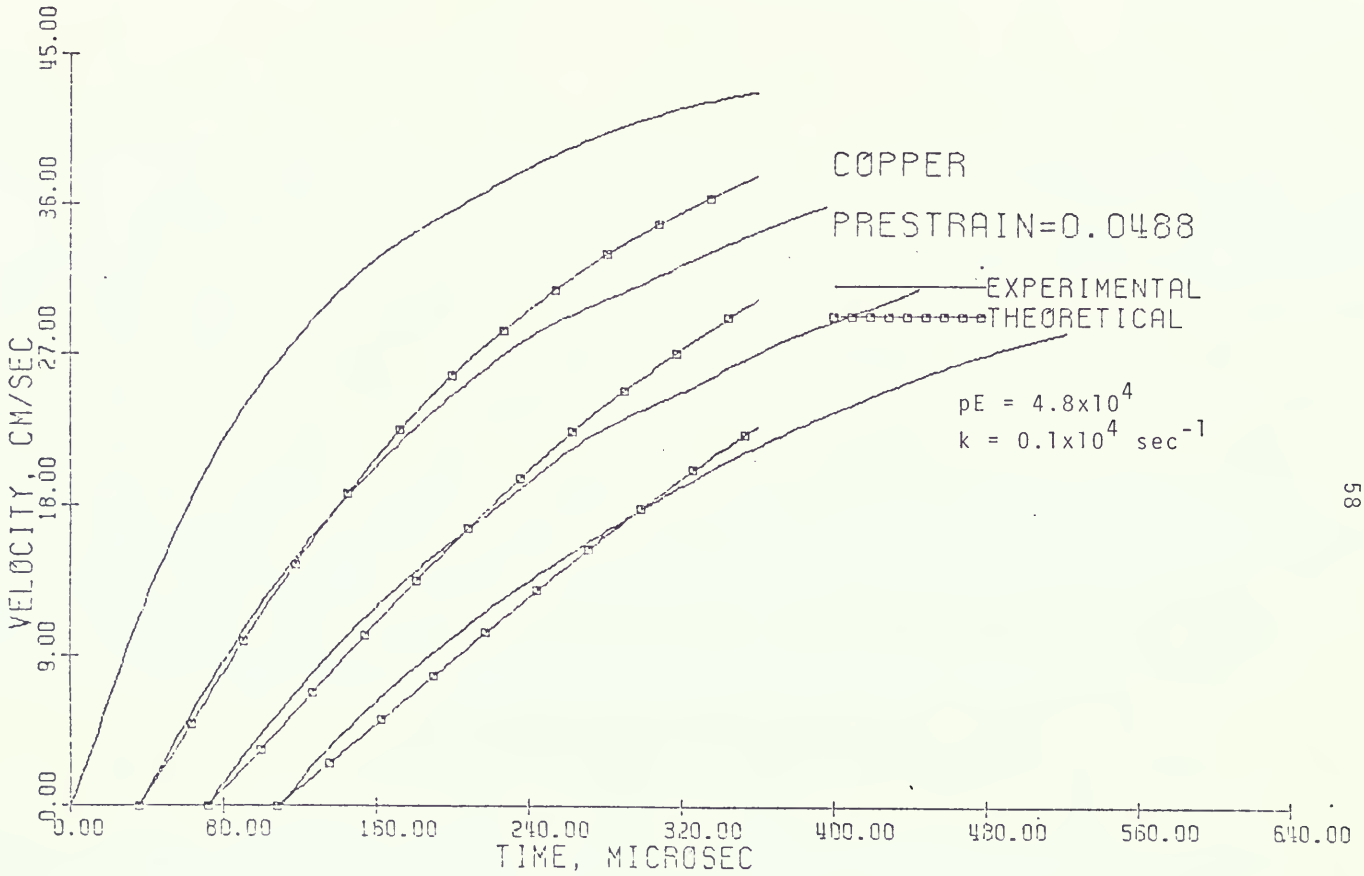

Figure 3.13 Particle Velocity Records (Copper Specimen No. 4, Prestrain 0.0488).

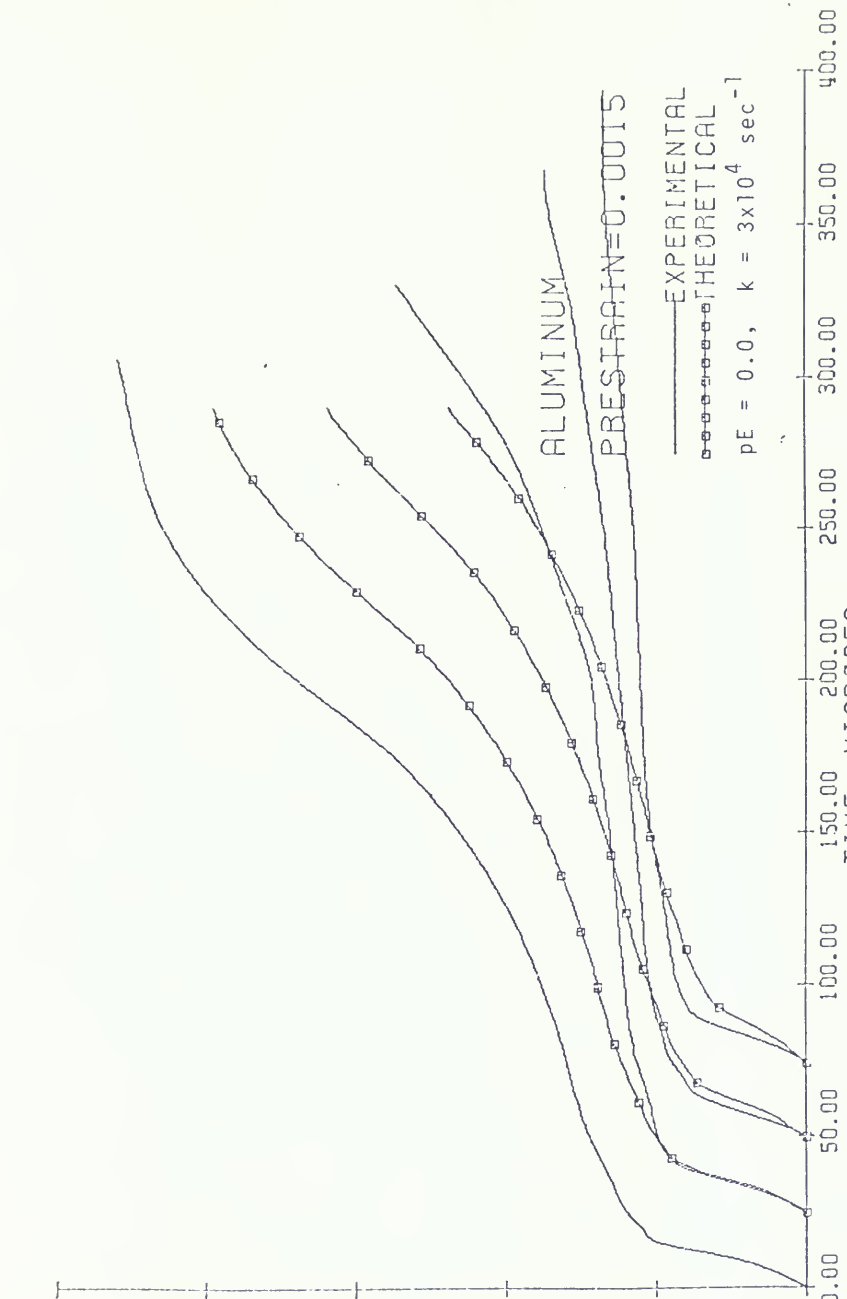

Figure 3.14 Particle Velocity Records (Aluminum Specimen No. 4, Prestrain 0.0015).

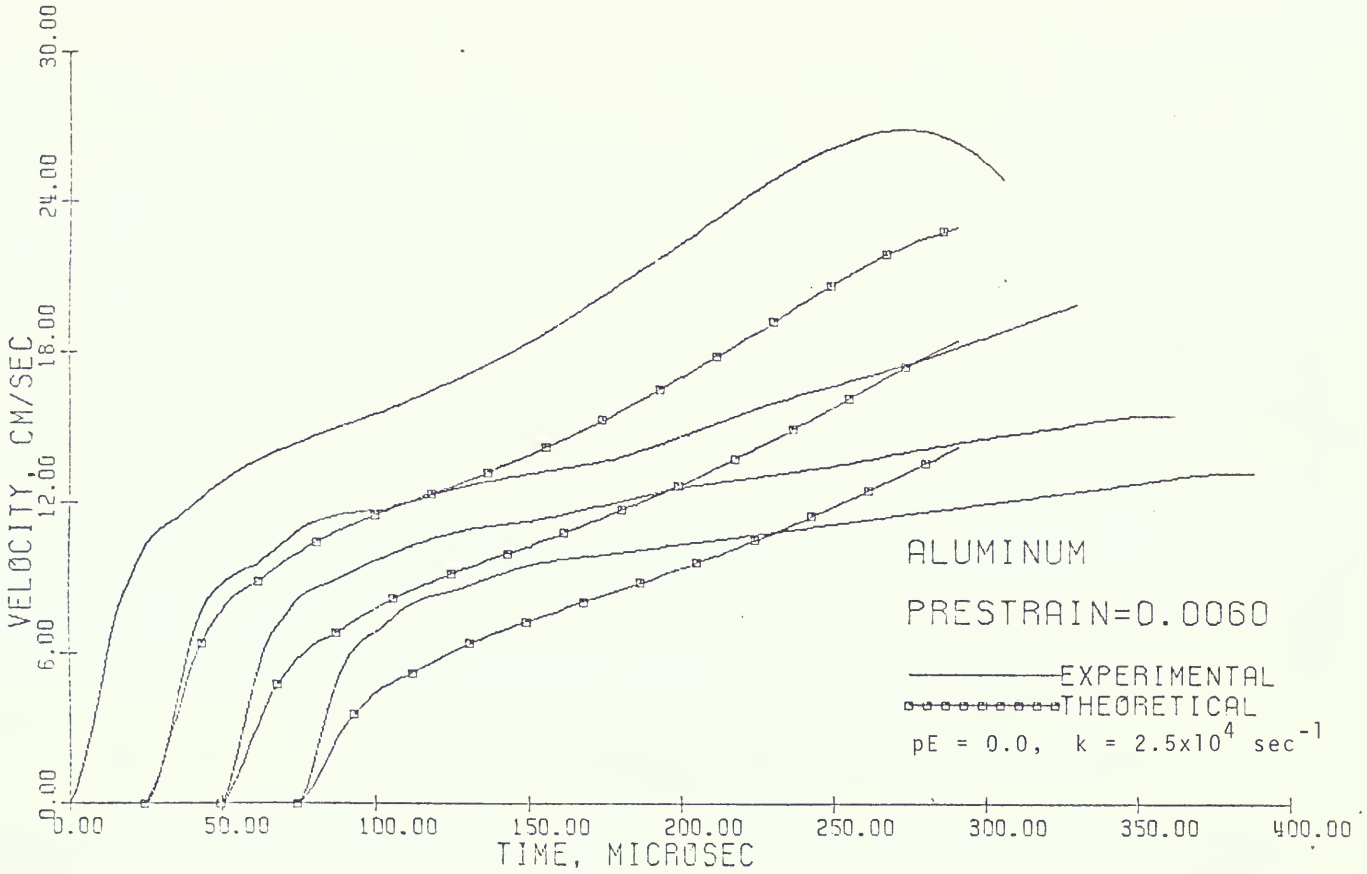

Figure 3.15 Particle Velocity Records (Aluminum Specimen No. 4, Prestrain 0.0060).

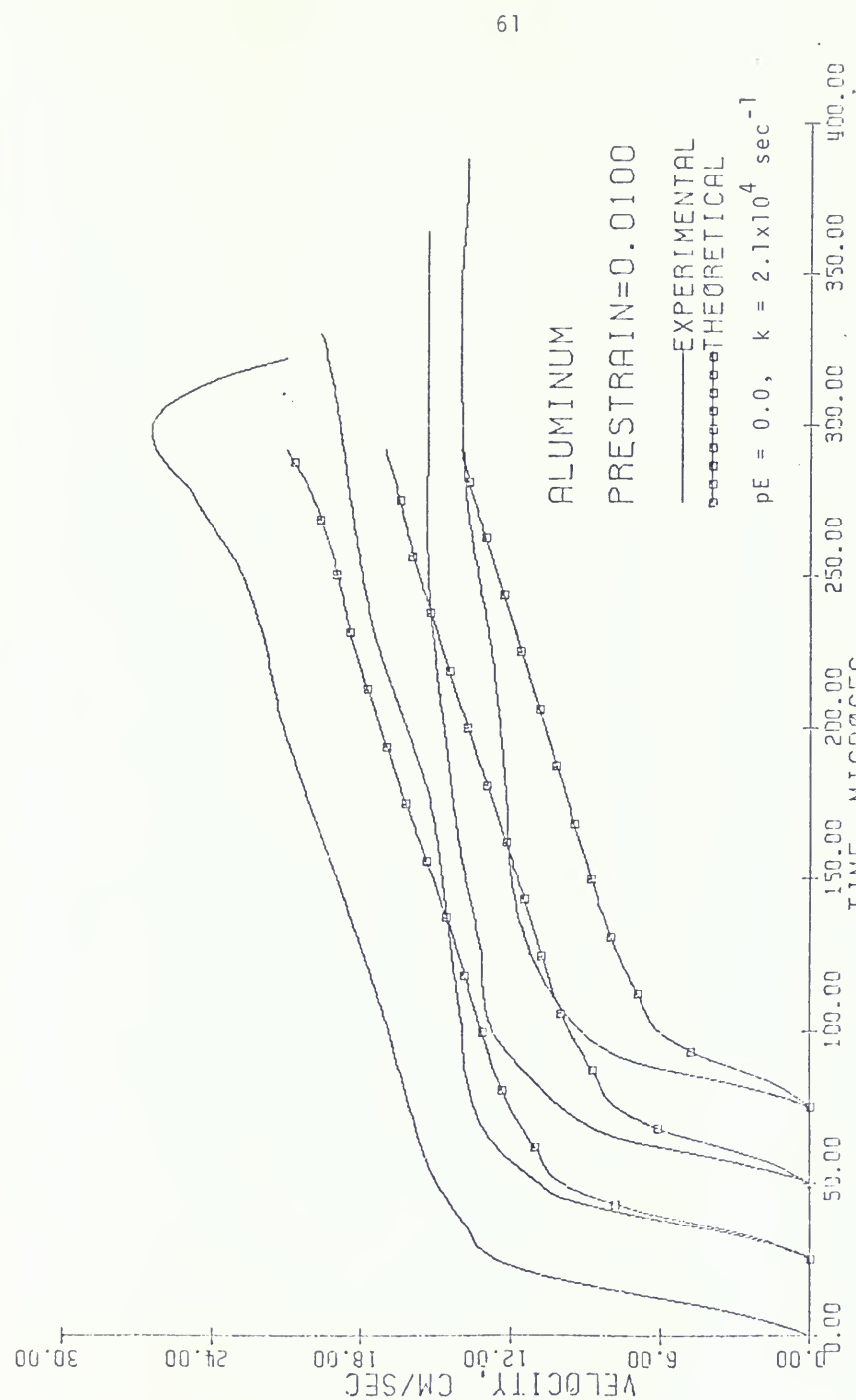

Figure 3.16 Particle Velocity Records (Aluminum Specimen No. 4, Prestrain 0.0100).

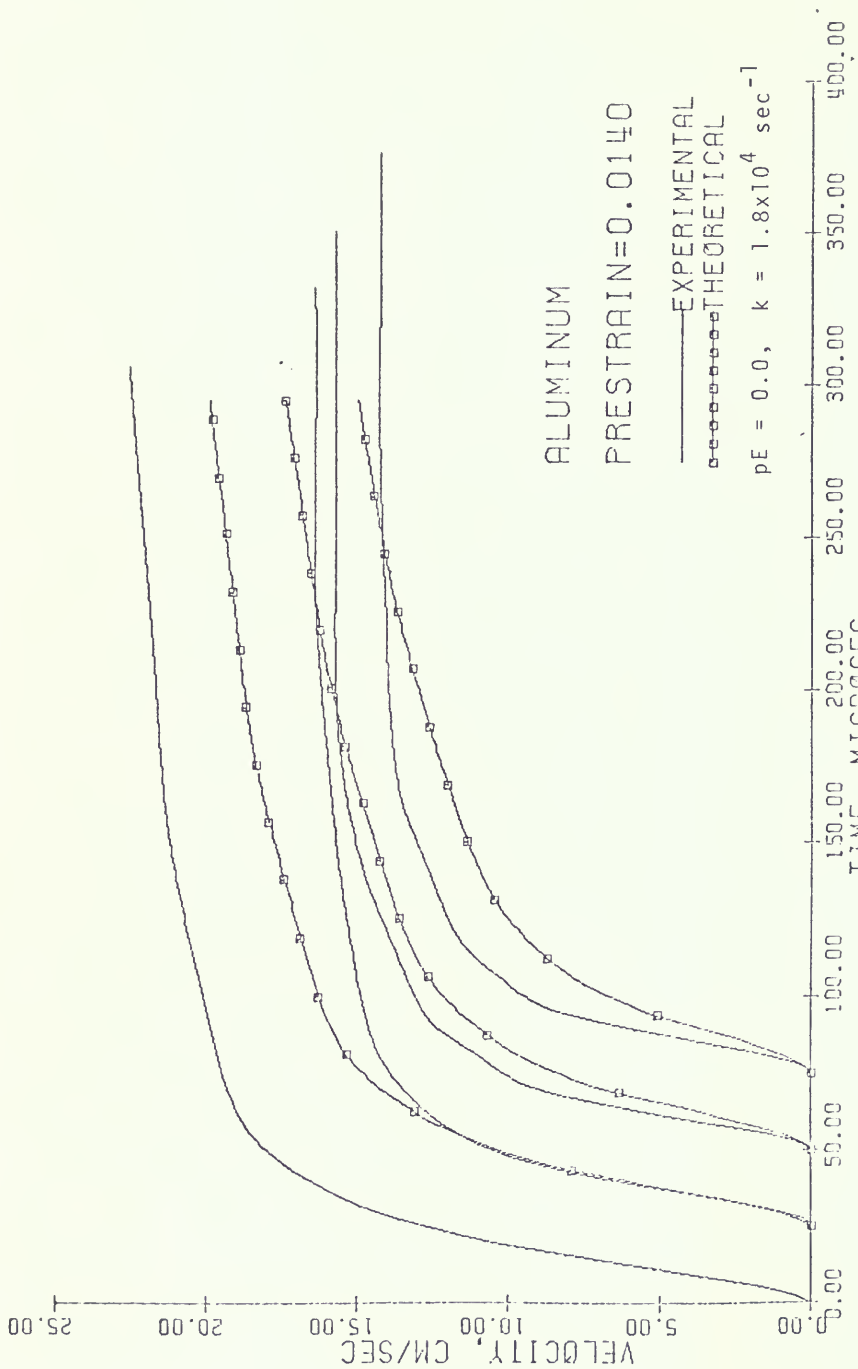

Figure 3.17 Particle Velocity Records (Aluminum Specimen No. 4, Prestrain 0.0140).

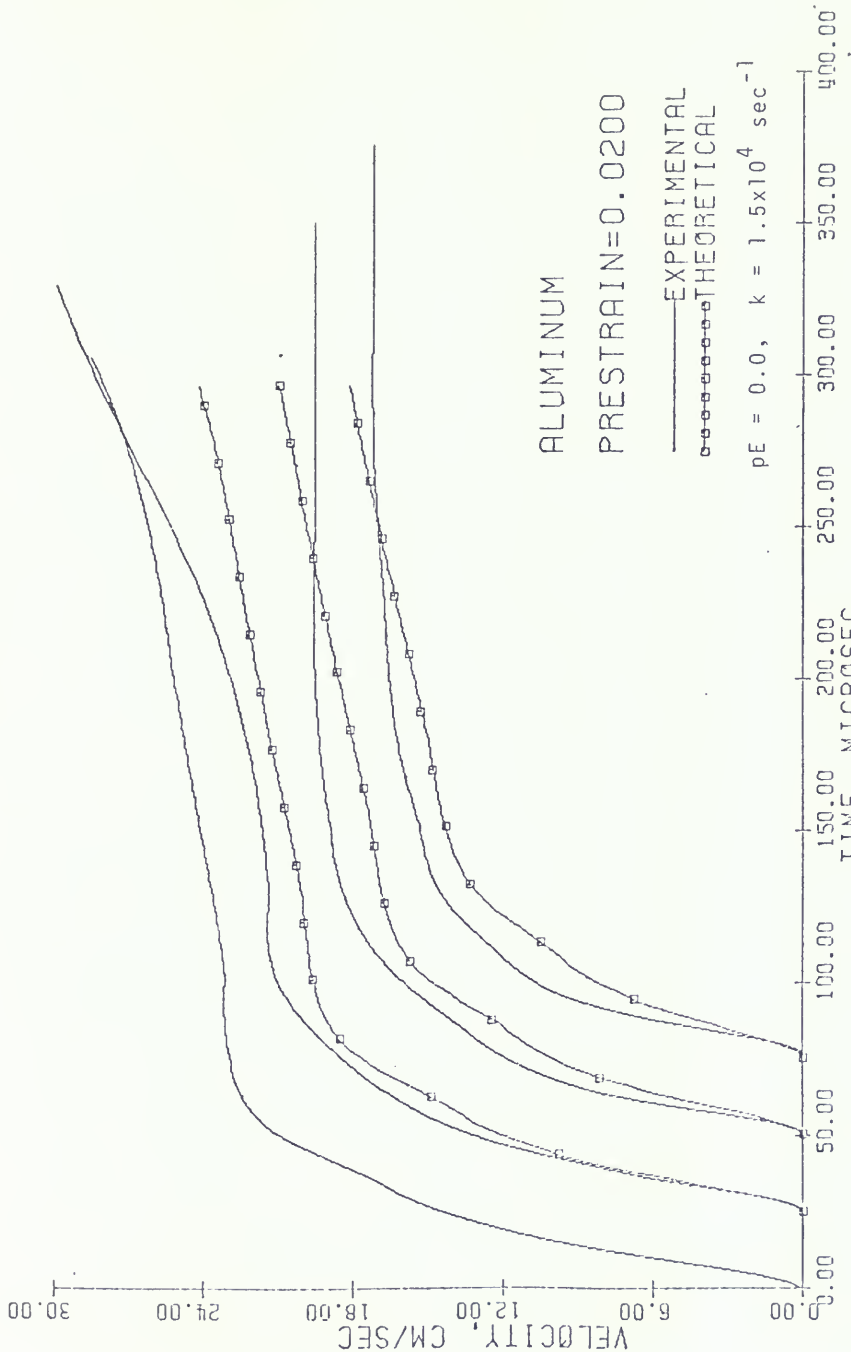

Figure 3.18 Particle Velocity Records (Aluminum Specimen No. 4, Prestrain 0.0200).

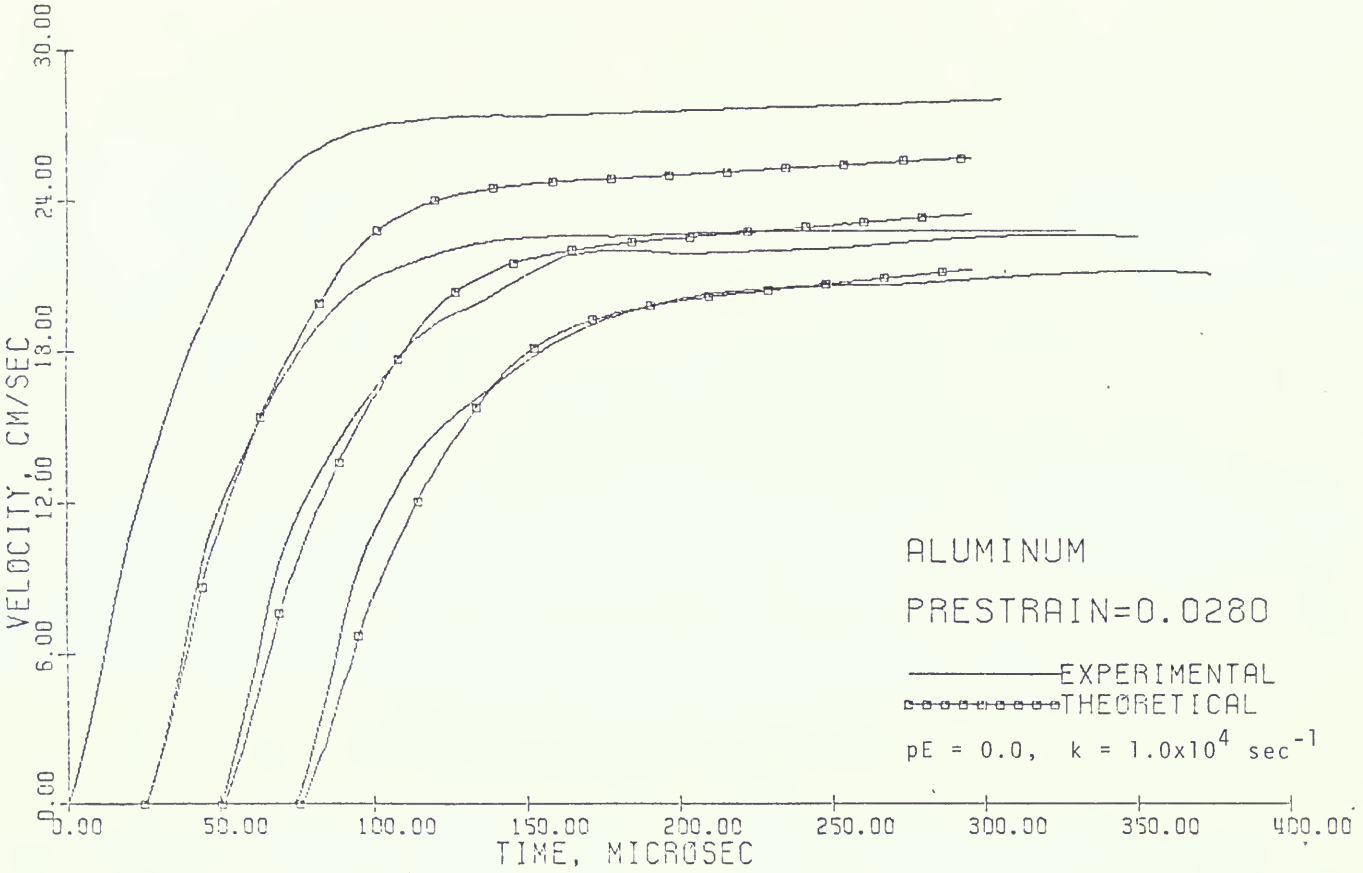

Figure 3.19 Particle Velocity Records (Aluminum Specimen No. 4, Prestrain 0.0280).

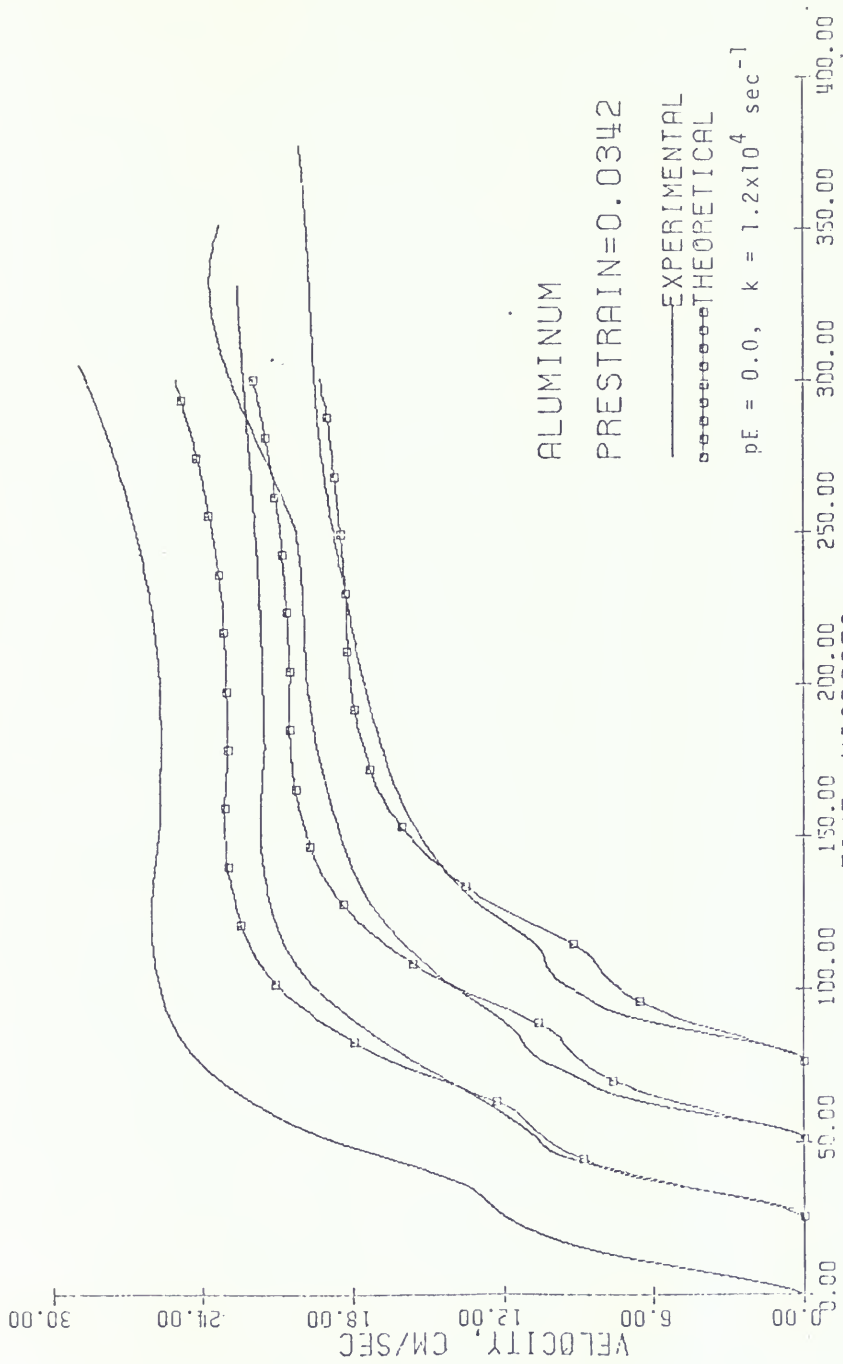

Figure 3.20 Particle Velocity Records (Aluminum Specimen No. 4, Prestrain 0.0342).

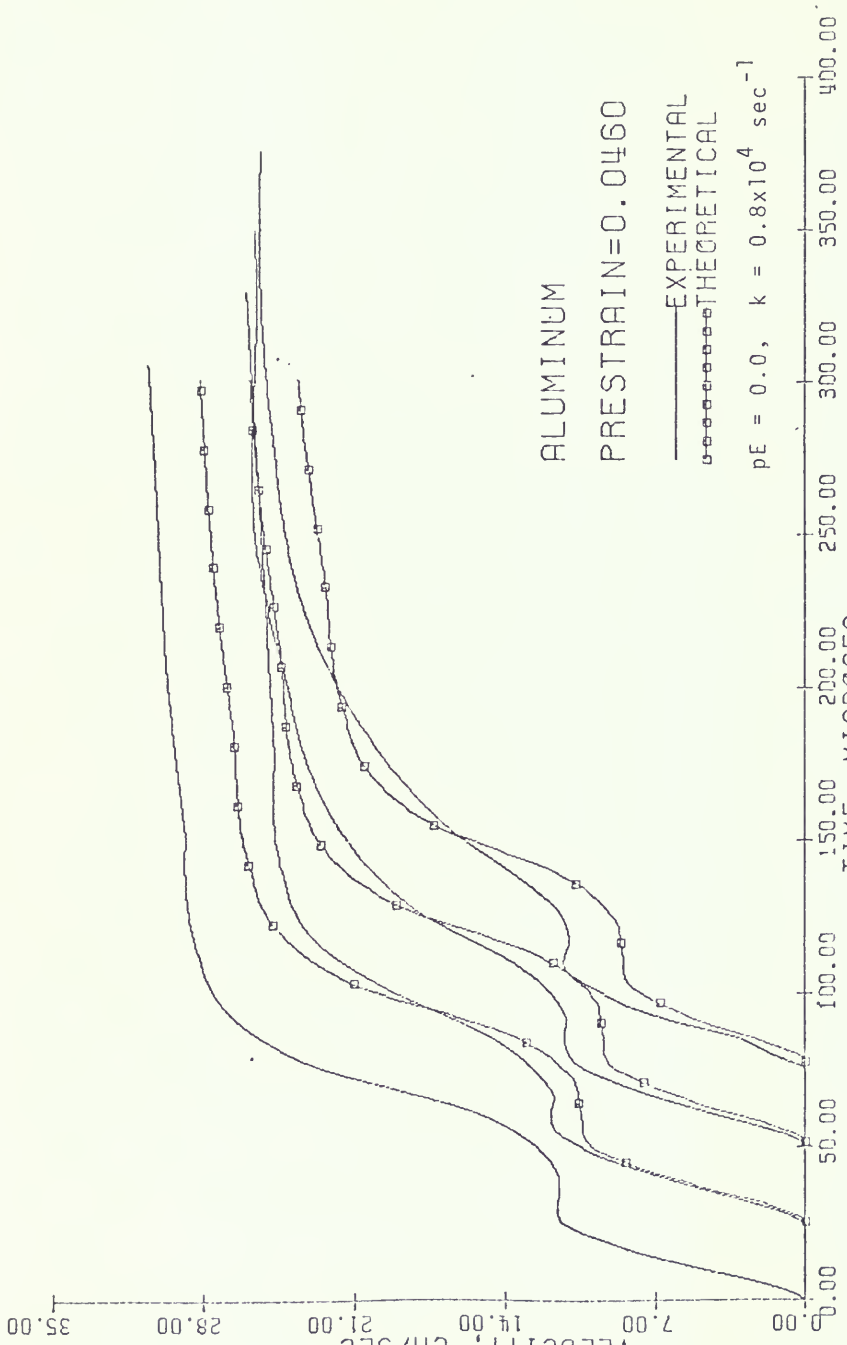

Figure 3.21 Particle Velocity Records (Aluminum Specimen No. 4, Prestrain 0.0460).

These phenomena were examined more fully by correlating parameters obtained from wave speed curve fitting with both prestrain and prestrain rate values.

3.4 Wave-Propagation Speed Curve Fitting and the Discovery of Prestrain and Prestrain Rate Dependence of the Incremental Waves

In order to use some simple parameters to characterize the family of wave-propagation speed functions, various kinds of curve fitting techniques were tried, among which the exponential function of equation (3.3) below was found to be the most adequate one. Although the two families of c(v) curves for copper and aluminum look so different in Figures 3.22 and 3.23, they could both be fitted well by this same exponential function , with different parameter values. It was found from the computer outputs that the wave-propagation speed lies between $c = c_o$ and $c = c_p$, where $c_o = \sqrt{E/\rho}$ and $c_p = \sqrt{(d\sigma/d\varepsilon)/\rho}$. (In finite wave-propagation c_p is defined as $c_p = \sqrt{(dS/de)/\rho}$. For the incremental wave the initial dimensions corresponding to true stress and strain values are the initial conditions.) The value of c_p decreases as the prestrain value is increased. The expression $\bar{c} = (c - c_p)/(c_o - c_p)$ was used as the nondimensional wave-propagation speed. $\bar{c}$ varies from 1 to 0 as c varies from c_o to c_p. The incremental velocity was also made nondimensional by dividing it by a velocity parameter v_c. The

form of the curve-fitting function was

$$\bar{c} = \exp[-(v/v_c)^n] \qquad (3.3)$$

in which v_c and n were determined from experimental data. This was done by taking the natural logarithm twice on both sides of equation (3.3), which was then reduced to a linear equation in variables $\ln[\ln(1/\bar{c})]$ and $\ln(v)$. The coefficients of this linear equation were then determined by linear regression. A simple computer program was written to do the computations for determining the values of v_c and n for all the 170 wave-propagation speed curves.

Some typical examples of the results of the curve fitting are shown in Figures 3.24 and 3.25. It can be seen that the fitted curves match very well with the experimental data. This kind of good quality of curve fitting was also true for all the other copper data and 65% of the other aluminum data. Tables 3.1 and 3.2 give the resulting values of v_c and n together with corresponding prestrain rate $\dot{e}_o$ and plastic wave speed for copper specimen No. 4 and aluminum specimen No. 4, respectively.

The parameter v_c expresses the degree of outwardness of the $\bar{c}$ curve from the origin. The larger the value of v_c is, the farther out the $\bar{c}$ curve lies. Parameter n expresses the curvature of the $\bar{c}$ curve. Since the value of n is very sensitive, the resulting value of n from curve fitting is not as reliable as is the value of v_c. This can be shown

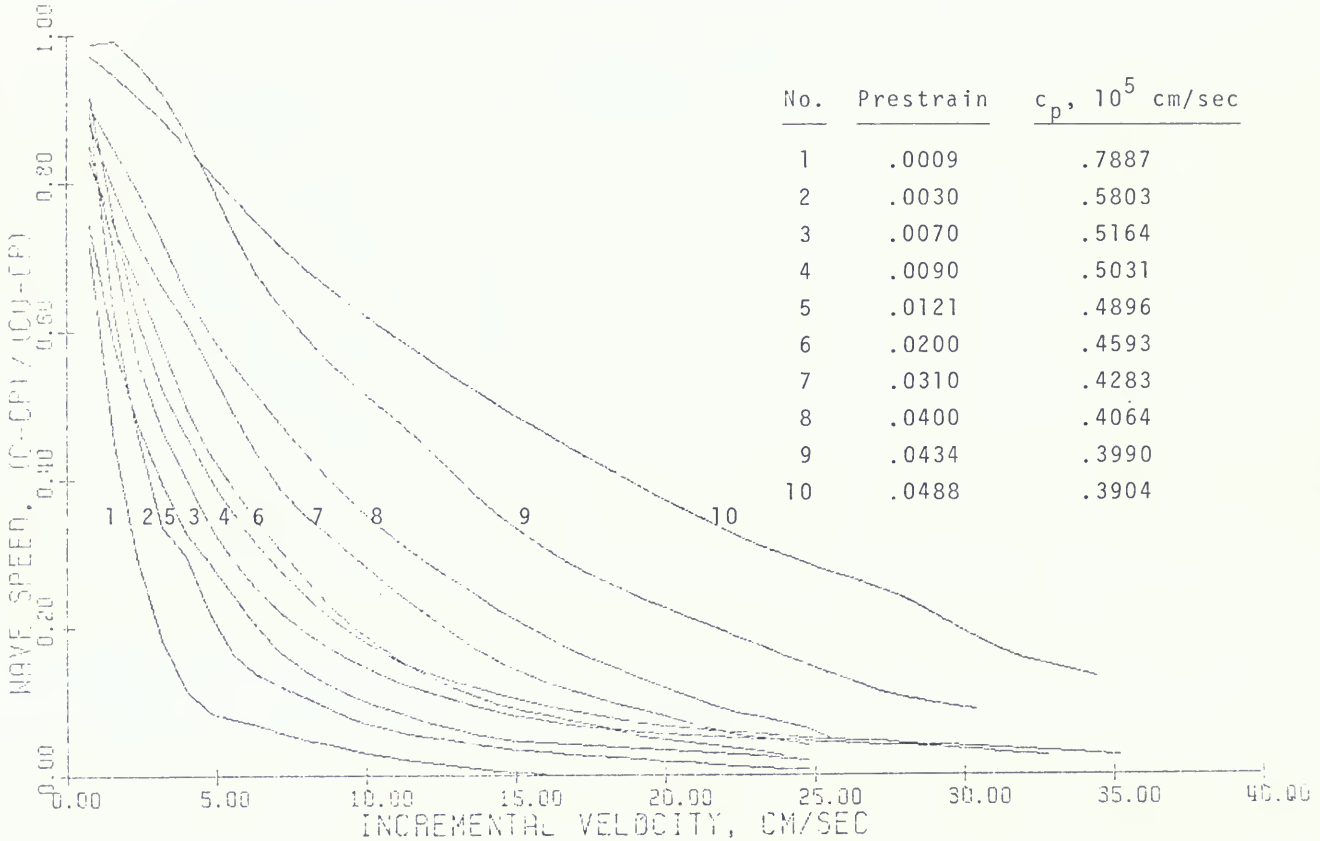

No.	Prestrain	c_p, 10^5 cm/sec
1	.0009	.7887
2	.0030	.5803
3	.0070	.5164
4	.0090	.5031
5	.0121	.4896
6	.0200	.4593
7	.0310	.4283
8	.0400	.4064
9	.0434	.3990
10	.0488	.3904

Figure 3.22 Family of Non-Dimensional Wave Speed Functions (Copper Specimen No.4).

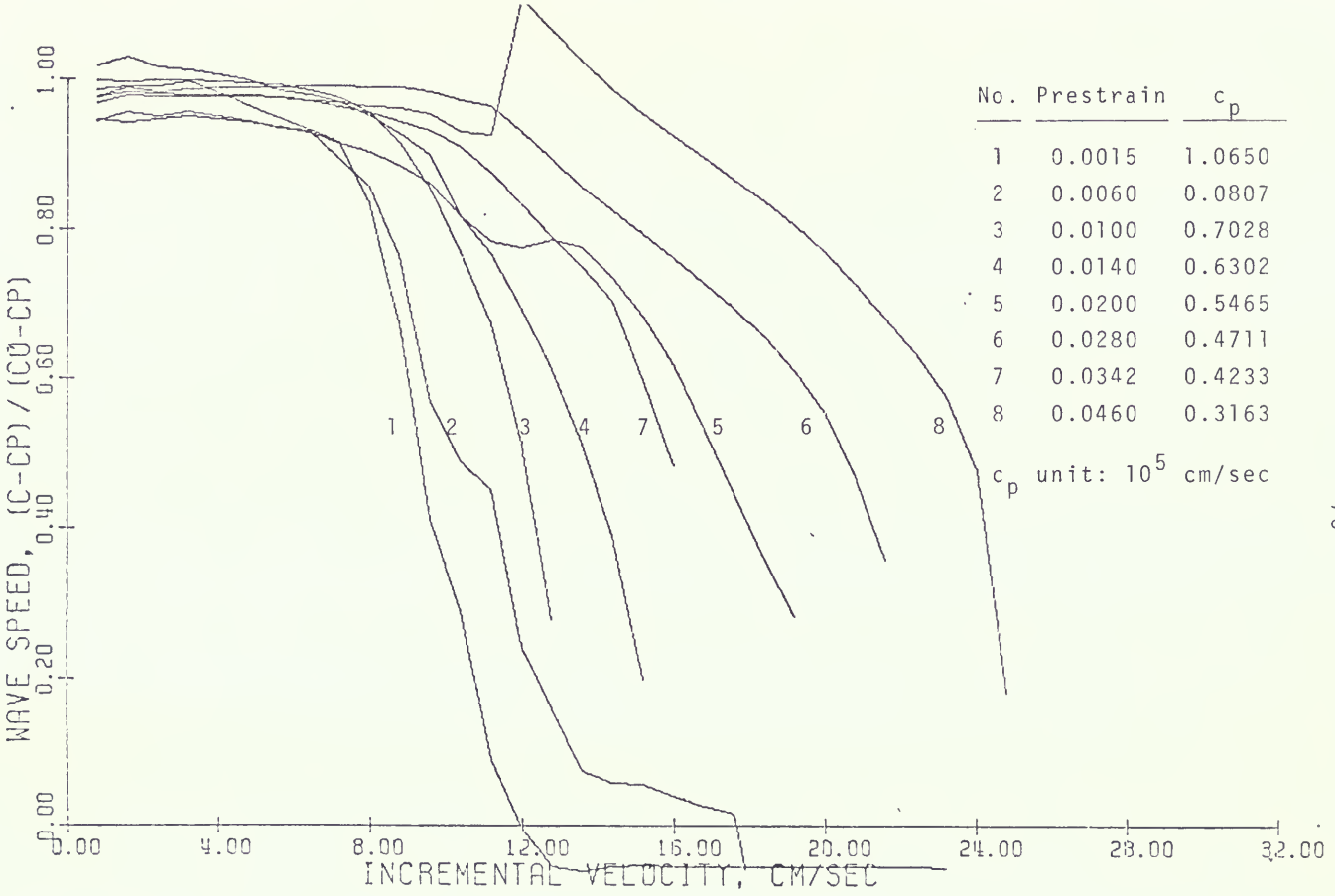

Figure 3.23 Family of Non-Dimensional Wave Speed Functions (Aluminum Specimen No. 4).

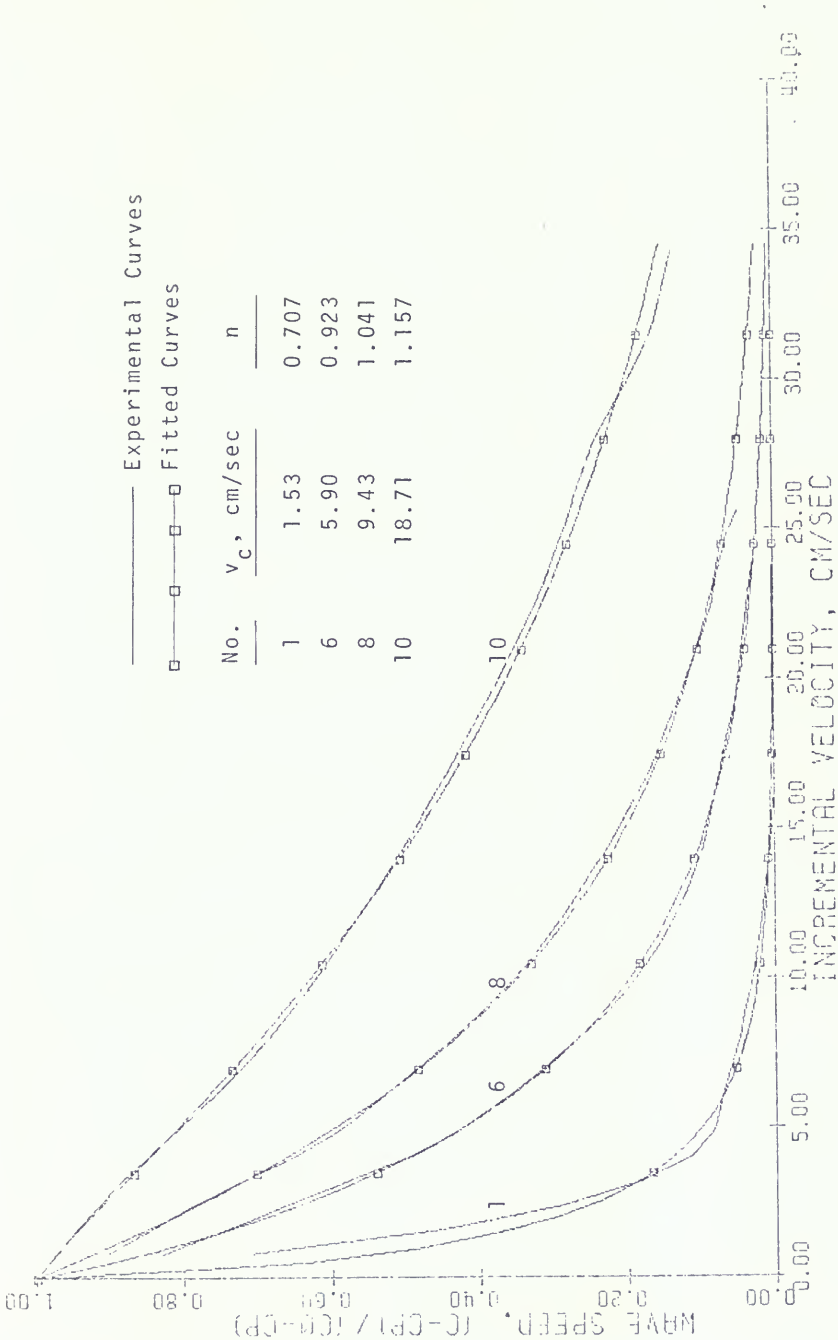

Figure 3.24 Examples of Wave-Propagation Speed Curve Fitting (Copper Specimen No.4).

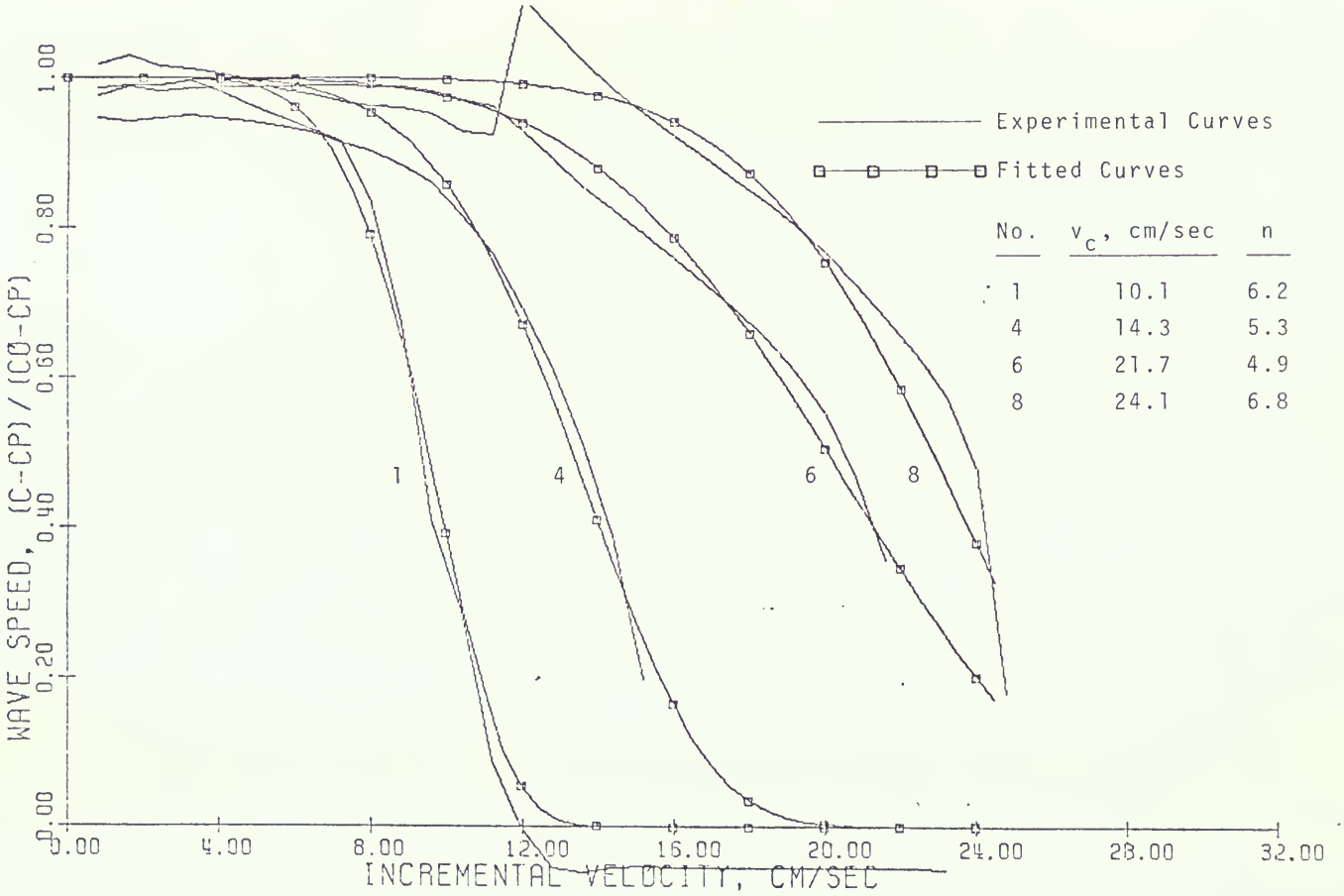

Figure 3.25 Examples of Wave-Propagation Speed Curve Fitting (Aluminum Specimen No. 4).

by taking the partial derivative of equation (3.3) with respect to n. We obtain

$$\Delta\bar{c}/\bar{c} = -[\ln(v/v_c)](v/v_c)^n \Delta n \qquad (3.4)$$

For example, if we choose n = 1.0 for copper and v/v_c = 0.8, a 10% variance in n, i.e., Δn = 0.1, will give $\Delta\bar{c}/\bar{c}$ = 1.8%. For aluminum the value of n is around 5. If v/v_c = 0.8 again and Δn = 0.5, then $\Delta\bar{c}/\bar{c}$ = 3.6%.

The values of v_c and n versus the prestrain value e_o for copper specimen No. 4 are plotted in Figures 3.26 and 3.27, respectively. At first glance the zigzag relation between v_c and prestrain e_o seems to mean that the results of wave-propagation speed contain some errors. By examining the relation carefully and correlating it with values of prestrain rate, it was found that whenever the value of $\dot{e}_o$ increased the value of v_c dropped. This phenomenon was checked on the results of three other copper specimens and five other aluminum specimens, which also showed the same character. Thus it was concluded that the character of small incremental waves propagated on the quasistatically deformed rod in the plastic region is influenced by both prestrain and prestrain rate.

At this stage, a quantitative relation among the parameter v_c and prestrain e_o and prestrain rate $\dot{e}_o$ was sought. It was found that on the e_o and $\log(\dot{e}_o)$ plane, shown in Figure 3.28, the contour lines of constant value of v_c are

close to a family of parallel straight lines. The following linear relation was assumed

$$me_o - \log_{10}(\dot{e}_o/\dot{e}_o^*) = k_1 v_c + k_2 \qquad (3.5)$$

where m is the slope of the contour lines in Figure 3.28, $\dot{e}_o^* = 10^{-5}$ sec^{-1} is an arbitrarily chosen reference value of the prestrain rate, and k_1 and k_2 are constants. Values of m, k_1 and k_2 were determined by the least square method. The left-hand side of equation (3.5) was defined as a precondition parameter $\xi = me_o - \log(\dot{e}_o/\dot{e}_o^*)$ in an attempt to express the dependence on e_o and $\dot{e}_o$ by a single parameter. The results for five aluminum and four copper specimens are listed in Table 3.3. Results of copper specimen No. 4 are also plotted in Figure 3.29.

It was found that the single parameter correlates the results for any one specimen fairly well, as in Figure 3.29. But, as can be seen from Table 3.3 the value of m in the precondition parameter definition was not constant for all specimens of one material.

It was not found possible to determine any correlation of the parameter n with the corresponding prestrain and prestrain rate values.

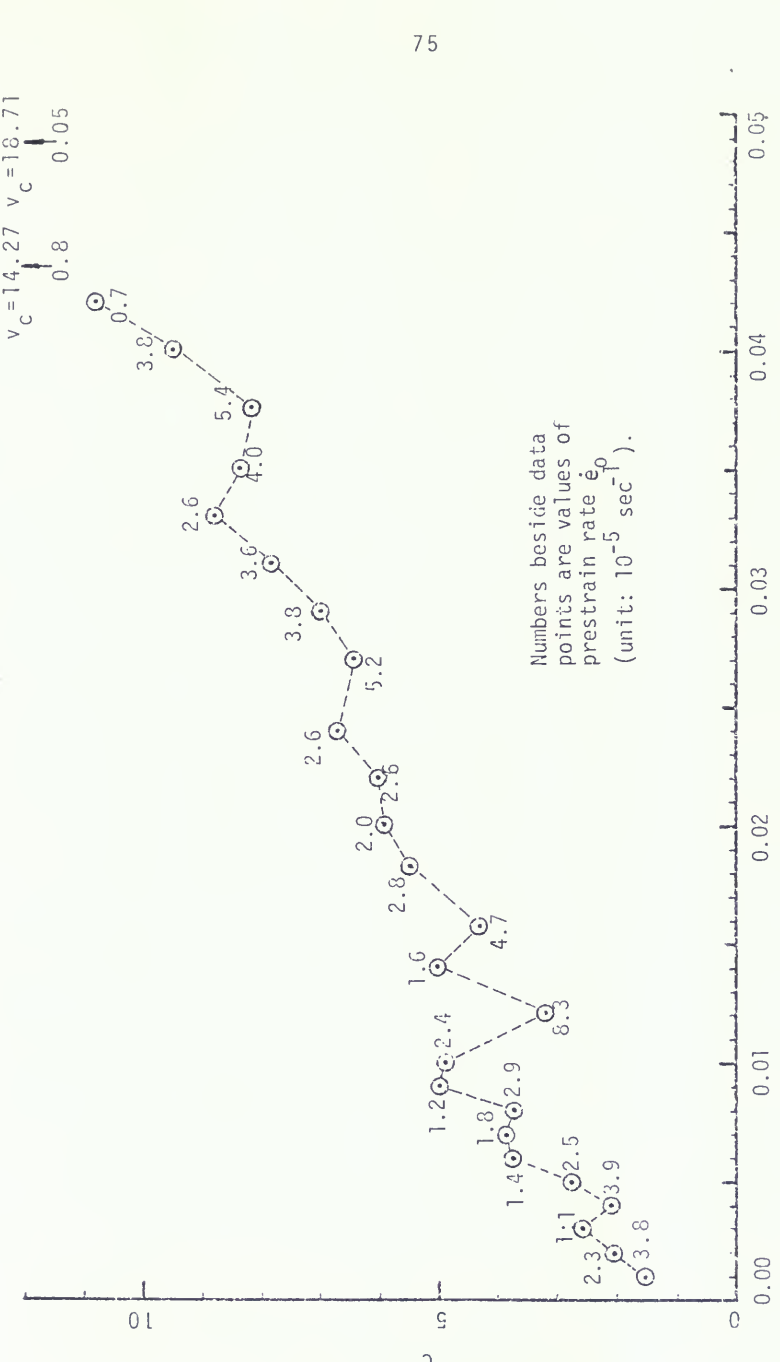

Figure 3.26 Wave Speed Parameter v_c versus Prestrain (Copper Specimen No. 4).

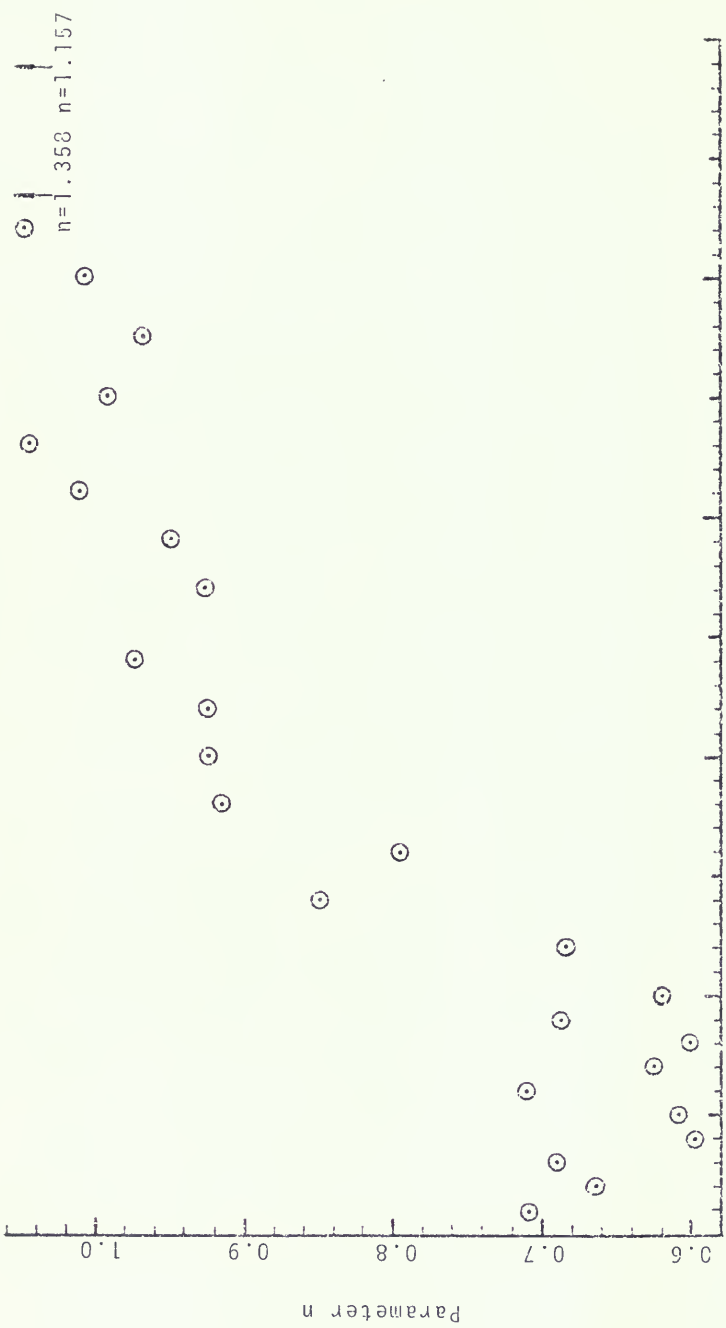

Figure 3.27 Wave Speed Parameter n versus Prestrain (Copper Specimen No. 4).

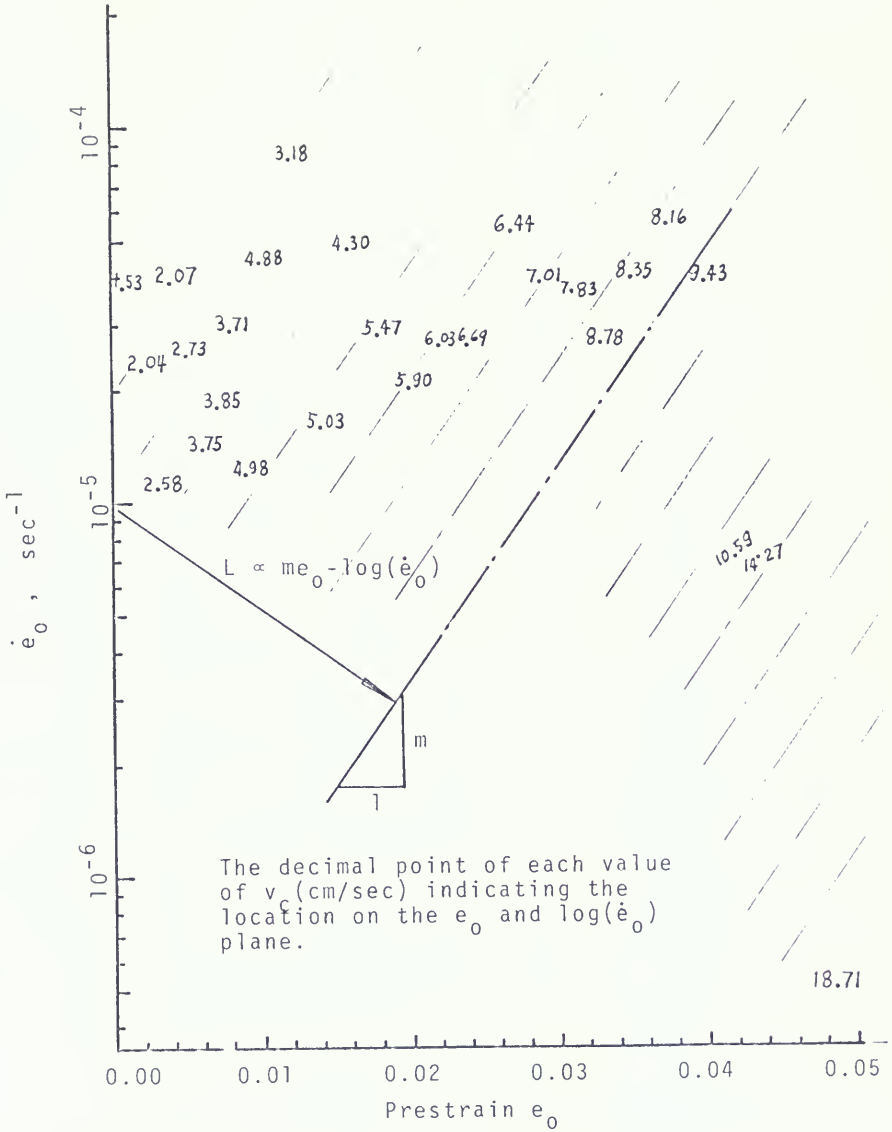

Figure 3.28 Values of v_c on the e_o and $\log(\dot{e}_o)$ Plane.

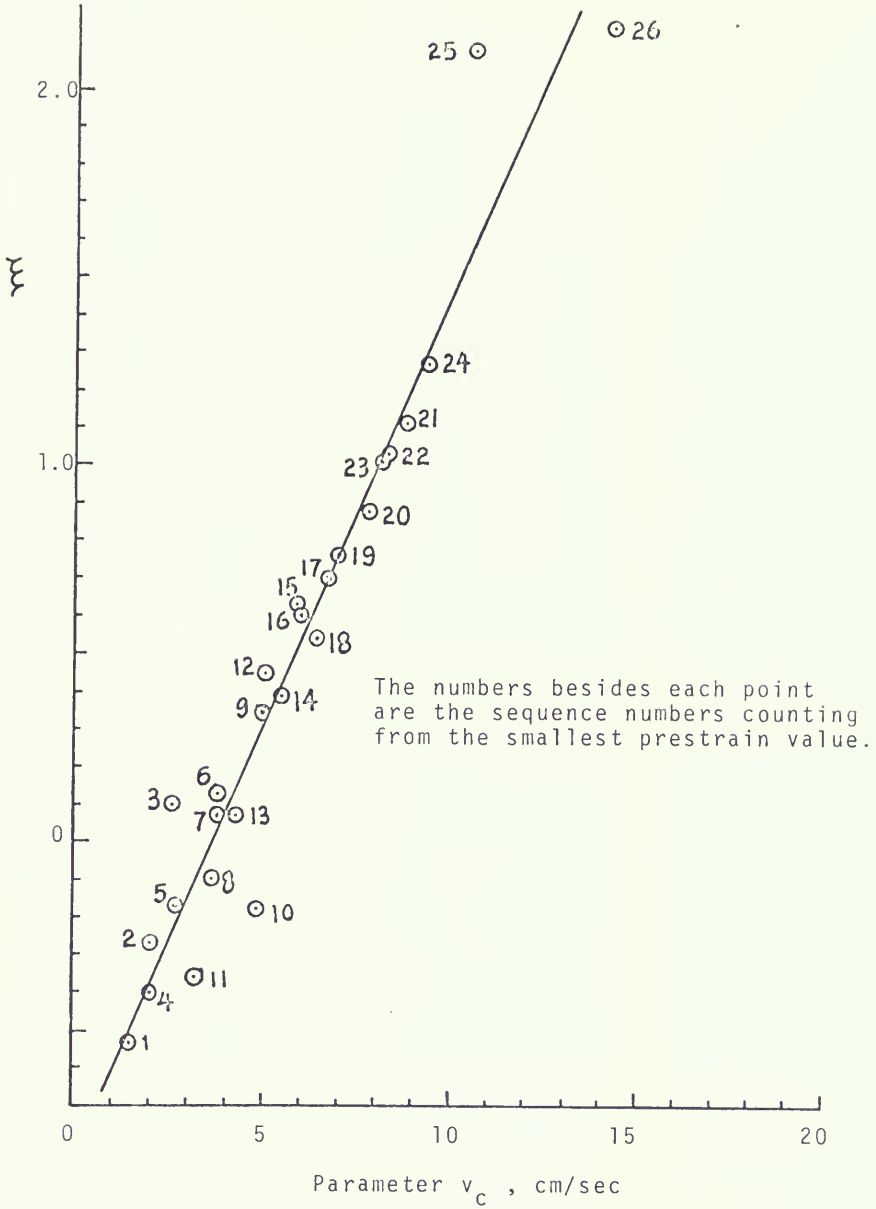

Figure 3.29 Relation Between v_c and the Precondition Parameter ξ.

Table 3.1 Values of Prestrain Rate and Wave Speed Function Parameters (Copper Specimen No.4)

e_o	$\dot{e}_o$, 10^{-5}/sec (1)*	(2)†	Ave.	v_c cm/sec	n	c_p 10^5 cm/sec
0.0009	4.02	3.51	3.8	1.53	0.707	0.7887
0.0020	2.38	2.12	2.3	2.04	0.663	0.6081
0.0030	1.12	1.07	1.1	2.58	0.688	0.5803
0.0040	3.93	3.89	3.9	2.07	0.597	0.5553
0.0050	2.55	2.50	2.5	2.73	0.606	0.5374
0.0060	1.37	1.48	1.4	3.75	0.709	0.5257
0.0070	--	1.82	1.8	3.85	0.624	0.5164
0.0080	2.59	3.09	2.9	3.71	0.600	0.5096
0.0090	1.00	1.35	1.2	4.98	0.686	0.5031
0.0100	3.67	5.15	4.4	4.88	0.619	0.4979
0.0121	7.90	8.70	8.3	3.18	0.683	0.4896
0.0140	1.17	2.03	1.6	5.03	0.847	0.4824
0.0160	4.85	4.57	4.7	4.30	0.794	0.4741
0.0180	2.42	3.12	2.8	5.47	0.914	0.4665
0.0200	1.50	2.04	2.0	5.90	0.923	0.4593
0.0220	3.00	2.24	2.5	6.03	0.923	0.4530
0.0240	2.92	2.31	2.6	6.69	0.971	0.4473
0.0270	5.53	4.87	5.2	6.44	0.925	0.4368
0.0290	3.42	4.18	3.8	7.01	0.946	0.4338
0.0310	3.42	3.74	3.6	7.83	1.007	0.4283
0.0330	2.25	2.97	2.6	8.78	1.041	0.4228
0.0350	3.93	3.98	4.0	8.35	0.988	0.4182
0.0376	5.27	5.53	5.4	8.16	0.966	0.4110
0.0400	3.09	4.41	3.8	9.43	1.041	0.4064
0.0420	0.42	1.02	0.7	10.59	1.060	0.4033
0.0434	0.42	1.16	0.8	14.27	1.358	0.3990
0.0488	0.08	0.03	0.05	18.71	1.157	0.3904

*From strain-time records.

†From load-time records.

Table 3.2 Values of Prestrain Rate and Wave Speed Function Parameters (Aluminum Specimen No.4)

e_o	$\dot{e}_o$, 10^{-5}/sec (1)*	(2)†	Ave.	v_c cm/sec	n	c_p 10^{-5} cm/sec
0.0015	--	2.6	2.6	10.1	6.2	1.0650
0.0030	--	2.4	2.4	9.7	7.8	0.9345
0.0060	17.2	16.0	16.6	11.4	5.1	0.8087
0.0080	5.2	6.2	5.7	11.4	5.8	0.7522
0.0100	4.0	5.2	4.6	12.6	6.4	0.7028
0.0120	3.6	4.4	4.0	14.7	5.5	0.6606
0.0140	2.4	4.1	3.3	14.3	5.3	0.6302
0.0160	9.8	5.1	7.5	14.6	5.6	0.6013
0.0200	--	0.2	0.2	17.5	4.6	0.5465
0.0250	4.8	5.7	5.3	16.9	7.4	0.5023
0.0280	3.7	4.1	3.9	21.7	4.8	0.4711
0.0300	1.6	1.8	1.7	22.8	4.0	0.4563
0.0342	--	14.2	14.2	16.4	5.2	0.4243
0.0400	--	5.9	5.9	23.8	3.6	0.3835
0.0460	--	3.5	3.5	24.1	6.8	0.3163

*From Strain-time records.

†From load-time records.

Table 3.3 Parameters for Functional Representation Giving v_c in Terms of e_o and $\dot{e}_o$.

Specimen No.	m	K_1(sec/cm)	K_2	Data Numbers
Aluminum - 1	20.8	0.11	-2.63	6
3	11.4	0.34	-0.91	14
4	48.4	0.16	-2.15	15
6	85.8	0.25	-3.39	13
7	34.2	0.08	-1.42	12
Copper - 1	96.3	0.44	-1.58	6
2	43.2	0.21	-0.72	22
3	114.8	0.61	-1.34	21
4	46.4	0.23	-0.85	27

CHAPTER 4

INTERPRETATION OF EXPERIMENTAL RESULTS BY VARIOUS THEORIES

4.1 Equation of Motion and Compatibility Condition for Incremental Waves of Small Amplitude

The governing equations for one-dimensional longitudinal wave propagation in a bar are derived under two general assumptions: (1) plane cross sections remain plane and (2) lateral inertia effects are negligible. It appears that both assumptions are fulfilled in the present experimental arrangement for the incremental wave considered. That the plane cross sections remain plane can be verified directly from the experimental results for the elastic wave shown in Figure 2.5 of Section 2.3. The strain-gage output indicates response from the surface while the velocity transducer indicates average response across the diameter of the cross section. The identity in these two signals verifies that the longitudinal particle velocity is uniform over a given transverse plane. Lateral inertia effects have been shown to be negligible after a wave has propagated a distance of one diameter from the impact location [see Bell (1966), De Vault (1965)]. In the present case, the first gage station was located 15 cm or 15 diameters from the impact collar attached on the rod. This first gage's output was used as the

boundary condition. Therefore the effects of lateral inertia are negligible in the region following the first gage station.

Lagrangian coordinates based on the initial dimensions of each prestrained configuration are used for describing the small incremental waves generated in that prestrained configuration. The coordinate $x = 0$ is chosen as the position of the first gage station at the instant when the leading edge of the incremental wave reaches the first gage station. The distance between adjacent gages at this time ($t = 0$) is equal to $12.7(1 + e_0)$ cm, where e_0 is the value of nominal prestrain. Let $u(x,t)$ be the displacement at time t of the cross section that was at position x at $t = 0$. Then

$$\varepsilon = \frac{\partial u}{\partial x} \tag{4.1}$$

$$v = \frac{\partial u}{\partial t} \tag{4.2}$$

where ε is the incremental strain and v is the incremental particle velocity at the section under consideration. In this chapter the symbols σ, ε and v will be used to represent the incremental quantities of stress, strain and velocity. Tensile incremental stress and strain are reckoned positive. Displacement and particle velocity in the positive x-direction are reckoned positive. Therefore in the present case, a tensile incremental wave is accompanied by

negative particle velocity. From equations (4.1), (4.2) the compatibility condition can be obtained as

$$\frac{\partial \varepsilon}{\partial t} = \frac{\partial v}{\partial x} \tag{4.3}$$

The equation of motion for an element of the bar can be derived from the impulse-momentum principle as

$$\frac{\partial \sigma}{\partial x} = \rho \frac{\partial v}{\partial t} \tag{4.4}$$

The material density ρ is assumed to be constant and independent of the prestrain value.

4.2 Boundary and Initial Conditions

The boundary condition for the theoretical solutions considered in this chapter was taken from the experimental particle velocity data of the first gage station. According to the sign convention mentioned in Section 4.1 the value of the velocity should be negative in the theoretical computations.

The initial conditions for the incremental stress, strain and velocity are

$$\sigma = \varepsilon = v = 0 \qquad \text{for} \quad t = o,\ x \geq 0 \tag{4.5}$$

These initial conditions are appropriate since in the duration of 10^{-4} sec (more than the time needed for the

incremental wave's leading edge to travel through the four gage stations) the prestress and prestrain of the quasistatic loading at a strain rate of the order of 10^{-5} sec^{-1} can be considered constant and the initial particle velocity can be considered zero.

4.3 Strain-Rate-Independent Theory

From the experimental results of Section 3.3, the wave-propagation speed for a given level of particle velocity is a constant value along the propagation distance through the four gage stations, as would be predicted by the simple wave solution of the one-dimensional strain-rate-independent theory. An exception occurs in the vicinity of the plateau in the particle velocity records for aluminum. Since the curves do not approach the same particle velocity plateau, it is apparent that no strain plateau is approached in the time of the experimental record. A very complete account of the rate-independent theory for finite amplitude plastic wave propagation is included in Cristescu (1967). In this section, the basic analytical method of the strain-rate-independent theory will be applied similarly for incremental waves by assuming that there exists a unique dynamic incremental stress-strain relation

$$\sigma = h(\varepsilon) \tag{4.6}$$

for a given incremental wave at a certain prestrain value. The dynamic response function is further assumed to be single-valued and to satisfy the conditions $dh/d\varepsilon \geq 0$ and $d^2h/d\varepsilon^2 \leq 0$. The present problem is of an inverse type, i.e., to find the function $h(\varepsilon)$ from the experimental data of the particle velocity.

Introducing equation (4.6) into (4.4) transforms the equation of motion to

$$\frac{\partial v}{\partial t} = \frac{1}{\rho} \frac{dh}{d\varepsilon} \frac{\partial \varepsilon}{\partial x} \tag{4.7}$$

Equation (4.7) and the compatibility equation (4.3) form a system of first order quasilinear partial differential equations. The characteristics are given by

$$\frac{dx}{dt} = \pm c(\varepsilon) \tag{4.8}$$

where

$$c(\varepsilon) = \left[\frac{1}{\rho} \frac{dh}{d\varepsilon}\right]^{1/2} \tag{4.9}$$

The differential relations satisfied along the characteristics are

$$dv = \pm c(\varepsilon)\, d\varepsilon \tag{4.10}$$

The upper and lower signs in equations (4.8) and (4.10) correspond to each other. It can be shown that the initial constant state of initial condition (4.5) gives a simple

wave solution. The characteristics of positive slope are a family of straight lines, and σ, ε, and v are constant values along each positive characteristic. The differential relation (4.10) becomes

$$dv = - c(\varepsilon)\, d\varepsilon \tag{4.11}$$

where the differentiation can be taken along any direction in the simple wave domain.

The incremental wave-propagation speed as a function of particle velocity was obtained from experimental data. The incremental response function $h(\varepsilon)$ can then be obtained from it, as follows. Combining (4.9) and (4.11) yields

$$d\sigma = - \rho c\, dv \tag{4.12}$$

Integrating (4.11) and (4.12), we obtain

$$\varepsilon(v_i) = - \int_0^{v_i} dv/c(v) \tag{4.13}$$

and

$$\sigma(v_i) = - \int_0^{v_i} \rho c(v)\, dv \tag{4.14}$$

If the integration in both equations (4.13) and (4.14) can be carried out explicity, then a closed form relation between σ and ε is obtained. Otherwise, the one-to-one correspondence between σ and ε can be obtained by integrating

(4.13) and (4.14) numerically with v_i increased by increment Δv at each step.

The fitted equation of wave-propagation speed, equation (3.3), can be rewritten as

$$c(v) = c_p + (c_o - c_p) \exp[-(v/v_c)^n] \qquad (4.15)$$

where values of c_p, v_c and n, constants at each prestrain, were given in Tables 3.1 and 3.2 for copper specimen No. 4 and aluminum specimen No. 4, respectively.

The integration was carried out by using a recursion formula. From equations (4.13) and (4.14), the numerical schemes are simply

$$\varepsilon_{i+1} = \varepsilon(v_{i+1}) = \varepsilon_i + \Delta v/c(\bar{v}_{i+1}) \qquad (4.16)$$

$$\sigma_{i+1} = \sigma(v_{i+1}) = \sigma_i + \rho c(\bar{v}_{i+1})\, \Delta v \qquad (4.17)$$

$$i = 1, 2, \ldots$$

where $\Delta v = |v_{i+1}| - |v_i|$, $\bar{v}_{i+1} = \frac{1}{2}(v_i + v_{i+1})$, $\sigma_1 = \varepsilon_1 = 0$, $v_i = (i-1)\,\Delta v$. (Note that the value of v is negative, $d\varepsilon = -dv/c = d|v|/c$, etc.).

In practice $\Delta v = 0.1$ cm/sec was used and the computation was carried out to $v = 40$ cm/sec. Convergence was checked by comparing with results obtained from $\Delta v = 0.2$ cm/sec; differences in the computed values of σ and ε at $v = 40$ cm/sec were less than 0.001%. Figures 4.1 and 4.2 show some examples of the incremental stress-strain curves at various

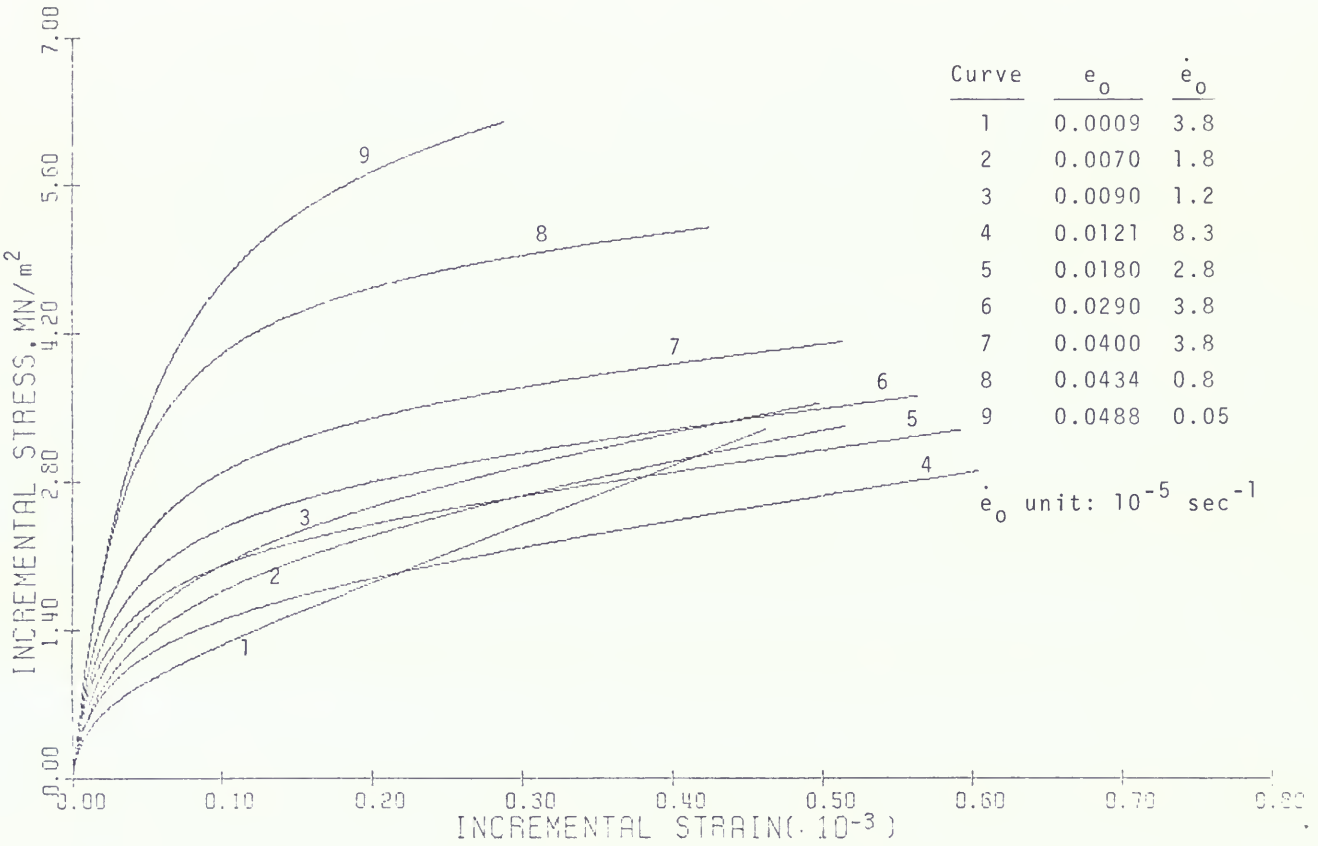

Figure 4.1 Dynamic Incremental Stress-Strain Curves (Copper Specimen No. 4).

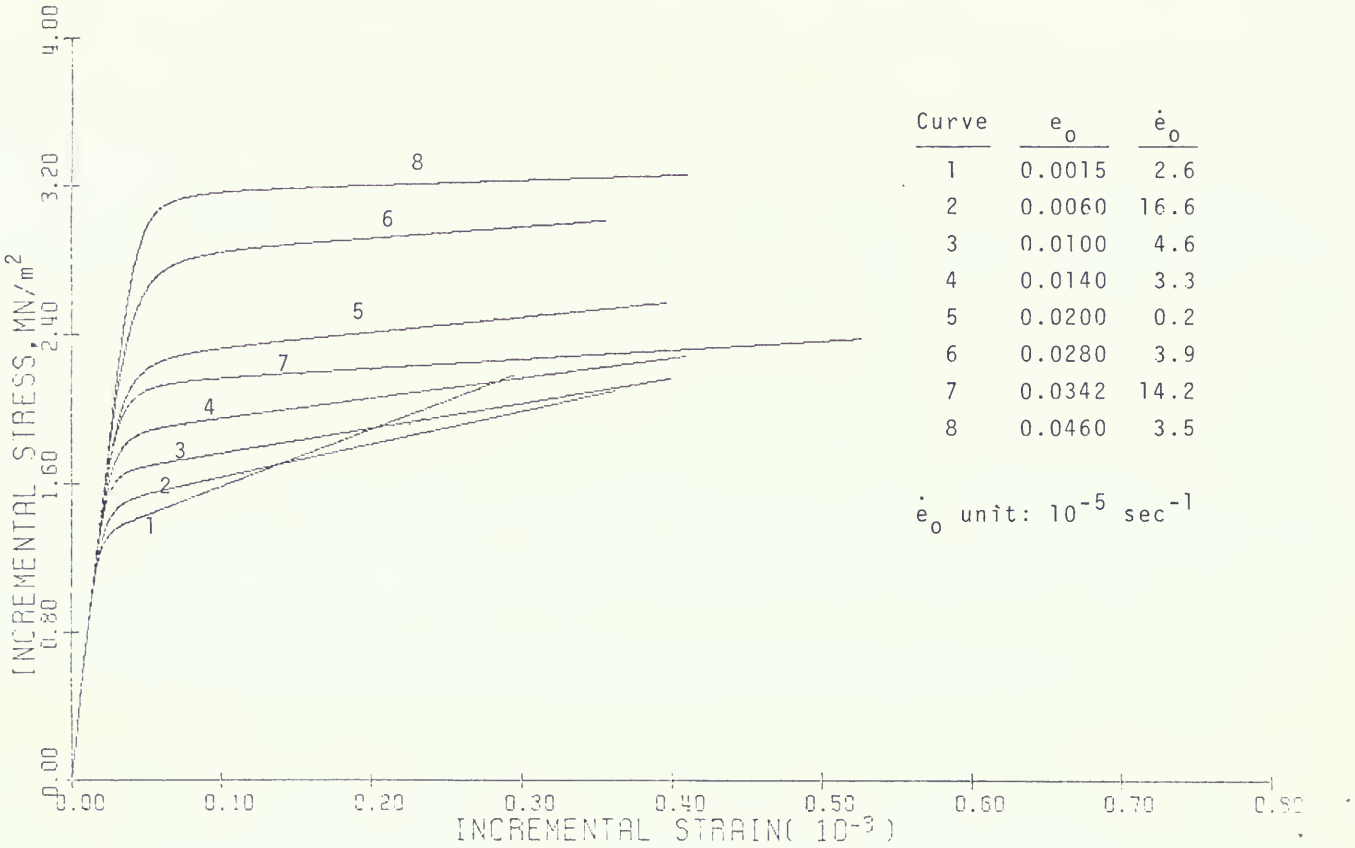

Curve	e_o	$\dot{e}_o$
1	0.0015	2.6
2	0.0060	16.6
3	0.0100	4.6
4	0.0140	3.3
5	0.0200	0.2
6	0.0280	3.9
7	0.0342	14.2
8	0.0460	3.5

$\dot{e}_o$ unit: 10^{-5} sec^{-1}

Figure 4.2 Dynamic Incremental Stress-Strain Curves (Aluminum Specimen No. 4).

prestrain levels for copper specimen No. 4 and aluminum specimen No. 4, respectively.

4.4 Strain-Rate-Dependent Theory

Since the first use of a semilinear rate-type constitutive equation by Sokolovsky (1948) and Malvern (1949) and the introduction of a quasilinear equation by Malvern (1949), several other kinds of rate-type constitutive equations have been investigated in many published papers [see Cristescu (1963), (1972), Lubliner (1964), Lubliner and Valathur (1969)].

In this section, two rate-type constitutive equations in terms of incremental stress and strain were considered and numerical solutions were obtained for incremental waves at several prestrain levels of one aluminum case and one copper case. The results show that the simple wave solution can also be approximated in certain types of constitutive laws of the strain-rate-dependent theory.

4.4.1 Constitutive Laws Considered

The general form of the quasilinear constitutive equation as suggested by Cristescu (1963) is

$$\dot{\varepsilon} = \phi(\sigma,\varepsilon)\dot{\sigma} + \psi(\sigma,\varepsilon) \tag{4.18}$$

where the dot represents the time derivative of the variable

at a material point x. Two special forms of equation (4.18) are considered, the first is the semilinear model of Malvern-type

$$\dot{\varepsilon} = \frac{1}{E}\dot{\sigma} + \frac{k}{E}[\sigma - A\varepsilon] \tag{4.19}$$

The second kind is a quasilinear model proposed by the present author as

$$\dot{\varepsilon} = [\frac{1}{E} + p\varepsilon]\dot{\sigma} + \frac{k}{E}[\sigma - A\varepsilon] \tag{4.20}$$

In equations (4.19) and (4.20), the parameters p and k are constants to be determined, E the Young's modulus and A the slope of the quasistatic true prestress-prestrain curve at the prestrain level where the incremental wave is generated. The term $A\varepsilon$ represents the approximate form of the quasi-static nominal stress-strain curve based on the initial dimensions of the prestrained state when the incremental wave started. $(\sigma - A\varepsilon)$ is the overstress. A restriction imposed on the instantaneous term $\phi(\sigma,\varepsilon)$ was suggested by Cristescu (1972). It was that whenever $\dot{\sigma} < 0$ or $\sigma < A\varepsilon$ the value of $\phi(\sigma,\varepsilon)$ should be switched to $1/E$.

4.4.2 Characteristics and Associated Interior Differential Equations

After introducing equation (4.18) into equation (4.3) and then combining with equation (4.4), we can write the resulting system of the equations in the following matrix form

$$\begin{bmatrix} \rho & 0 \\ 0 & \phi \end{bmatrix} \begin{Bmatrix} v_t \\ \sigma_t \end{Bmatrix} + \begin{bmatrix} 0 & -1 \\ -1 & 0 \end{bmatrix} \begin{Bmatrix} v_x \\ \sigma_x \end{Bmatrix} = \begin{Bmatrix} 0 \\ -\psi \end{Bmatrix} \tag{4.21}$$

where the subscripts t and x denote partial differentiation. The theory for systems of first order quasilinear partial differential equations, as represented by equation (4.21), is given in Jeffrey and Taniuti (1964). The characteristic wave speeds associated with such a system are the roots of the determinantal equation

$$\begin{vmatrix} \rho c & 1 \\ 1 & c\phi \end{vmatrix} = 0 \tag{4.22}$$

With $c = 1/\sqrt{\rho\phi}$ the characteristic equations are

$$dx = \pm\, c\, dt \tag{4.23}$$

The null vector $\underset{\sim}{\ell}^T = [\ell_1, \ell_2]$ for equation (4.21), which corresponds to the characteristic wave speed c, is given by

$$[\ell_1, \ell_2] \begin{bmatrix} \rho c & 1 \\ 1 & \phi c \end{bmatrix} = [0, 0] \tag{4.24}$$

Choosing an arbitrary scale factor such that $\ell_1 = 1$ in equation (4.24), we get

$$\underset{\sim}{\ell}^T = [-c\phi, 1] \tag{4.25}$$

The interior differential equation corresponding to the characteristic given by dx = c dt is given by

$$[-c\phi,\ 1]\begin{bmatrix}\rho & 0\\ 0 & \phi\end{bmatrix}\begin{Bmatrix}dv\\ d\sigma\end{Bmatrix} = [-c\phi,\ 1]\begin{Bmatrix}0\\ -\psi\end{Bmatrix} dt \qquad (4.26)$$

which is rewritten as

$$d\sigma - \rho c\, dv = -\frac{\psi}{\phi}\, dt, \qquad dx = +\, c\, dt \qquad (4.27)$$

For the negative characteristic given by dx = - c dt, we replace (+c) by (-c) in equation (4.27).

4.4.3 Semilinear Model — Numerical scheme

The governing differential equations given in (4.19) and (4.27) are written in the finite difference form with $\phi = 1/E$ and $\psi = k(\sigma - A\varepsilon)/E$ in the present case. The characteristic wave speed c of equation (4.22) becomes a constant, equal to the elastic bar wave speed $c_0 = \sqrt{E/\rho}$. The system of finite difference equations is

$$\Delta\sigma - E\,\Delta\varepsilon = -[\sigma - A\varepsilon]k\,\Delta t \quad \text{along } dx = 0 \qquad (4.28)$$

$$\Delta\sigma \pm \rho c_0\,\Delta v = -[\sigma - A\varepsilon]k\,\Delta t \quad \text{along } dx = \pm c_0\, dt \qquad (4.29a,b)$$

Figure 4.3(i) shows the solution domain in the x-t plane. Mesh point types involved are sketched in the same figure with labels (ii), (iii), (iv) and (v). This is the

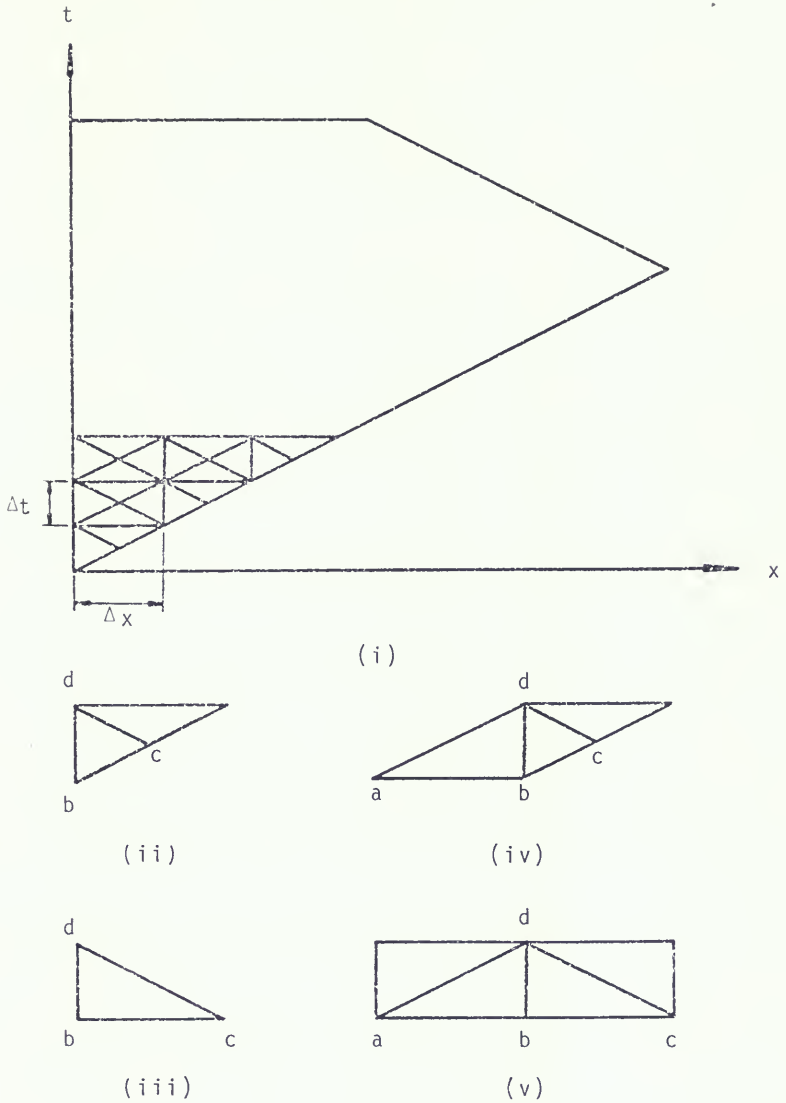

Figure 4.3 Schematics of Solution Domain and Mesh Point Types for Semilinear Model.

same algorithm as that given by Bianchi (1963) and Banerjee (1972).

The unknowns at a typical point are stress and strain for the boundary and stress, strain and velocity for a general interior point. These are determined by solving appropriate selected set of equations from equations (4.28) and (4.29a,b) as follows:

General boundary point [Ref. Figure 4.3(iii)]

Solution is known at points b and c. Solution at point d is obtained from

$$\sigma_d - \sigma_c + \rho c_o(v_d - v_c) = -\frac{1}{2}k[\sigma_d + \sigma_c - A(\varepsilon_d + \varepsilon_c)]\,\Delta t \qquad (4.30)$$

$$\sigma_d - \sigma_b - E(\varepsilon_d - \varepsilon_b) = -\frac{1}{2}k[\sigma_d + \sigma_b - A(\varepsilon_d + \varepsilon_b)]\,\Delta t \qquad (4.31)$$

Mesh point type 4.3(ii), representing the first point to be computed, is governed by equations identical to those above, except that Δt in equation (4.30) is replaced by $0.5\,\Delta t$.

General interior point [Ref. Figure 4.3(v)]

Solution at points a, b, c is known. Solution at point d is obtained from

$$\sigma_d - \sigma_a - \rho c_o(v_d - v_a) = -\frac{1}{2}k[\sigma_d + \sigma_a - A(\varepsilon_d + \varepsilon_a)]\,\Delta t \qquad (4.32)$$

$$\sigma_d - \sigma_c + \rho c_o(v_d - v_c) = -\frac{1}{2}k[\sigma_d + \sigma_c - A(\varepsilon_d + \varepsilon_c)]\,\Delta t \qquad (4.33)$$

$$\sigma_d - \sigma_b - E(\varepsilon_d - \varepsilon_b) = -\frac{1}{2}k[\sigma_d + \sigma_b - A(\varepsilon_d + \varepsilon_b)]\,\Delta t \qquad (4.34)$$

Mesh point behind leading wave [Ref. Figure 4.3(iv)]

The difference equations are the same as equation (4.32) through (4.34), except that Δt in equation (4.33) is replaced by $0.5\ \Delta t$.

A Fortran IV computer program was written to perform the computation. Because of the linear prestress-prestrain function assumed in the overstress term of equation (4.19), direct solution from the linear simultaneous difference equations is possible. In order to make the actual gage stations fall on mesh points exactly in each case for various prestrain levels, the mesh size is controlled by an integer parameter, denoted by NX, which represents the number of intervals between two adjacent gage stations. Mesh size dimensions Δx and Δt are obtained from

$$\Delta x = \frac{(1 + e_o)\, d}{NX} \tag{4.35}$$

$$\Delta t = \frac{\Delta x}{c_o} \tag{4.36}$$

where d is the distance between two adjacent gage stations at zero prestrain and e_o is the value of prestrain. NX = 16 was chosen in the computations, and thus the value of Δt varies from 0.7736 μsec to 0.8123 μsec as the prestrain increases from zero to 0.05 in the aluminum case, $\Delta t \simeq 1.1$ μsec in the copper case. Boundary data were read at constant

time intervals from the experimental results. These were then interpolated by using the cubic Lagrangian step-by-step routine to get values at the mesh points with intervals of Δt obtained in each case. Convergence of the computation was checked by seeing that halving the mesh step (doubling the value of NX) did not produce any observable change in the solution.

Results of the numerical computation will be discussed in detail in Section 4.4.5. Some remarks are given here. In general the semilinear model of the Malvern type does not give a simple wave solution. Some authors recommended the use of a nonlinear function of overstress to get a better result. However, Banerjee (1972) has obtained solutions for the semilinear model with both linear and exponential overstress and for the quasilinear model with linear overstress in a torsional incremental wave case. By checking the results carefully, it was found that the result of the exponential overstress model made no substantial improvement over that of linear overstress. It was the quasilinear model which gave the best result among the three models considered. Therefore a quasilinear model was considered next.

4.4.4 Quasilinear Model — An Integro-Differential Approach and Numerical Scheme

The behavior of the theoretical solution for the quasilinear constitutive model

$$\dot{\varepsilon} = [\frac{1}{E} + p\varepsilon]\dot{\sigma} + \frac{k}{E}[\sigma - A\varepsilon] \qquad (4.20)$$

in the incremental wave propagation will be considered. The parameters p and k are two constants to be determined by matching the theoretical solutions with the experimental results for incremental waves at various prestrain levels.

(i) Remarks concerning the choice of the function $\phi(\sigma,\varepsilon)$

The introduction of the instantaneous plastic response term was first made by Cristescu (1963) on a purely phenomenological basis, in order to give a better description of the dynamic plastic response of a material. However, Holt et al. (1967) performed tests with a series of commercial aluminum alloys and found that stress-strain curves at the higher strain rates of 10^{-2} sec^{-1} to 10^{3} sec^{-1} were all coincident. This means that for representing the behavior of that particular material in that high strain rate range, the existence of a single dynamic stress-strain curve can be assumed. Most authors have determined the dynamic response function ϕ by assuming a simple form of dynamic stress-strain curve, such as $\sigma = \beta\varepsilon^{n}$ [see Cristescu (1972), Banerjee (1972)]. This always resulted in a complicated

form of the function ϕ itself. The solution to the consequent system of differential equations then required a computer time of the order of minutes in a third-generation computer. The cost problem became critical in the present work, since solutions for several cases at various prestrain levels of a series of incremental wave tests were to be investigated. For this reason, the simple form of $\phi = 1/E + p\varepsilon$ was proposed and a solution procedure was found such that the computing time needed to obtain a solution was reduced to about half a minute. The function $\phi = 1/E + p\varepsilon$ gives an instantaneous response curve of the form

$$\sigma = \frac{1}{p} \ln(1 + pE\varepsilon) \tag{4.37}$$

This curve is qualitatively satisfactory, since it is a single-valued function with $\partial\sigma/\partial\varepsilon > 0$, $\partial^2\sigma/\partial\varepsilon^2 < 0$.

A restriction proposed by Cristescu (1972), on the form of ϕ in equation (4.18) is that the slope of the instantaneous response curve must lie between the slopes of the elastic curve and of the relaxation boundary at the same strain. For the present case this requires

$$A < \frac{E}{1 + pE\varepsilon} < E \tag{4.38}$$

which was always satisfied.

(ii) Formulation of the interior differential equations in an integro-differential form

It will be shown that the quasilinear constitutive equation (4.20) may be solved for $\varepsilon(t)$ in terms of $\sigma(t)$ and t. Thus, one of the unknown variables is eliminated, and the resulting system of differential equations can be solved in a more efficient way.

Consider equation (4.20), which represents the constitutive law assumed for a material point x.

$$\dot{\varepsilon} = [\frac{1}{E} + p\varepsilon]\dot{\sigma} + \frac{k}{E}[\sigma - A\varepsilon] \qquad (4.20)$$

The initial condition is

$$\sigma = \varepsilon = 0 \qquad \text{at} \quad t = 0 \qquad (4.39)$$

(In this discussion time t = 0 represents the moment when the leading edge of the incremental wave just arrives at x. This differs from the initial time of Section 4.2). The solution to equation (4.20) without the second terms on the right-hand side may be written as

$$\varepsilon(t) = -\frac{1}{pE} + we^{p\sigma(t)} \qquad (4.40)$$

where w = constant. The solution to the complete equation (4.20) may then be given by the variation of parameter technique [Hildebrand (1962), Suliciu et al. (1974)] as

$$\varepsilon(t) = -\frac{1}{pE} + w(t)\, e^{p\sigma(t)} \qquad (4.41)$$

where now $w(t)$ is a variable to be determined. Introducing the initial condition (4.39) into equation (4.41), gives

$$w(0) = \frac{1}{pE}$$

We make the change of variable

$$w(t) = \frac{1}{pE} + w_1(t) , \qquad w_1(0) = 0 \qquad (4.42)$$

and substitute equation (4.41) into equation (4.20) to get

$$\dot{w}_1 + \frac{Ak}{E} w_1 = \frac{k}{E}\{[\sigma(t) + \frac{A}{pE}]\, e^{-p\sigma(t)} - \frac{A}{pE}\} \qquad (4.43)$$

Solution to equation (4.43) may be obtained by applying the variation of parameter method once again. The result is

$$w_1(t) = \frac{k}{E}\, e^{-\frac{Ak}{E}t} \int_0^t q(s)\, ds - \frac{1}{pE}(1 - e^{-\frac{Ak}{E}t}) \qquad (4.44)$$

where

$$q(s) = [\sigma(s) + \frac{A}{pE}] \exp[\frac{Ak}{E}s - p\sigma(s)] \qquad (4.45)$$

Substituting equations (4.44) and (4.42) in equation (4.41), we get an explicit representation for ε in terms of σ and t,

$$\varepsilon(t) = \frac{1}{pE}\,[F\{\sigma(t), t\} - 1] \qquad (4.46)$$

where $F\{\sigma(t),t\}$ is a functional depending on the (unknown) history of $\sigma(t)$, given by

$$F\{\sigma(t),t\} = pk \int_0^t [\sigma(s) + \frac{A}{pE}] \exp\{p[\sigma(t) - \sigma(s)] - \frac{Ak}{E}(t - s)\}\, ds + \exp[p\sigma(t) - \frac{Ak}{E}t] \tag{4.47}$$

In order to incorporate it with the equations of motion and compatibility, equation (4.46) is differentiated with respect to t, giving

$$\frac{\partial \varepsilon}{\partial t} = \frac{F\{\sigma,t\}}{E} \frac{\partial \sigma}{\partial t} + \frac{k}{E}\sigma + \frac{Ak}{pE^2} [1 - F\{\sigma,t\}] \tag{4.48}$$

where for brevity $F\{\sigma(t),t\}$ has been written as $F\{\sigma,t\}$. By comparing equation (4.48) with the general form of quasilinear constitutive equation (4.48), the values of the functions ϕ and ψ in equation (4.21) at any time can be expressed in terms of the value of $F\{\sigma,t\}$ as

$$\phi = F\{\sigma,t\}/E \tag{4.49}$$

$$\psi = \frac{k}{E}\sigma + \frac{Ak}{pE^2} [1 - F\{\sigma,t\}] \tag{4.50}$$

By applying the results of Section 4.4.2, we obtain the characteristic wave speed of equation (4.22) in terms of $F\{\sigma,t\}$ as

$$c = 1/\sqrt{\rho F\{\sigma,t\}/E}$$

or

$$c = c_0/\sqrt{F\{\sigma,t\}} \tag{4.51}$$

where c_0 is the elastic bar wave speed. The interior differential equations associated with the characteristic equations

$$\frac{dx}{dt} = \pm c = \pm \frac{c_0}{\sqrt{F\{\sigma,t\}}} \tag{4.52}$$

may then be obtained from equation (4.27) as

$$d\sigma \mp \rho c\, dv = k\left[\frac{A}{\rho E}\left(1 - \frac{1}{F\{\sigma,t\}}\right) - \frac{\sigma}{F\{\sigma,t\}}\right] dt \tag{4.53}$$

Only two unknown variables σ and v are involved in the integration of equation (4.53). The strain is obtained from equation (4.46) after solution for σ has been obtained. Some difficulties are observed from solving equation (4.53), since the values of $F\{\sigma,t\}$ are not known a priori, because $\sigma(t)$ is not known and equation (4.47) for $F\{\sigma,t\}$ contains an integration from $s = 0$ to $s = t$ with the integrand a function of $\sigma(s)$. A recursion formula of numerical integration was found that decouples the history dependence of $\sigma(t)$ in $F\{\sigma,t\}$ as follows

$$F_n = \exp(p\sigma_n - \alpha t_n) + pk \exp[p(\sigma_n - \sigma_{n-1}) - \alpha\,\Delta t]\{F_{n-1} + \Delta t[A_1 + \tfrac{1}{2}(\sigma_n + \sigma_{n-1})] \exp[\tfrac{1}{2}(\sigma\,\Delta t - p(\sigma_n - \sigma_{n-1}))]\} \tag{4.54}$$

where $\alpha = Ak/E$, $A_1 = A/pE$, $\Delta t = t_n - t_{n-1}$ and the subscripts n and n-1 represent the function values at $t = t_n$ and $t = t_{n-1}$, respectively. All the (n-1)-subscripted quantities are known from the previous iteration. Therefore, equation (4.54) makes the value of the function F depend explicitly on σ_n, the present unknown value of stress. This makes the iteration procedure of solving for σ and v at a mesh point become possible. The numerical scheme is described in the following.

(iii) Numerical scheme

The method of integration consists of integrating equation (4.53) along the corresponding characteristic curves, defined by equation (4.52). These two families of characteristic curves have variable slopes in the loading domain. However, the grid used in integration was a regular one with constant slopes $\pm c_0$. Figure 4.4 shows schematically the solution domain and types of grids. The standard Courant-Isaacson-Rees procedure [see Jeffrey and Taniuti (1964)] was applied and the convergence of iterations is assured, since $c \leq c_0$.

General interior point [Ref. Figure 4.4(iii)]

The solution is known at points a, b and c. Points L and R are intersections of lines $\overline{ab}$ and $\overline{bc}$ with the lines $\overline{Ld}$ and $\overline{Rd}$ tangent to characteristic curves at point d. Finite difference formulations of equation (4.53) along the characteristics $\overline{Ld}$ and $\overline{Rd}$ may be written as

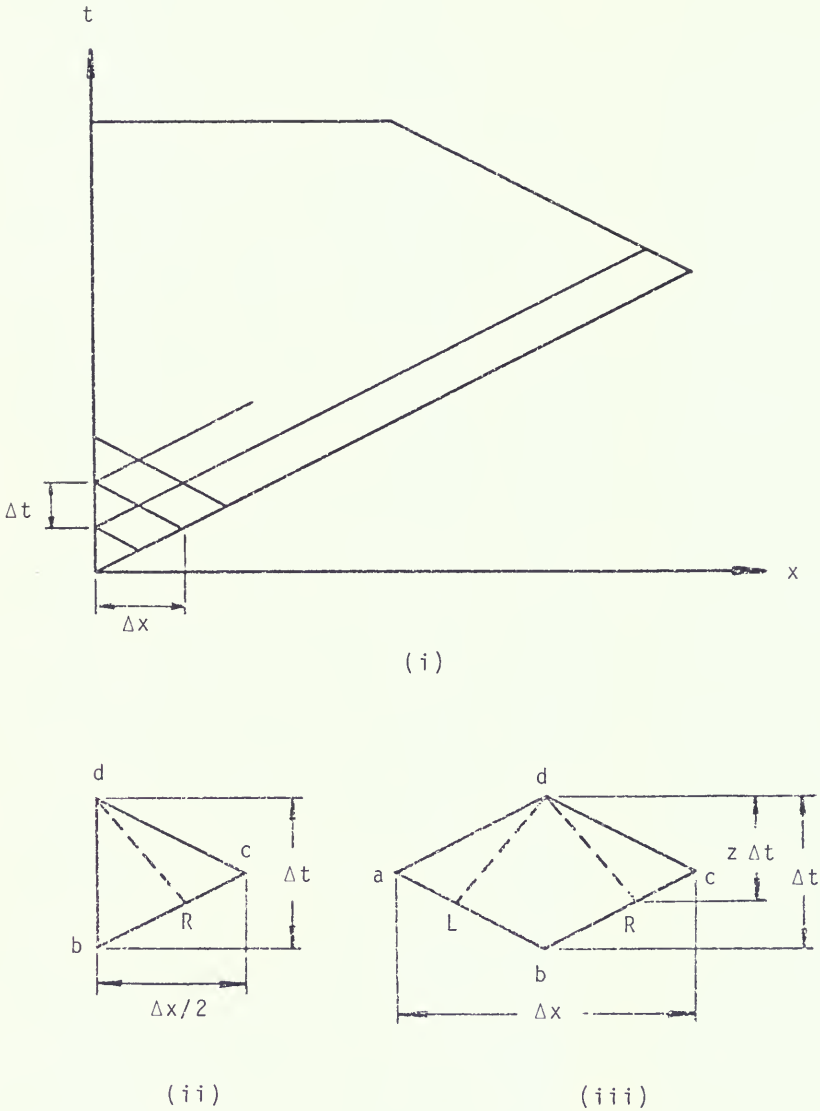

Figure 4.4 Schematics of Solution Domain and Mesh Point Types for Quasilinear Model.

$$\sigma_d - \sigma_L - \frac{\rho c_o}{\sqrt{F_d}} (v_d - v_L) = [A_1(1 - \frac{1}{F_d}) - \frac{1}{F_d} \frac{\sigma_d + \sigma_L}{2}] kz \Delta t \qquad (4.55)$$

$$\sigma_d - \sigma_R + \frac{c_o}{\sqrt{F_d}} (v_d - v_R) = [A_1(1 - \frac{1}{F_d}) - \frac{1}{F_d} \frac{\sigma_d + \sigma_R}{2}] kz \Delta t \qquad (4.56)$$

where $A_1 = A/pE$ and F_d is unknown and depends on σ_d as given by equation (4.54). The meaning of parameter z can be perceived from Figure 4.4(iii), and it can be shown that

$$z = \frac{\sqrt{F_d}}{1 + \sqrt{F_d}} \qquad (4.57)$$

The variables σ_R, σ_L, v_R and v_L in equations (4.55) and (4.56) can be replaced by the following expressions from linear interpolation,

$$\begin{aligned} \sigma_R &= \sigma_b + r(\sigma_c - \sigma_b) \\ \sigma_L &= \sigma_b + r(\sigma_a - \sigma_b) \\ v_R &= v_b + r(v_c - v_b) \\ v_L &= v_b + r(v_a - v_b) \end{aligned} \qquad (4.58)$$

where $r = \overline{bR}/\overline{bc} = \overline{bL}/\overline{ba} = 2/(1 + \sqrt{F_d})$ (4.59)

Substituting equation (4.58) into equation (4.55) and (4.56), we obtain the solutions for σ_d and v_d

$$\sigma_d = \frac{s_1}{2}\,[2\sigma_b(1 - r) + r(\sigma_a + \sigma_c)] + s_2 + rs_3(v_c - v_a) \quad (4.60)$$

$$\sigma_d = \frac{1}{2}\,[2v_b(1 - r) + r(v_a + v_c)] + rs_4(\sigma_c - \sigma_a) \quad (4.61)$$

where

$$s_1 = \frac{2F_d - kz\ \Delta t}{2F_d + kz\ \Delta t} \quad (4.62a)$$

$$s_2 = \frac{2A_1(F_d - 1)\ kz\ \Delta t}{2F_d + kz\ \Delta t} \quad (4.62b)$$

$$s_3 = \frac{c_o\sqrt{F_d}}{2F_d + kz\ \Delta t} \quad (4.62c)$$

$$s_4 = \frac{2F_d - kz\ \Delta t}{4\ c_o\sqrt{F_d}} \quad (4.62d)$$

The iteration proceeds by assuming first $\sigma_d = \sigma_d^{(0)} = \sigma_b$. The values of F_d and also z, r, s_1, s_2, s_3, s_4 are evaluated next. First solutions $\sigma_d^{(1)}$, $v_d^{(1)}$ can then be obtained from equations (4.60) and (4.61). The process is repeated by using $\sigma_d = \lambda\sigma^{(1)} + (1 - \lambda)\ \sigma_d^{(0)}$, or in general $\sigma_d = \lambda\sigma_d^{(n)} + (1 - \lambda)\ \sigma_d^{(n-1)}$, until the prescribed agreement is obtained between the successive σ_d values. The parameter λ is used here to improve the rate of convergence, since otherwise some kind of slowly convergent oscillation occurs. In the final computation, $\lambda = 0.9$ was used, and it resulted in an

accuracy of $|[\sigma_d^{(n)} - \sigma_d^{(n-1)}]/\sigma_d^{(n)}| < 0.00005$ in an average of 4 iterations. If $\lambda = 1.0$ is used, i.e., $\sigma_d = \sigma_d^{(n)}$, the number of iterations required is around 25.

General boundary points [Ref. Figure 4.4(ii)]

The only unknown is the value of stress at point d. The particle velocity values are given on the boundary points. The iteration scheme is the same as that of the general interior points, except that equations (4.60) and (4.61) are replaced by

$$\sigma_d = 2s_3[(v_b - v_d) + r(v_c - v_d)] + s_1[\sigma_b(1 - r) + r\sigma_c] + s_2 \qquad (4.63)$$

The mesh-size controlling parameter was arranged in a way similar to that used in the semilinear model. The values of Δt used were around 2.0 μsec for both copper and aluminum specimens. Halving of this step size did not produce any significant change in results but increased the computer time. The total computer time on the IBM system 360/70 was around 30 seconds for a loading duration of 350 μsec. Computer program is given in Appendix A-2.

4.4.5 Numerical Results

(i) Results for copper

Experimental results of specimen No. 4 were used for comparison with the numerical solutions by theoretical models. It was found that some substantial discrepancies exist

between the solution by the semilinear model and the experimental data. A typical example is given in Figure 4.5 for the case of prestrain e_o = 0.0290. The discrepancies are mainly: (1) the v-t curve shapes are different and (2) the propagation speed of a given level of particle velocity is not a constant according to the numerical solution by the semilinear model but varies by as much as about 30% in this case.

Most of the effort was therefore spent on matching the solutions according to the quasilinear model with the experimental velocity records by determining the parameters p and k in equation (4.20) of the quasilinear constitutive model. Numerical solutions of seven cases at prestrains equal to 0.0009, 0.0070, 0.0180, 0.0290, 0.0400, 0.0434 and 0.0488 were obtained first. The cost criterion in these parameter identification studies was set by comparing the wave speed curve fitting parameters v_c and n of the numerical solutions to the corresponding experimental values in each case. The solution by the quasilinear model is also not a simple wave solution in general. The maximum variation of the propagation speed of a given level of particle velocity between values computed from stations 1-2 and from stations 3-4 can, however, be controlled to be under 15%. The values of v_c and n from the propagation speed between stations 1-2 were used in the parameter identification studies. The parameter values resulting from these studies are given in Table 4.1.

Figures 3.7 through 3.13 show comparisons between particle velocity records computed with these resulting parameter values and the experimental records at stations 2, 3, and 4 for the seven cases. Some remarks will be given here.

(a) The value of n indicates the wave shape. This factor is the difficult one to match. It can be seen from the results in Table 4.1 that the value of n from the quasilinear solution at e_o = 0.0290 is much improved over that of the semilinear solution.

(b) The obtained parameters p and k depend on the precondition parameter ξ rather than depending on the prestrain value alone. Curves of p and k versus ξ are plotted in Figure 4.6

(c) It was later found that the choice of p and k to match the particle velocity records did not have a unique result. Also an unreasonable incremental stress-strain curve was found in the results of the case e_o = 0.0009, as will be seen in Section 4.5.

Nevertheless, at that time, three other cases were computed by using values of p and k predicted from Figure 4.6. One case is e_o = 0.0121 of specimen No. 4 and the other two cases are e_o = 0.0100 and e_o = 0.0461 of specimen No. 2. Cases of specimen No. 2 were picked since the values of m, k_1, and k_2 in Table 3.3 are close for the two specimens.

Results are shown in Figures 4.7 through 4.9. It appears that these results are as good as those of the seven cases previously shown in Figures 3.7 through 3.13.

(ii) Results for aluminum

Experimental results of specimen No. 4 were used for comparison with the numerical computation. Eight cases at prestrain values of 0.0015, 0.0060, 0.0100, 0.0140, 0.0200, 0.0280, 0.0342 and 0.0460 were examined. From the previous experience in dealing with the copper data, the quasilinear model was tried first. It turned out that for most cases the solution looked better if the value of p was on the order of 10^{-12} cm^2/dyne or $pE \simeq 1.0$ (Double precision is needed in the computation). It was checked that these solutions were identical to solutions of the semilinear model. Therefore the semilinear model was used to analyze the experimental data of the aluminum specimen.

Results of the eight cases are shown in Figure 3.14 through 3.21. It can be seen from Figure 3.14 through 3.16 that no reasonable solutions were obtained for these cases. For the rest of the cases, the parameter k was determined by matching the velocity solution of the station No. 4 with the experimental data. From this point of view, the solutions of the semilinear model are only qualitatively good. The dependence of the parameter k on the precondition factor ξ is shown in Figure 4.10. Some discussion concerning the incremental stress-strain relation of the numerical solutions will be given in Section 4.5.

Table 4.1 Related Parameters in Computer Solution of Rate-Dependent Theories.

	EXPERIMENTAL			THEORETICAL			
e_o	ξ	v_c cm/sec	n	pE	k 10^4 sec^{-1}	v_c cm/sec	n
Copper No. 4							
0.0009	-0.54	1.53	0.707	24.0	3.5	1.55	0.68
				9.6	6.0	0.88	0.39
0.0070	0.07	3.85	0.624	16.8	3.0	3.85	0.62
0.0180	0.39	5.47	0.914	12.0	2.0	5.44	0.77
0.0290	0.76	7.01	0.946	10.2	1.6	7.07	0.77
				0.0	5.0	7.66	0.56
0.0400	1.27	9.43	1.041	9.6	0.5	9.5	0.87
0.0434	2.17	14.27	1.358	6.6	0.1	14.5	0.89
0.0488	3.56	18.71	1.157	4.8	0.1	19.6	0.92
				3.0	1.0	22.2	0.89
0.0121	-0.35	3.18	0.683	20.9	3.4	2.7	0.59
Copper No. 2							
0.0100	-0.10	3.35	0.706	18.0	3.3	2.83	0.57
0.0461	1.50	9.81	0.976	8.9	0.6	10.59	0.75
Aluminum No. 4							
0.0015	-0.34	----------		0.0	3.0		
0.0060	-0.93	----------		0.0	2.5		
0.0100	-0.18	----------		0.0	2.1		
0.0140	0.16	----------		0.0	1.8		
0.0200	1.67	----------		0.0	1.5		
0.0280	0.76	----------		0.0	1.0		
0.0342	0.50	----------		0.0	1.2		
0.0460	1.68	----------		0.0	0.8		

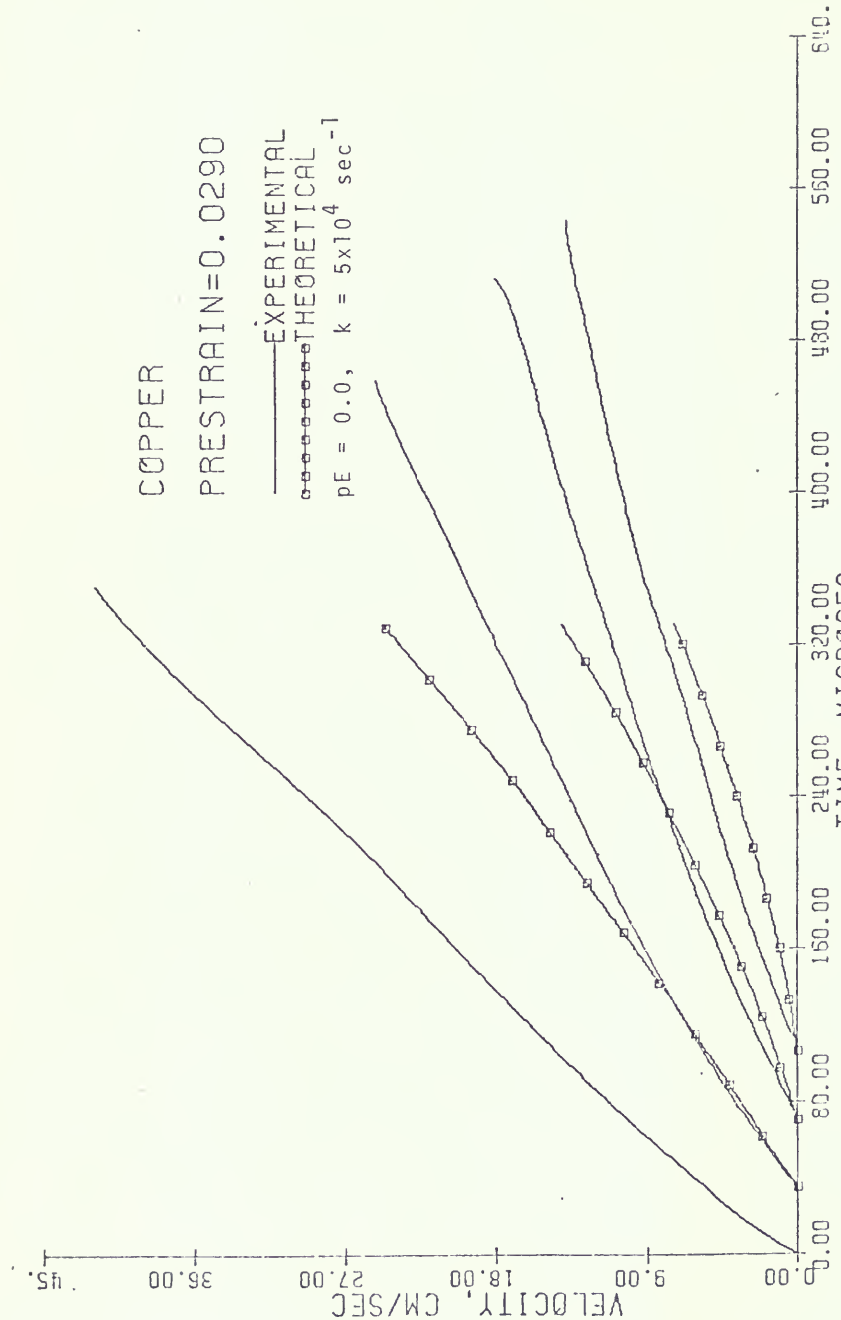

Figure 4.5 Particle Velocity Solution of Semilinear Model (Copper Specimen No. 4, Prestrain 0.0290).

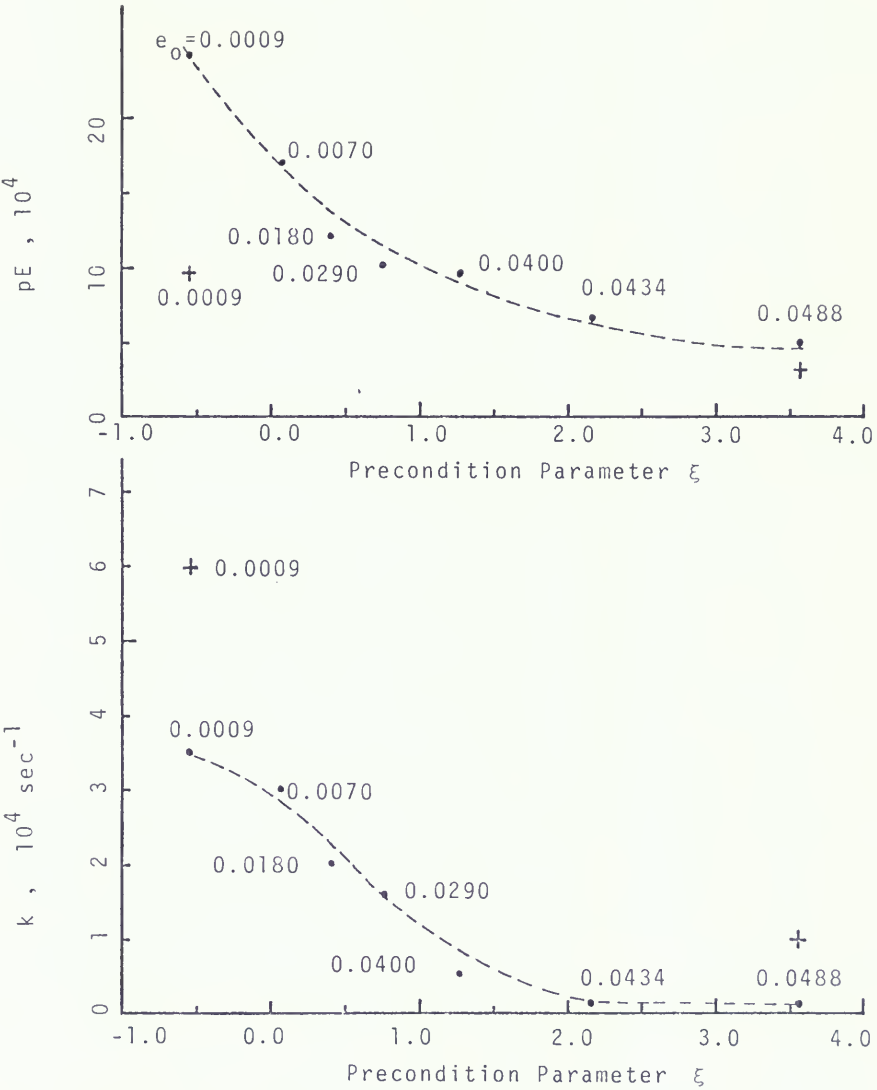

Figure 4.6 Relations Between Parameters in the Quasilinear Model and Precondition Parameter.

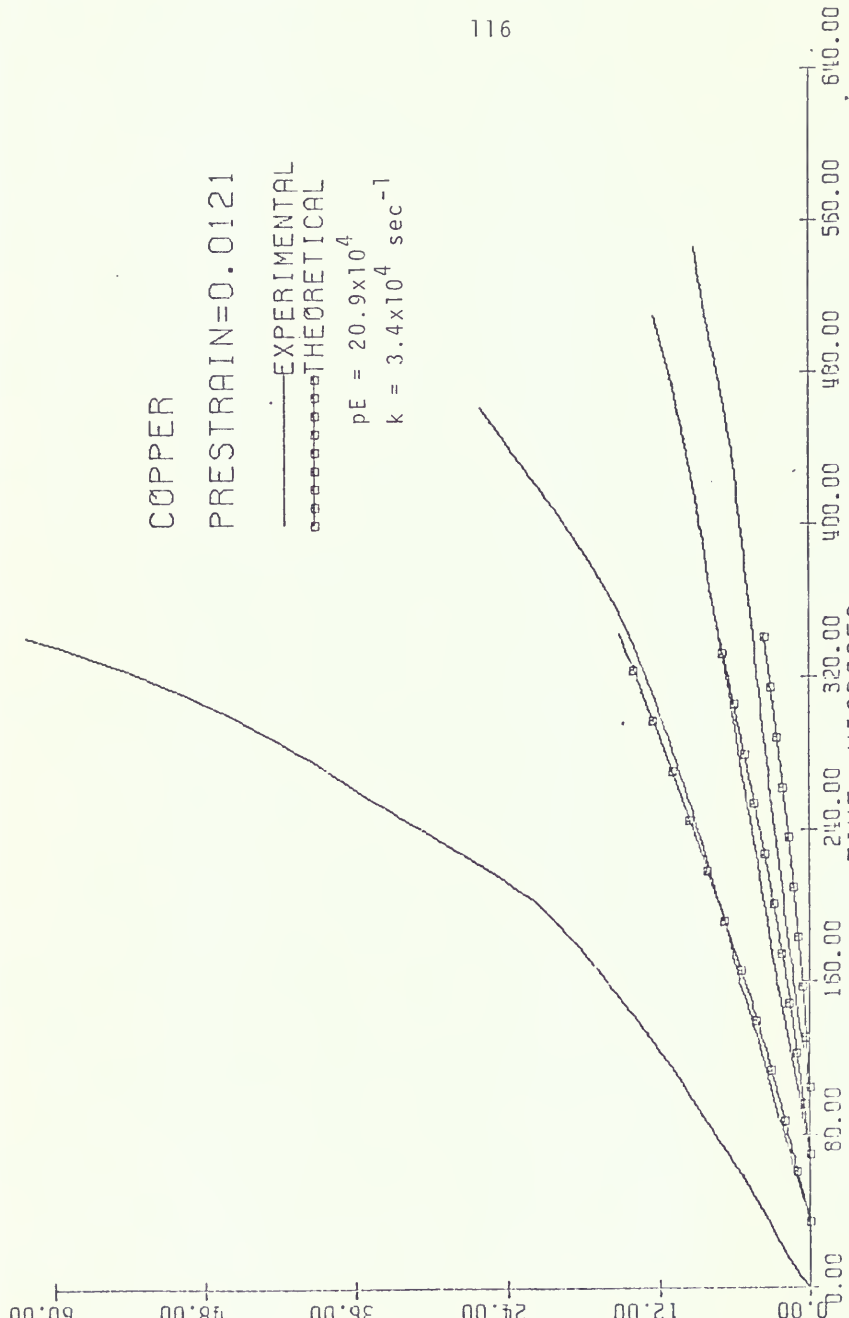

Figure 4.7 Particle Velocity Solution of Quasilinear Model (Copper Specimen No. 4, Prestrain 0.0121).

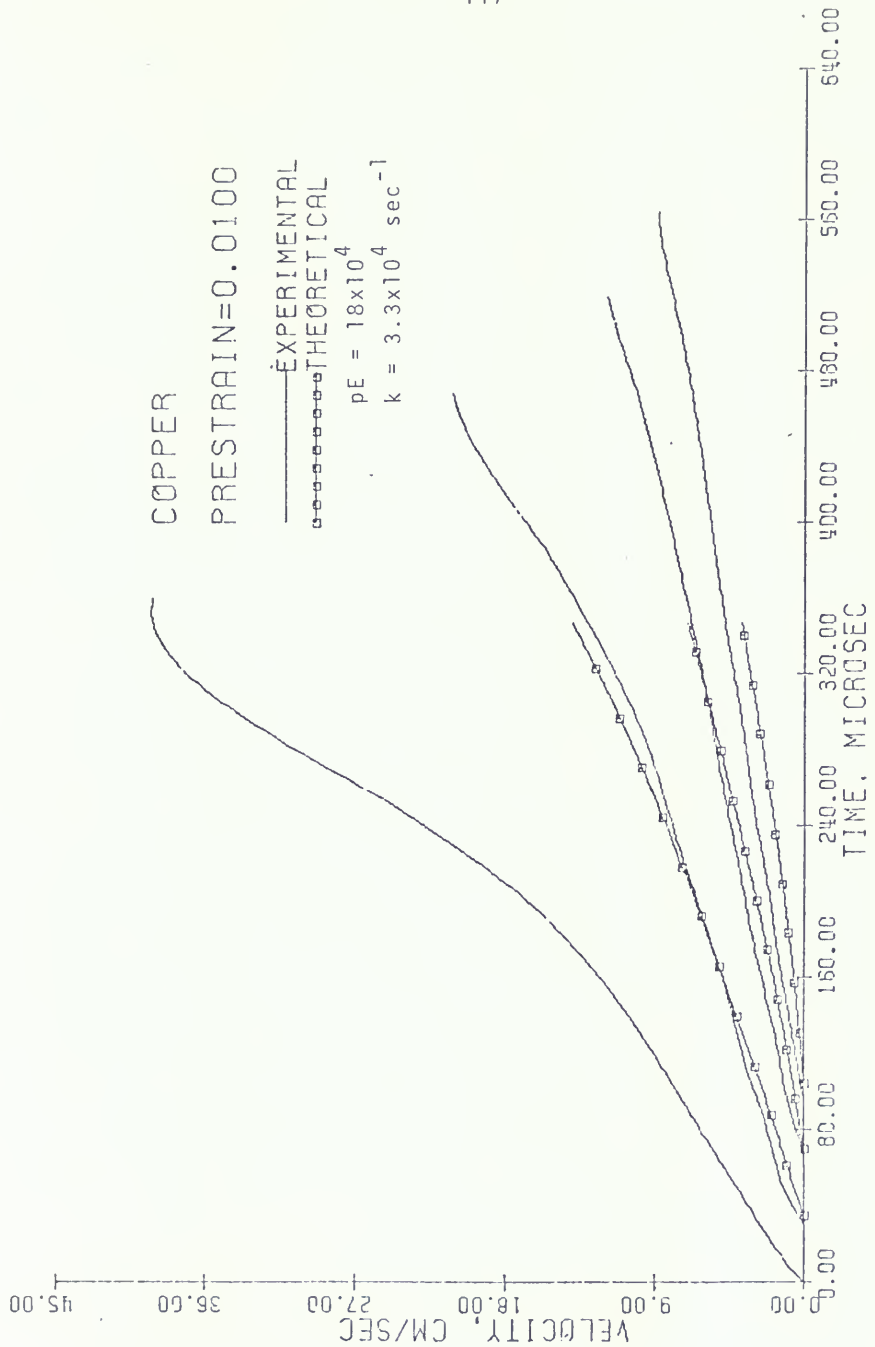

Figure 4.8 Particle Velocity Solution of Quasilinear Model (Copper Specimen No. 2, Prestrain 0.0100).

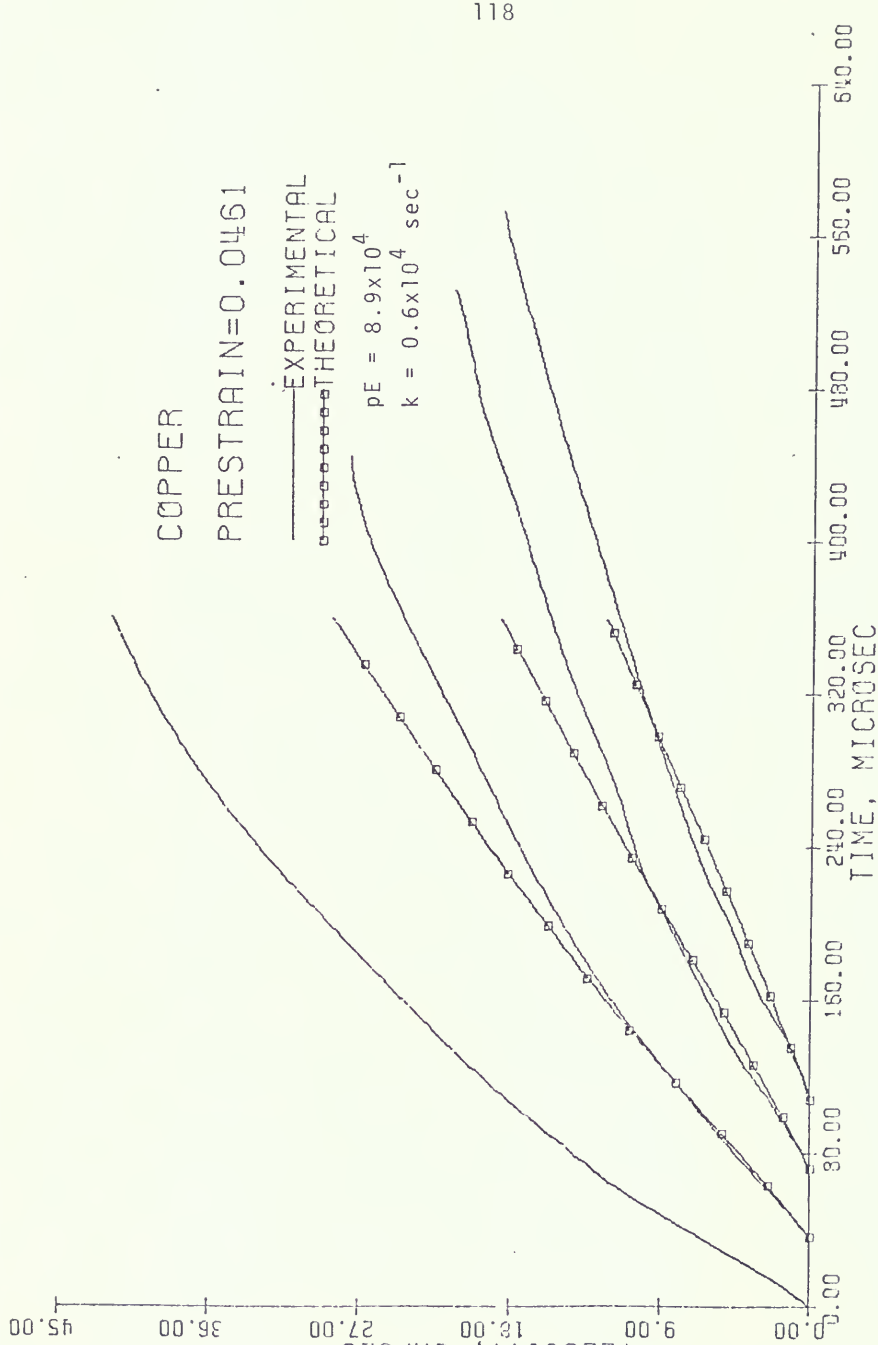

Figure 4.9 Particle Velocity Solution of Quasilinear Model (Copper Specimen No. 2, Prestrain 0.0461).

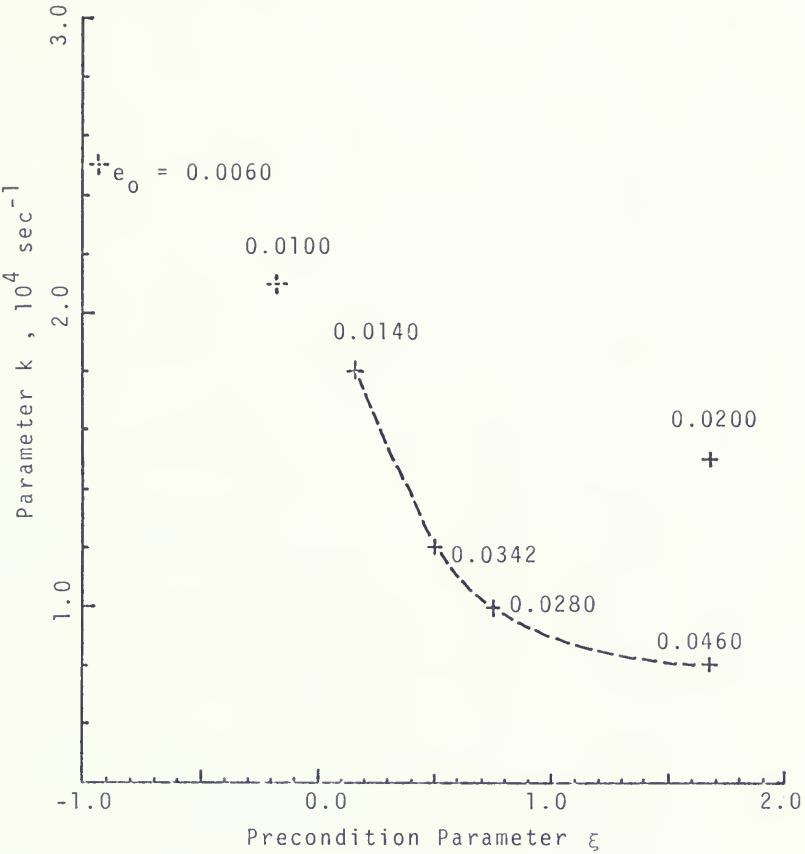

Figure 4.10 Relations Between Parameter in Semilinear Model and Precondition Parameter.

4.5 Comparative Study of the Strain-Rate-Independent and Strain-Rate-Dependent Theories

The results for copper will be discussed first. The incremental stress-strain curves obtained from the numerical solutions of rate-dependent models will be compared with the curves obtained from rate-independent theory. The results of the experimental data suggest strongly that a simple wave solution exists in the loading domain considered. Also, the curve fitting for the wave speed function is a very good approximation as shown in Figure 3.24. The incremental stress-strain curves shown in Figure 4.1 are thus very reasonable. Examples of cases at e_0 = 0.0009, 0.0070, 0.0290 and 0.0488 are given in Figures 4.11 through 4.14 for comparison to demonstrate some properties of the rate-dependent models.

In Figure 4.11 the curve marked RI is the one given by the rate-independent model, which is believed reasonable. At the higher incremental strains it becomes parallel to the quasistatic curve indicated by the heavy solid line marked QC. The curve marked QM-A1 is the curve at station No. 1 (the boundary for the solution), according to the quasilinear model with parameter values previously selected by parameter identification to match the velocity profiles. It is clear that although this gives a good match to the velocity profiles (see Figure 3.7), the resulting incremental stress-strain curve is unreasonable. It even falls below the quasistatic curve.

Curve QM-B1 of Figure 4.11 resulted at station No. 1 from another solution with parameter choice B ($pE = 0.96 \times 10^5$ and $k = 60{,}000\ \text{sec}^{-1}$). This is a much more reasonable curve, which lies close to the rate-independent curve, although its slope at the higher incremental strains is less than that of the rate-independent curve. Particle velocity predictions with parameter choice B are shown in Figure 4.15. They appear little different from those shown in Figure 3.7 (obtained with parameter choice A). This shows that the parameter identification procedure does not produce unique results for p and k, as was noted in remark (3) of Section 4.4.5 (i). The curves marked IC-A and IC-B are the instantaneous response curves of the quasilinear theory for the two parameter choices.

This example, led to the suggestion that the restriction of inquality (4.38) on the instantaneous curve should be strengthened as follows for use in the parameter choices:

$$\frac{dh(\varepsilon)}{d\varepsilon} \leq \frac{E}{1 + pE\varepsilon} \leq E \qquad (4.64)$$

where $h(\varepsilon)$ is the function in equation (4.6). Inequality (4.64) is not a necessary restriction; it may be violated and solution may still be a good approximation. From the incremental stress-strain curves of Figures 4.11 through 4.14 it appears that this inequality (4.64) is more important for cases with small prestrain or smaller values of precondition

parameter ξ than for cases with larger values of ξ. Figure 4.12 for the original solution for the case $e_0 = 0.0070$ shows that a tendency similar to that of the curve QM-A1 of Figure 4.11 exists as the inequality (4.64) is violated. Figure 4.13 gives a comparison between a semilinear solution (SM-A) and quasilinear one (QM-B). This shows that the incremental stress-strain curves of the quasilinear model are more like the rate-independent curves than are those of the semilinear model. Curves QM-A1 and QM-A2 in Figure 4.14 show that a simple wave solution can be approached as the rate sensitivity parameter k becomes small. The instantaneous response curve IC-A did violate the inequality (4.64), but the result is not so serious as in the case of Figure 4.12. Curves QM-B1 and QM-B2 in Figure 4.14 show that a similar solution with a better result in the σ-ε curve of station No. 1 is obtained by using another pair of p, k values. In this case the value of k is larger and the simple wave solution is no longer approached. The particle velocity solution is given in Figure 4.16.

From the above analysis, it is concluded that the relations between p, k and ξ shown in Figure 4.6 have to be revised in the region of small ξ and that there exist many pairs of the parameters p and k which can yield a good approximate solution. Values of p and k depend on precondition parameter ξ, but the result is not unique. The choice of the form $(1/E + p\varepsilon)$ for $\phi(\sigma,\varepsilon)$ seems to be adequate for

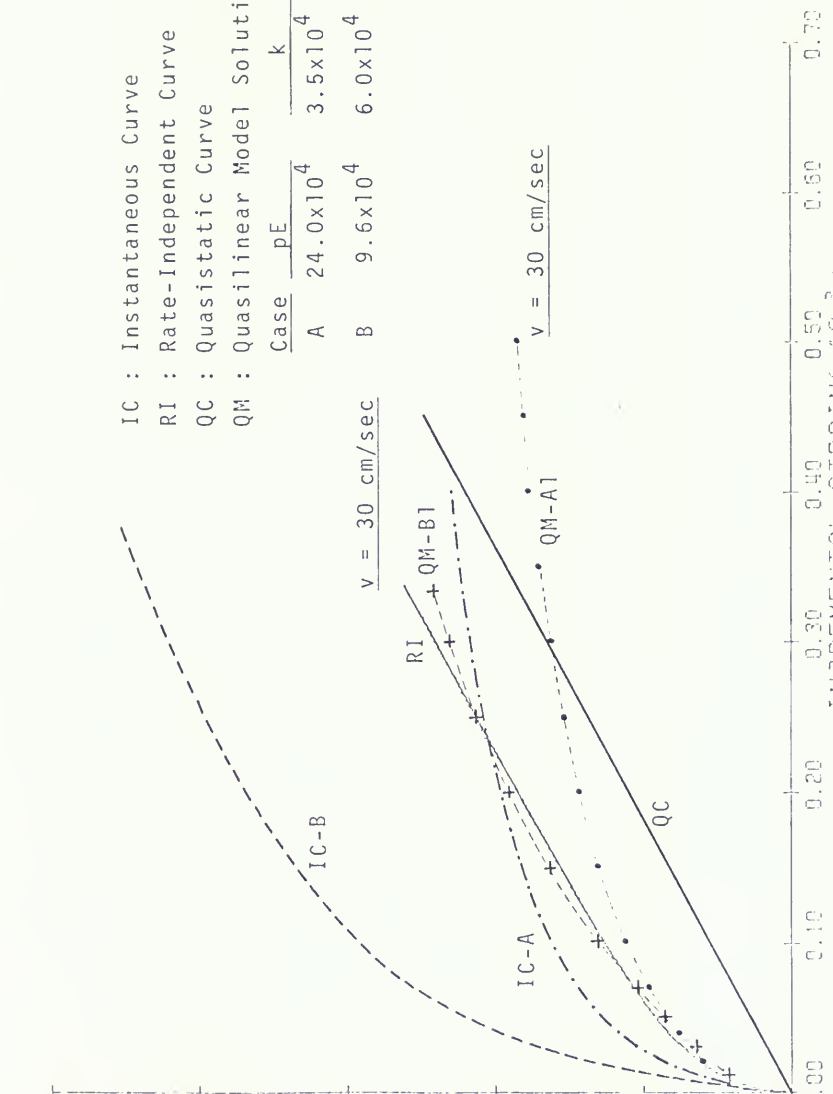

Figure 4.11 Comparisons of Incremental Stress-Strain Curves (Copper Specimen No. 4, Prestrain 0.0009).

Figure 4.12 Comparisons of Incremental Stress-Strain Curves (Copper Specimen No. 4, Prestrain 0.0070).

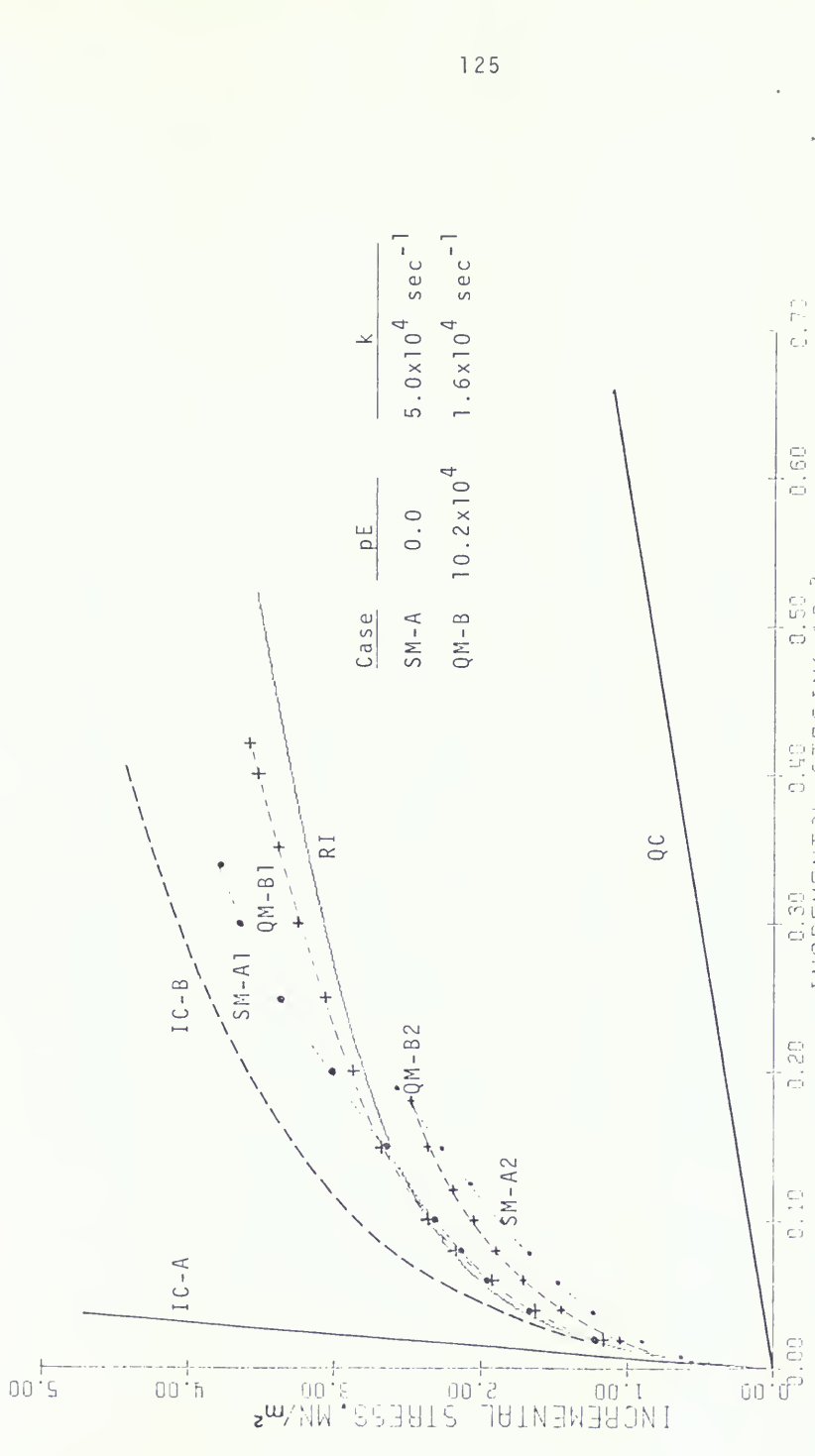

Figure 4.13 Comparisons of Incremental Stress-Strain Curves (Copper Specimen No. 4, Prestrain 0.0290).

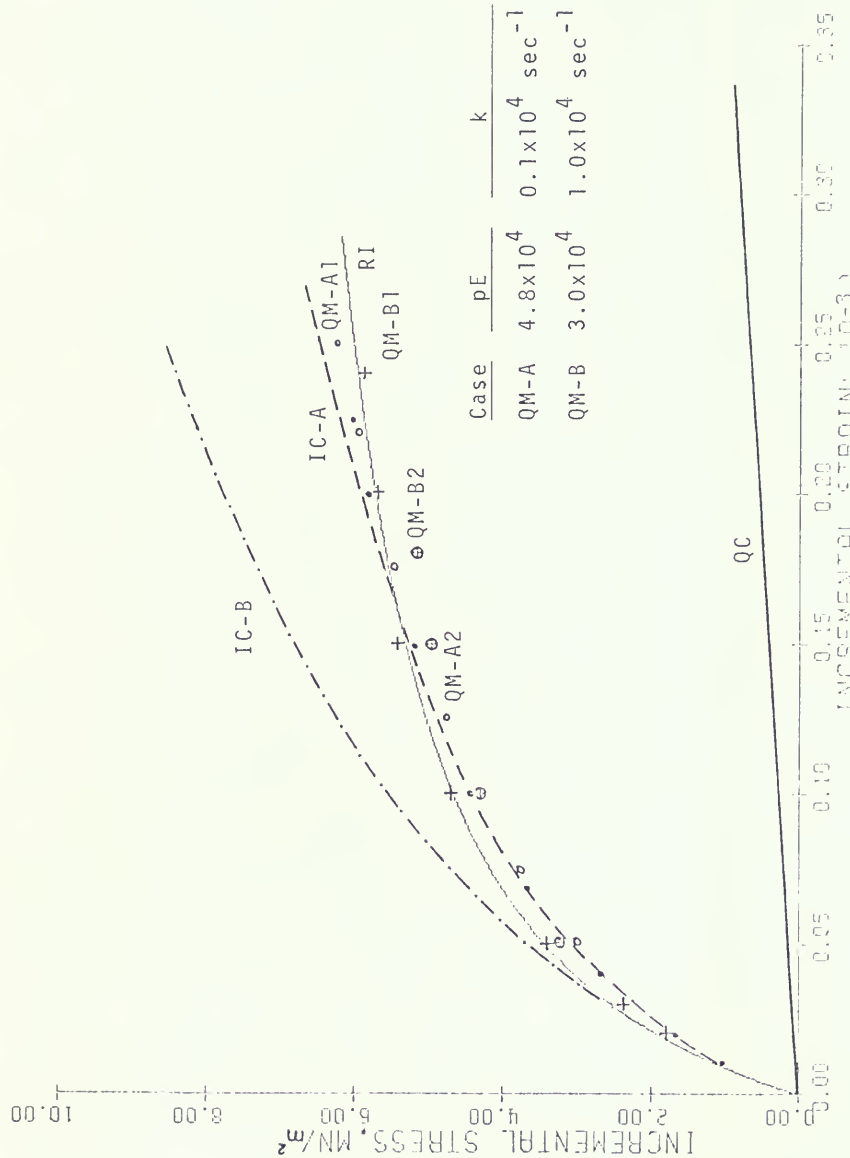

Figure 4.14 Comparisons of Incremental Stress-Strain Curves (Copper Specimen No. 4, Prestrain 0.0488).

Figure 4.15 Particle Velocity Solution of Quasilinear Model (Copper Specimen No. 4, Prestrain 0.0009).

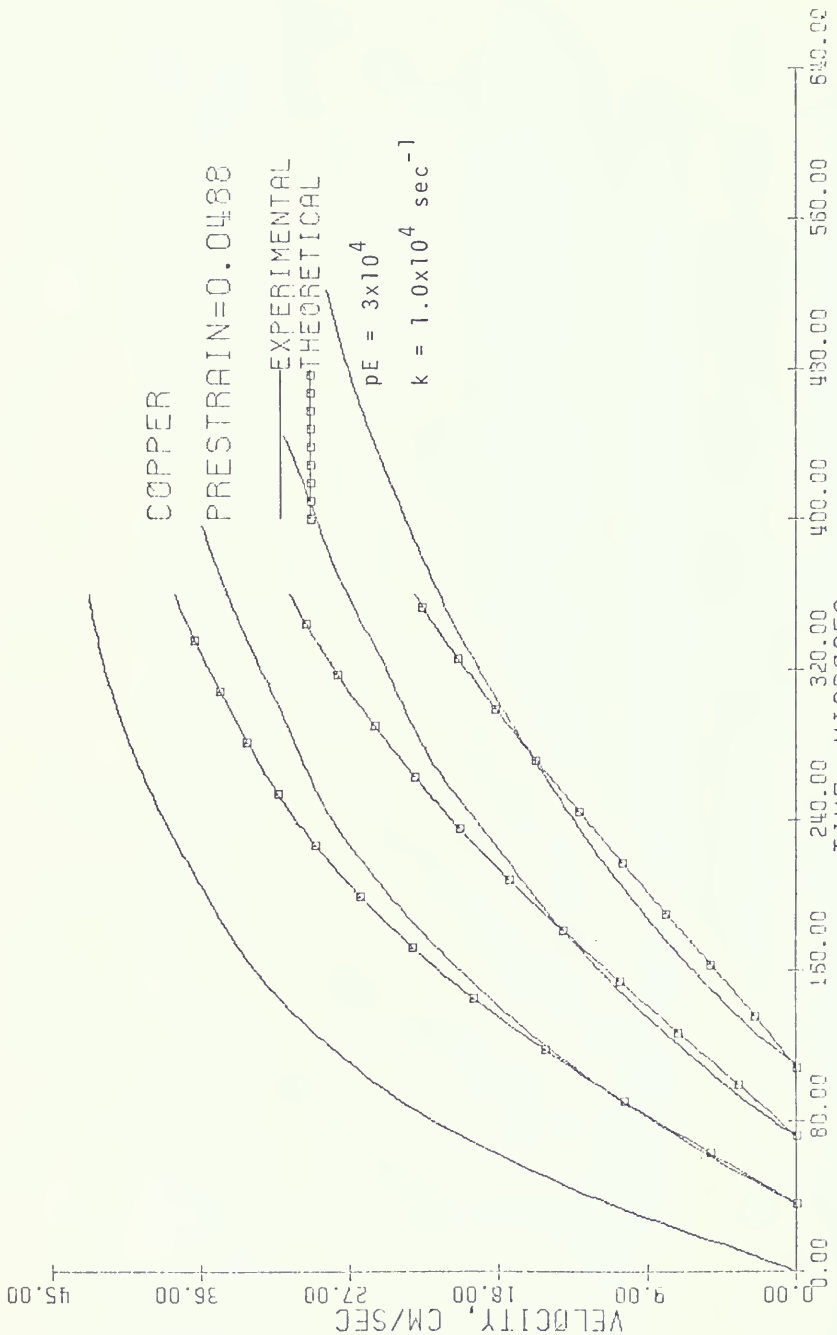

Figure 4.16 Particle Velocity Solution of Quasilinear Model (Copper Specimen No. 4, Prestrain 0.0488).

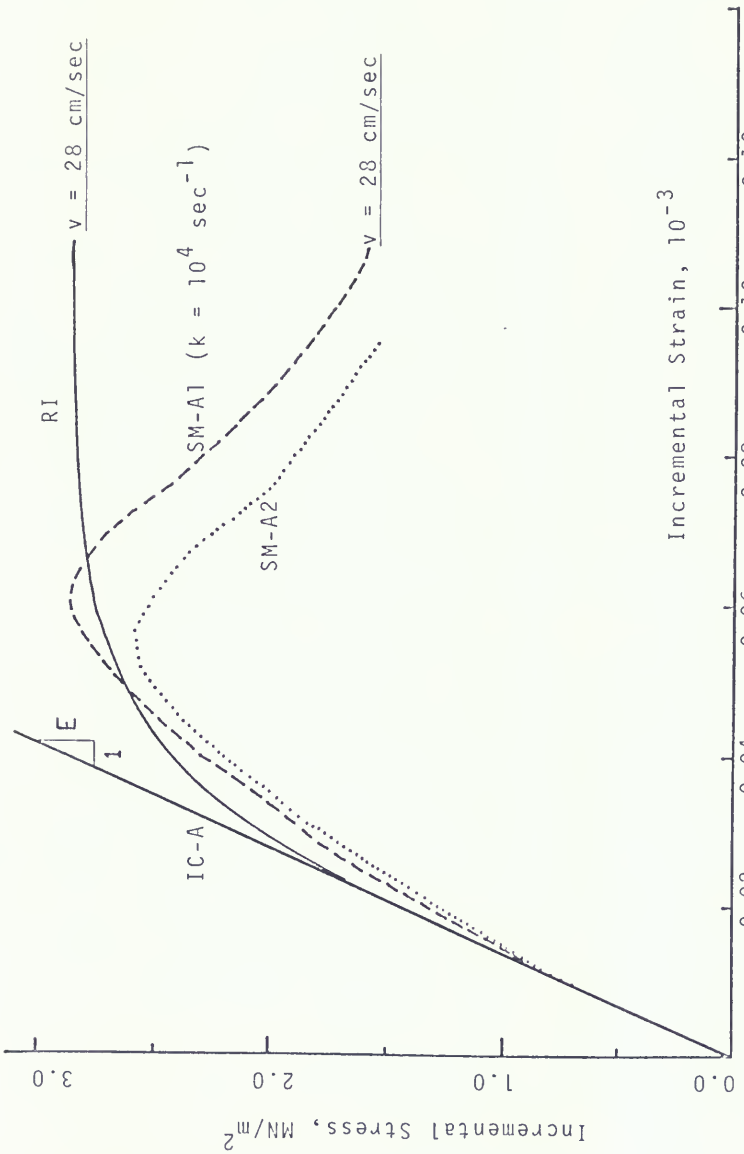

Figure 4.17 Comparisons of Incremental Stress-Strain Curves (Aluminum Specimen No. 4, Prestrain 0.0280).

the small incremental waves in copper rods considered.

The inequality (4.64) appears to be an effective constraint to ensure that the parameters chosen to match the particle velocity records for the copper rods also give a reasonable incremental stress-strain curve. It also proved to be an expedient practical guide to a simplified procedure for choosing the parameters p and k as follows. First a value of p was chosen as large as possible in the expected ε range, which satisfied the inequality. Then it was found that the parameter k could be chosen by the parameter identification procedure to match the velocity records. This parameter identification procedure was much simpler than the previous one of exploring combinations of the two parameters p and k.

Results for the aluminum specimen will be discussed next. In general the solution by the rate-dependent model is not satisfactory quantitatively. Each incremental stress-strain curve in Figure 4.2 is almost bilinear. (These curves were obtained by using the rate-independent theory.) It is understandable from the above analysis and inequality (4.64) that a semilinear model with instantaneous curve $\sigma = E\varepsilon$ is more adequate than a quasilinear model with the instantaneous curve $\sigma = \frac{1}{p} \ln(1 + pE\varepsilon)$. By checking through Figures 3.14 to 3.21 it is seen that in general the solution by a semilinear model is qualitatively satisfactory for most cases except the cases at $e_0 = 0.0015$, 0.0060 and

0.0100. One important fact supporting the solution of the semilinear model is that in the experimental records the particle velocity plateau approached decayed along the propagation distance x. This dynamic relaxation phenomenon cannot be explained by the simple wave solution of rate-independent theory. Most incremental stress-strain curves of Figure 4.2 were obtained by assuming that the particle velocity continuously increased to 40 cm/sec, which was not true in the experiments. As shown in Figure 3.23, many wave speed functions ceased at a certain velocity level. An example of an incremental stress-strain curve obtained from the numerical solution with the semilinear model is given in Figure 4.17 for comparison with the rate-independent one. The stress relaxation shown in the semilinear solutions is qualitatively not unreasonable in view of the continued straining at the particle velocity plateaus.

About the results of aluminum, more study is needed. From the results of the experiment it appears that the behavior of aluminum is very complex. We can conclude only that the small incremental wave can be described qualitatively by using a semilinear model of the Malvern type for cases at $e_0 > 0.0100$. The rate-sensitivity constant k is also found to be dependent on the precondition parameter ξ.

CHAPTER 5

SUMMARY AND CONCLUSIONS

A series of incremental wave tests were performed on annealed aluminum 1100-F and commercially pure copper rods under quasistatic preloading. An electromagnetic transducer was used to obtain measurements of particle velocity at four stations along the rod. The strain rates of the quasistatic preloading were in the range of 10^{-6} to 10^{-4} sec^{-1}, while strain rates of the order of 1.0 sec^{-1} were achieved in the incremental waves.

Test results indicated that except near the plateau in the records for aluminum any given level of incremental particle velocity propagates along the rod with a constant speed, not affected by the strain rate within the small range of the incremental-wave strain rates encountered. However, the wave-speed function of particle velocity differed noticeably for the incremental waves generated at different prestrain levels. An exponential function with two parameters was found to be able to fit the various wave speed functions of both materials. The results then indicated that one of the parameters, the major one, v_c, depends not only on the level of prestrain but also on the value of prestrain rate. This discovery shows another physical property of metal under incremental loading, in

addition to the well-known phenomenon of the leading edge propagating at the elastic bar wave speed.

This dependence on the prestrain rate may be related to a phenomenon observed by Klepaczko et al. (1974), who found the response to a sudden rate change in a torsional test to be dependent on the preceding strain rate history. They did not examine wave propagation but measured average stress-strain response along a short specimen.

Some preliminary efforts were made to describe quantitatively the dependence of the incremental waves on both prestrain and prestrain rate. A new parameter composed of these two variables was introduced, which was called the precondition parameter ξ in the text. The possibility of interpreting the prestrain-rate dependence from the point of view of the strain-rate difference between the incremental wave and quasistatic preloading should not be excluded, although not enough evidence exists to show this.

Both strain-rate-dependent theory and strain-rate-independent theories were compared with the results of the experiment. Based on the simple wave solution of rate-independent theory, incremental stress-strain curves were obtained for both cases of aluminum and copper. Quasilinear and semilinear rate-type constitutive models with linearized terms of $\phi(\sigma,\varepsilon)$ and $\psi(\sigma,\varepsilon)$ were proposed. Numerical computer solutions were obtained for incremental waves at various prestrain levels of both aluminum and copper specimens.

The velocity records obtained from the first gage station (15 diameters from the impact transmitting collar) were used as input boundary conditions.

An integro-differential approach was introduced for obtaining numerical computer solutions with the quasilinear model. It turned out that this technique is a very efficient one in solving the system of partial differential equations of nonlinear wave propagation.

Numerical solutions show that the proposed quasilinear constitutive equation is an adequate one to describe the copper material. In the copper cases, it was found that matching the particle velocity records does not guarantee correctness of the solution. An additional check on the solution was made by comparing the incremental stress-strain curve with the stress-strain curve obtained from the rate-independent theory. When the two agreed approximately a good match to the particle velocity records was always obtained. Therefore a stronger inequality condition was proposed [inequality (4.64)], which proved to be a sufficient (though not always necessary) condition for determining the correct range for parameter p in the instantaneous plastic term $\phi(\sigma,\varepsilon)$. By adjusting the two parameters in the quasilinear constitutive equation, a simple wave solution with its different dynamic stress-strain curve for each prestrain level could be well approximated by the quasilinear model.

The experimental results for the aluminum specimen show the phenomenon of dynamic relaxation which could not be described from the simple wave solution of the strain-rate-independent theory. Computer solution with the semi-linear model was able to describe it qualitatively. However, more efforts should be made in the future to describe the experimental data of incremental waves generated at small prestrain levels.

Further study in this area should include the following: (1) A series of tests with increasing amplitude of impact for generating the incremental waves would be useful, since larger amplitude usually results in larger values of strain rate. (2) The quasistatic preloading should be controlled at a given constant prestrain rate for a test of one speciman. Incremental wave tests should be performed on several specimens at various constant prestrain rate values differing from each other by a magnitude of the order of 10^{-5} sec^{-1}. (3) A longer copper rod is preferred so that reflection from the end will not reach the gage stations before particle velocity reaches a constant level. The dynamic relaxation phenomenon can then be checked in copper.

APPENDIX

COMPUTER PROGRAM

A-1 Velocity Data Processing Program

```
C      MAIN DATA PROCESSING FOR INCREMENTAL WAVE PROPAGATION
       LOGICAL*1 YVEL(51),YCO(51),YCP(51)
       INTEGER TWAVE(20),TSPEED(20),XTIME(20),XVEL(20),DATE(5)
       COMMON NC,DT,DV,T(4,20),V(4,300),GAUSS(4),B(15,94),C(4,100),BV(100
      1),NS1(8),STRAIN,SLOPE,NT(4),TRSLOP
       COMMON/CONST/TMAX,TMIN,VMAX,VMIN,BV2,BV1
       DIMENSION CA(4,101),CB(4,101),RV(300),RT(300),TT(20),VV(20),CC(4,1
      101)
       READ(5,100) IDATA
C      IDATA IS NUMBER OF DATA PICTURES TO BE PROCESSED IN ONE RUN
       READ(5,600) (DATE(I),I=1,5)
       READ(5,610) (YVEL(I),I=1,51)
       READ(5,610)  (YCO(I),I=1,51)
       READ(5,610)  (YCP(I),I=1,51)
       READ(5,600) (TWAVE(I),I=1,20)
       READ(5,600) (TSPEED(I),I=1,20)
       READ(5,600)  (XTIME(I),I=1,20)
       READ(5,600)   (XVEL(I),I=1,20)
  100 FORMAT(I2)
  600 FORMAT(20A4)
  610 FORMAT(51A1)
C      GIVE MATERIAL CONSTANTS
C      RHO: GM/C.C.    E: DYNES/CM**2    CO: CM/SEC
       CO=5.13E+05
       E=7.1E+11
       RHO=2.699
       CPMAX=15.0
C
       CALL DATA1
C
       NC2=NC*2
       DO 555 III=1,IDATA
C
       CALL DATA2
       WRITE(6,105) (DATE(JJ),JJ=1,5)
       WRITE(6,310) STRAIN,SLOPE
       WRITE(6,106) RHO,E,CO
       CALL MAGFLD(STRAIN)
       CALL WAVE
C
       CP=(SLOPE/RHO)**0.5
       CPTRUE=(TRSLOP/RHO)**0.5
C      INTERPOLATING VELOCITY-TIME CURVE AND PLOT RESULTS
       DO 5 I=1,NC
       M=NT(I)
       DO 10 K=1,M
       TT(K)=T(I,K)
  10   VV(K)=V(I,K)
```

```
C
      CALL LAGRAN(TT,VV,1,NT(I),RT,RV,DT,NN,NNN,20,300)
      NS1(I)=NN
      NS1(I+NC)=NNN
      DO 15 J=NN,NNN
   15 V(I,J)=RV(J)
    5 CONTINUE
C     GIVE ZERO TO REMAINING V(I,J) OUTSIDE J=NN,NNN
      NTV=NS1(NC2)
      DO 50 I=1,NC
      NA=NS1(I)-1
      DO 25 J=1,NA
   25 V(I,J)=0.
      NB=NS1(I+NC)+1
      IF(NB.GE.102) GO TO 50
      DO 30 J=NB,NTV
   30 V(I,J)=0.
   50 CONTINUE
      RT(1)=0.0
      WRITE(6,200)
      WRITE(6,110) (DATE(JJ),JJ=1,5)
      WRITE(6,310) STRAIN,SLOPE
      DO 56 K=1,NTV
      RT(K)=(K-1)*DT
   56 WRITE(6,210) RT(K),V(1,K),V(2,K),V(3,K),V(4,K)
      DO 58 I=1,4
   58 WRITE(7,220) (V(I,K),K=1,NTV)
  220 FORMAT(6E12.6)
      GO TO 555
      CALL PLOT10(RT,V,TMAX,TMIN,VMAX,VMIN,NTV,NC,TWAVE,YVEL,XTIME)
      WRITE(6,310) STRAIN,SLOPE
      WRITE(6,110) (DATE(JJ),JJ=1,5)
C     CALCULATE WAVE SPEED AND PLOT RESULTS
      CALL SPEED(L3,STRAIN,RT)
      WRITE(6,319)
      WRITE(6,110) (DATE(JJ),JJ=1,5)
      WRITE(6,310) STRAIN,SLOPE
      DO 70 K=1,L3
   70 WRITE(6,320) BV(K),(C(I,K),I=1,4)
      DO 60 I=1,NC
      DO 60 J=1,L3
      IF(C(I,J).LE.1.0) GO TO 61
      CA(I,J)=C(I,J)/CO
      CB(I,J)=C(I,J)/CP
      CC(I,J)=C(I,J)/CPTRUE
      GO TO 60
   61 CB(I,J)=-100.
      CA(I,J)=-100.0
```

```
      CC(I,J)=-100.0
   60 CONTINUE
      CALL PLOT10(BV,CA,BV2,BV1,1.1,0.1,L3,NC,TSPEED,YCO,XVEL)
      WRITE(6,110) (DATE(JJ),JJ=1,5)
      WRITE(6,310) STRAIN,SLOPE
C
      CALL PLOT10(BV,CB,BV2,BV1,CPMAX,0.0,L3,NC,TSPEED,YCP,XVEL)
      WRITE(6,300) STRAIN,SLOPE,CP
      WRITE(6,110) (DATE(JJ),JJ=1,5)
      CALL PLOT10(BV,CC,BV2,BV1,CPMAX,0.0,L3,NC,TSPEED,YCP,XVEL)
      WRITE(6,300) STRAIN,TRSLOP,CPTRUE
      WRITE(6,110) (DATE(JJ),JJ=1,5)
  555 CONTINUE
  105 FORMAT(1H1,//,11X,'TEST DATE : ',5A4)
  110 FORMAT(   11X,'TEST DATE : ',5A4)
  106 FORMAT(/,11X,'DENSITY=',F6.3,' GM/C.C.',/,11X,'YOUNGS MODULUS=',
     1E10.3,'DYNES/CM**2',/11X,'BAR WAVE SPEED=',E10.3,' CM/SEC')
  300 FORMAT(   11X,'INITIAL PRE-STRAIN = ',F6.4,7X, 'SLOPE OF STRESS-S
     1TRAIN CURVE = ',E10.4,' DYNE/CM**2',/,11X,'PLASTIC WAVE SPEED = ',
     2E10.4,'CM/SEC')
  310 FORMAT(   11X,'INITIAL PRE-STRAIN = ',F6.4,7X,' SLOPE OF STRESS-S
     1TRAIN CURVE = ',E10.4,' DYNE/CM**2')
  319 FORMAT(1H1,///,11X,'TABLE FOR WAVE SPEED VERSUS INCREMENTAL PARTIC
     1LE VELOCITY',//,11X,'UNIT IN CM/SEC',///, 7X,'VELOCITY',11X,'WAVE S
     1PEED',/)
  320 FORMAT(11X,F6.2,4(7X,E10.4))
  200 FORMAT(1H1,///,11X,'INCREMENTAL WAVE IN TERMS OF PARTICLE VELOCITY
     1',//,11X,'VELOCITY UNIT : CM/SEC',//,11X,'TIME,SEC',8X,'V1',8X,'V2'
     1',8X,'V3',8X,'V4',/)
  210 FORMAT(11X,E10.4,4(4X,F6.2))
      STOP
      END



      SUBROUTINE DATA1
      COMMON NC,DT,DV,T(4,20),V(4,300),GAUSS(4),B(15,94),C(4,100),BV(100
     1),NS1(8),STRAIN,SLOPE,NI(4),TRSLOP
      COMMON/LOCAT/STR(2),ZA(2),ZB(2),XA,XB,YA,YB,NOP(8,4),XC(15),YC(15)
      COMMON/CONST/TMAX,TMIN,VMAX,VMIN,BV2,BV1
      READ(5,200) STR(1),ZA(1),ZB(1),STR(2),ZA(2),ZB(2)
      READ(5,300) XA,XB,YA,YB
      READ(5,400) NC,DT,DV
      DO 10 I=1,8
      READ(5,600) (NOP(I,J),J=1,4)
   10 CONTINUE
```

```
      READ(5,610) (XC(I),I=1,15)
      READ(5,610) (YC(I),I=1,15)
      DO 5 I=1,15
5     READ(5,100) (B(I,J),J=1,94)
      TMAX=100.0*DT
      TMIN=0.0
      VMAX=50.0
      VMIN=0.0
      BV2=100.0*DV
      BV1=0.0
100   FORMAT(24F3.0)
200   FORMAT(6F6.4)
300   FORMAT(2(F8.6,F5.3))
400   FORMAT(I1,F8.2,F3.1)
600   FORMAT(1X,4I2)
610   FORMAT(15F4.1)
      RETURN
      END
```

```
      SUBROUTINE DATA2
      COMMON NC,DT,DV,T(4,20),V(4,300),GAUSS(4),B(15,94),C(4,100),BV(100
     1),NS1(8),STRAIN,SLOPE,NT(4),TRSLOP
      COMMON/VT/PT(20),PV(4,20),CV(4),AM(4),TC(4),DELTA
      READ(5,100) STRAIN,SLOPE,TRSLOP,(NT(I),I=1,NC)
      M=20
      READ(5,200) (PT(J),J=1,M)
      DO 6 I=1,NC
      M=NT(I)
6     READ(5,300) (PV(I,J),J=1,M)
      READ(5,600) (TC(I),I=1,NC)
      READ(5,400) (CV(I),I=1,NC)
      READ(5,500) (AM(I),I=1,NC),DELTA
100   FORMAT(F4.4,2E9.4,4I2)
200   FORMAT(20F2.1)
300   FORMAT(20F3.2)
400   FORMAT(4F5.4)
500   FORMAT(4E10.5,E9.3)
600   FORMAT(4F3.2,F4.2)
      RETURN
      END
```

```
      SUBROUTINE MAGFLD(EPS)
      COMMON NC,DT,DV,T(4,20),V(4,300),GAUSS(4),B(15,94),C(4,100),BV(100
     1),NS1(8),STRAIN,SLOPE,NT(4),TRSLOP
      COMMON/LOCAT/STR(2),ZA(2),ZB(2),XA,XB,YA,YB,NOP(8,4),XC(15),YC(15)
      DIMENSION X(4),Y(4),G(4,15),W(9),ZM(4)
      WRITE(6,101)
      DATA ZM/4.0,16.7,29.4,42.1/
      DO 5 I=1,NC
      Z=((ZA(2)*ZM(I)+ZB(2))*(EPS-STR(1))-
     1    (ZA(1)*ZM(I)+ZB(1))*(EPS-STR(2)))/(STR(2)-STR(1))
      ZN=Z*2.+1.0
      X(I)=XA*Z+XB
      Y(I)=YA*Z+YB
      WRITE(6,100) X(I),Y(I),Z
      NN=ZN
      DO 6 L=1,15
    6 G(I,L)=B(L,NN)+(B(L,NN+1)-B(L,NN))*(2.*Z-NN+1)
    5 CONTINUE
C     MAKE INTERPOLATION IN X-Y PLANE AND USE TRAPZOID'S RULE
C     TO CALCULATE GAUSS(4), THE EFFECTIVE MAGNETIC FIELD INTENSITY
      D=1.0
      N=9
      DN=D*(N+1)/(N-1)/2.0
      U=D/(N-1)
      DO 15 I=1,NC
      P=Y(I)-DN
      DO 16 K=1,N
      W(K)=P+K*U
      NE=LOCATE(X(I),W(K))
      M1=NOP(NE,1)
      M2=NOP(NE,2)
      M3=NOP(NE,3)
      M4=NOP(NE,4)
      R=(X(I)-XC(M1))/0.5
      Q=(W(K)-YC(M1))/0.5
      W(K)=G(I,M1)+(G(I,M2)-G(I,M1))*R+
     1                (G(I,M4)-G(I,M1))*Q+R*Q*
     1     (G(I,M1)+G(I,M3)-G(I,M2)-G(I,M4))
   16  CONTINUE
      A=0.0
      NN=N-1
      DO 20 J=2,NN
   20 A=A+W(J)
      GAUSS(I)=(W(1)+W(N)+2.0*A)/NN/2.0*3.03
   15 CONTINUE
      WRITE(6,102)
      WRITE(6,100) (GAUSS(I),I=1,4)
```

```
  101 FORMAT(  ////,11X,'LOCATION IN MAGNETIC FIELD OF EACH VELOCITY TRA
     1NSDUCER AT IMPACT',//,11X,'UNIT IN CENTIMETER',//,11X,'X(N-S DIREC
     2TION)',4X,'Y(DEPTH)',12X,'Z(ROD AXIAL)')
  100 FORMAT(11X,4(F10.3,10X))
  102 FORMAT(11X,'EFFECTIVE MAGNETIC INTENSITY FOR EACH TRANSDUCERS'//
     1,11X,'UNIT IN GAUSS',/)
      RETURN
      END



      SUBROUTINE WAVE
      COMMON NC,DI,DV,T(4,20),V(4,300),GAUSS(4),B(15,94),C(4,100),BV(100
     1),NS1(8),STRAIN,SLOPE,NT(4),TRSLOP
      COMMON/VT/PT(20),PV(4,20),CV(4),AM(4),TC(4),DELTA
C     TIME PART
      DO 5 I=1,2
      M=NT(I)
      DO 5 J=1,M
    5 T(I,J)=TC(1)*AM(1)+(PT(J)-TC(I))*AM(I)
      DO 6 I=3,4
      M=NT(I)
      DO 6 J=1,M
    6 T(I,J)=TC(1)*AM(1)+(PT(J)-TC(I))*AM(I)-DELTA
C     PARTICLE VELOCITY PART
C     SF=1.0CM/(LENGTH OF 1 CM-DIVISION ON PICTURE)
      SF=1.0084
      DO 25 I=1,NC
      M=NT(I)
      DO 25 J=1,M
   25 V(I,J)=90909.14*CV(I)*SF*PV(I,J)/GAUSS(I)
C     VELOCITY IN CM/SEC
      RETURN
      END
      FUNCTION LOCATE(X,Y)
C     X,Y ARE COORDINATE VALUE
C     NE IS ELEMENT NUMBER WHERE (X,Y) RESIDE
      DO 1 L=1,4
    2 AL=0.5*(2-L)
      IF(Y.LT.AL) GO TO 1
      IF(X.GT.0.0) NE=L
      IF (X.LE. 0.0) NE=4+L
      GO TO 33
    1 CONTINUE
   33 CONTINUE
      LOCATE=NE
      RETURN
```

```
      END



      SUBROUTINE SPEED(L3,FP,Q)
      COMMON NC,DT,DV,T(4,20),V(4,300),GAUSS(4),B(15,94),C(4,100),BV(100
     1),NS1(8),STRAIN,SLOPE,NT(4),TRSLOP
      DIMENSION X(4,100),L(3),Q(300)
CCCCCCCCCCCCCCCCCCCCCCCCCCCCCCCCCCCCCCCCC
C                                         C
C     DL IS DISTANCE BETWEEN  VELOCITY TRANSDUCERS
C     L3  NUMBER OF EVALUATIONS OR POINTS TO BE PLOTTED
C     Q(101) IS TIME ARRAY
C                                         C
CCCCCCCCCCCCCCCCCCCCCCCCCCCCCCCCCCCCCCCCC
      DL=12.7*(1.+FP)
      NC1=NC-1
      DO 5 I=1,NC1
      N=NS1(I+4)
      N1=NS1(I+5)
      IF(V(I,N)-V(I+1,N1)) 21,22,22
  21  L(I)=V(I,N)/DV-1
      GO TO 5
  22  L(I)=V(I+1,N1)/DV-1
  5   CONTINUE
      DO 9 I=1,NC1
      IF(L(I).GE.100) L(I)=99
  9   CONTINUE
      L1=L(1)
      L2=L1+1
      DO 30 K=1,L2
  30  BV(K)=(K-1)*DV
      DO 10 I=1,NC
      IF (I.EQ.1) LL=L(1)
      IF (I.NE.1) LL=L(I-1)
      DO 15 K=1,LL
      M=1
  7   IF(V(I,M).GT.BV(K)) GO TO 3
      M=M+1
      GO TO 7
  3   M2=M
      M1=M-1
      X(I,K)=Q(M1)+(BV(K)-V(I,M1))*(Q(M2)-Q(M1))/(V(I,M2)-V(I,M1))
  15  CONTINUE
  10  CONTINUE
      DO 50 I=1,NC
```

```
      IF(I.EQ.NC) GO TO 65
      LL=L(I)
      DO 60 K=1,LL
      IF(ABS(X(I+1,K)-X(I,K))-1.0E-06) 11,11,12
   11 C(I,K)=0.
      GO TO 60
   12 C(I,K)=DL/(X(I+1,K)-X(I,K))
   60 CONTINUE
      GO TO 50
   65 LL=L(I-1)
      DO 70 K=1,LL
   70 C(I,K)=(NC-1)*DL/(X(NC,K)-X(1,K))
   50 CONTINUE
      DO 80 I=2,NC
      IF(I.NE.NC) LL=L(I)+1
      IF(I.EQ.NC) LL=L(NC1)+1
      DO 55 K=LL,L1
   55 C(I,K)=0.
   80 CONTINUE
      L3=L1
      RETURN
      END
```



```
      SUBROUTINE LAGRAN(PT,PV,ITA,ITB,RT,RV,DT,NN,NNN,MA,MB)
      DIMENSION ZT(4),ZV(4),PT(MA),PV(MA),RT(MB),RV(MB)
C     PT,PV INPUT,    ITA,ITB  1ST&LAST ELEMENT NO. OF ARRAY PT,INTERPOLATING
C     EXECUTED BETWEEN THEM.     RT,RV OUTPUT ,  NN,NNN: 1ST&LAST NO. OF RT,RV
      N=(PT(ITB)-PT(ITA))/DT
      NN=PT(ITA)/DT+2
      NNN=NN+N
      M=ITA
      L=ITB-1
      I2=ITA+1
      DO 5 K=NN,NNN
      RT(K)=(K-1)*DT
      IF(RT(K).LE.PT(I2)) GO TO 7
      IF(RT(K).GT.PT(L)) GO TO 4
      IF(RT(K)-PT(M+1)) 4,4,3
   3  M=M+1
      DO 10 I=1,4
      ZT(I)=PT(I+M-2)
   10 ZV(I)=PV(I+M-2)
      GO TO 4
   7  DO 15 I=1,4
```

```
      ZT(I)=PT(I+M-1)
15    ZV(I)=PV(I+M-1)
4     RV(K)=0.
      DO 30 I=1,4
      ZTI=ZT(I)
      A=1.0
      DO 20 J=1,4
      IF(J.EQ.I) GO TO 20
      A=A*(RT(K)-ZT(J))/(ZTI-ZT(J))
20    CONTINUE
30    RV(K)=RV(K)+A*ZV(I)
5     CONTINUE
      RETURN
      END



      SUBROUTINE PLOT10(X,Y,XMAX,XMIN,YMAX,YMIN,NPTS,NPL,TITLE,YTITLE,
     1LABEL)
      REAL*4 X(NPTS),Y(NPL,NPTS),XSC(11)
      INTEGER TITLE(20),LABEL(20)
      LOGICAL*1 SP,SPACE,DIV,BAR,MINUS,PLUS,$PT,LINE(101),
     .          SYMB(10),YTITLE(51)
      DATA SPACE/' '/,BAR/'|'/,MINUS/'-'/,PLUS/'+'/,
     .     SYMB/'A','B','C','D','5','6','7','8','9','0'/
      IF(NPL .EQ. 1) SYMB(1) = SYMB(10)
      WRITE(6,120) (TITLE(II),II=1,20)
      XR = XMAX - XMIN
      YR = YMAX - YMIN
      RYS = 0.0
      IYT = 52
      DO 70 I3 = 1,11
      DO 70 I4 = 1,5
      IYT=IYT-1
      IF(I3.EQ.11) GO TO 15
      IF(I3.NE.1) GO TO 20
      IF(I4.NE.1) GO TO 20
15    DIV=PLUS
      SP=MINUS
      K=0
      DO 40 I5=1,11
      K=K+1
      LINE(K)=DIV
      IF(I5.EQ.11) GO TO 40
      DO 41 I6=1,9
      K=K+1
```

```
   41  LINE(K)=SP
   40  CONTINUE
       GO TO 45
   20  CONTINUE
       SP = SPACE
       DIV=BAR
       IF(I4.NE.1) GO TO 25
       DIV=PLUS
   25  LINE(1)=DIV
       LINE(101)=DIV
       DO 30 IL=2,100
   30  LINE(IL)=SPACE
   45  CONTINUE
       IYTR = 52 - IYT
       $PT = .FALSE.
       IF (I4 .NE. 1) GO TO 50
       $PT = .TRUE.
       YSC = YMAX - RYS*YR/10.
       RYS = RYS + 1.0
   50  DO 60 I7 = 1,NPL
       DO 60 I7A = 1,NPTS
       IX = 100.*(X(I7A)-XMIN)/XR + 1.49999
       IY = 50.*(Y(I7,I7A)-YMIN)/YR + 1.49999
       IF (IY .NE. IYT) GO TO 60
       IF((IX .LT. 1) .OR. (IX .GT. 101)) GO TO 60
       LINE(IX) = SYMB(I7)
   60  CONTINUE
       IF($PT) WRITE(6,1000) YTITLE(IYTR),YSC,(LINE(II),II=1,101)
       IF(.NOT.$PT) WRITE(6,1100) YTITLE(IYTR),(LINE(II),II=1,101)
       IF(I3 .EQ. 11) GO TO 80
   70  CONTINUE
   80  RXS = 0.0
       DO 90 I8 = 1,11
       XSC(I8) = XMIN + RXS*XR/10.
   90  RXS = RXS + 1.0
       WRITE(6,1200) (XSC(II),II=1,11,2),(XSC(II),II=2,11,2)
       WRITE(6,130) (LABEL(II),II=1,20)
  120  FORMAT('1',32X,20A4/)
  130  FORMAT( /30X,20A4/)
 1000  FORMAT(3X,A1,2X,G12.5,1X,101A1)
 1100  FORMAT(3X,A1,15X,101A1)
 1200  FORMAT(4X,6G20.3/14X,5G20.3)
       RETURN
       END
```

A-2 Quasilinear Model Program

```
      SUBROUTINE QORD(A,QP,AK,NX,NT,RHO,E,CO,DT,DELTA,BV,SS,VEL,SN,T)
      DIMENSION N(4),S(2,400),V(2,400),W(2,400),F(400),SS(4,300),
     1VEL(4,300),SN(4,300),BV(300),T(300)
      WT=0.9
      RC=RHO*CO
      AKT=AK*DT
      AL=A*AK/E
      P=QP
      A1=A/(P*E)
      PK=P*AK
      AT=A1*AKT
      N(1)=1
      N(2)=NX+1
      N(3)=N(2)+NX
      N(4)=N(3)+NX
      K2=N(2)
      K3=N(3)
      K4=N(4)
      JM=NT+(NX/2)*3
      DO 20 J=1,JM
      S(1,J)=0.0
      V(1,J)=0.0
      W(1,J)=0.0
20    CONTINUE
      LNT=NT-(NX/2)*3
      DO 5 I=2,NT
      V(1,1)=BV(I-1)
      V(2,1)=BV(I)
      IF(I-LNT) 2,2,3
3     M=M-2
      GO TO 1
2     M=JM-I+1
1     J=1
      LL=0
45    SD=S(1,J)
4     X=P*(SD-S(1,J))-AL*DT
      W(2,J)=EXP(X)*(W(1,J)+DT*EXP(-X/2)*(A1+(SD+S(1,J))/2))
      F(J)=EXP(P*SD-AL*(I-1)*DT)+PK*W(2,J)
      FF=F(J)
      RF=RC*FF**0.5
      G=2.0/(1.0+FF**0.5)
      Z=G*FF**0.5/2.0
      QG=1.0-G
      DA=2.0*FF-Z*AKT
      DB=2.0*FF+Z*AKT
      SA=DA/DB
      SB=2.0*AT*Z*(FF-1.0)/DB
      U=RF/DB
```

```
      Q=DA/(4.0*RF)
      S(2,J)=SA/Q*(V(1,J)*OG+G*V(1,J+1)-V(2,J))
     1+SA*(S(1,J)*OG+G*S(1,J+1))+SB
      LL=LL+1
      RATIO=(S(2,J)-SD)/S(2,J)
      IF(ABS(RATIO)-DELTA) 11,11,12
12    SD=WT*S(2,J)+(1.0-WT)*SD
      GO TO 4
11    CONTINUE
      S(2,J)=(SD+S(2,J))/2.0
41    WRITE(6,200) J,S(2,J),V(2,J),F(J),LL
      IF(I.EQ.NT) GO TO 28
      DO 10 J=2,M
65    SD=S(1,J)
6     X=P*(SD-S(1,J))-AL*DT
      W(2,J)=EXP(X)*(W(1,J)+DT*EXP(-X/2)*(A1+(SD+S(1,J))/2))
      F(J)=EXP(P*SD-AL*(I-1)*DT)+PK*W(2,J)
      FF=F(J)
      RF=RC*FF**0.5
      G=2.0/(1.0+FF**0.5)
      Z=G*FF**0.5/2.0
      OG=1.0-G
      DA=2.0*FF-Z*AKT
      DB=2.0*FF+Z*AKT
      SA=DA/DB
      SB=2.0*AT*Z*(FF-1.0)/DB
      U=RF/DB
      Q=DA/(4.0*RF)
      S(2,J)=SA*(S(1,J)*OG+G*(S(2,J-1)+S(1,J+1))*0.5)
     1+SB+U*G*(V(1,J+1)-V(2,J-1))
      V(2,J)=V(1,J)*OG+G*(V(2,J-1)+V(1,J+1))*0.5
     1+Q*G*(S(1,J+1)-S(2,J-1))
      RATIO=(S(2,J)-SD)/S(2,J)
      IF(ABS(RATIO)-DELTA) 13,13,14
14    SD=WT*S(2,J)+(1.0-WT)*SD
      GO TO 6
13    S(2,J)=(SD+S(2,J))/2.0
10    CONTINUE
      WRITE(6,300) I,V(2,1),V(2,K2),V(2,K3),V(2,K4)
300   FORMAT(11X,I3,4F20.6)
28    DO 15 K=1,4
      KK=N(K)
      II=I+(K-1)*NX/2
      IF(II.GT.NT) GO TO 15
      SS(K,II)=S(2,KK)
      VEL(K,II)=-V(2,KK)
      SN(K,II)=(F(KK)-1.0)/(P*E)
15    CONTINUE
```

```
      DO 17 J=1,M
      S(1,J)=S(2,J)
      V(1,J)=V(2,J)
17    W(1,J)=W(2,J)
5     CONTINUE
      DO 16 K=1,4
      MK=1+(K-1)*NX/2
      DO 16 I=1,MK
      SS(K,I)=0.0
      VEL(K,I)=0.0
      SN(K,I)=0.0
16    CONTINUE
      DO 26 I=1,NT
26    T(I)=(I-1)*DT
200   FORMAT(31X,I5,3E20.6,5X,I3)
      RETURN
      END
```

BIBLIOGRAPHY

Alter, B. E. K., and Curtis, C. W., "Effect of Strain Rate on the Propagation of a Plastic Strain Pulse Along A Lead Bar," J. Appl. Phys., vol. 27, No. 9, Sept., 1956, pp. 1079-1085.

Baker, W. E., and Yew, C. H., "Strain-Rate Effect in the Propagation of Torsional Plastic Waves," J. Appl. Mech., vol. 33, Dec., 1966, pp. 917-923.

Banerjee, A. K., Plastic Stress Waves In Prestressed Thin-Walled Tubes: Numerical Analysis by Rate-Dependent Theories, Ph.D. Thesis, University of Florida, 1972.

Banerjee, A. K., and Malvern, L. E., "Computation of Incremental Torsional Plastic Waves with Rate-Dependent Models," Int. J. Solids Structures, vol. 11, 1975, pp. 347-355.

Bell, J. F., "Propagation of Plastic Waves in Prestressed Bars," U. S. Navy Contract N6-onr-243, Tech. Rept. No. 5, Johns Hopkins University, Baltimore, Md., June, 1951.

Bell, J. F., "Determination of Dynamic Plastic Strain Through the Use of Diffraction Gratings," J. Appl. Phys., vol. 27, No. 10, Oct., 1956, pp. 1109-1113.

Bell, J. F., "Propagation of Large Amplitude Waves in Annealed Aluminum," J. Appl. Phys., vol. 31, No. 2, Feb., 1960a, pp. 277-282.

Bell, J. F., "Study of Initial Conditions in Constant Velocity Impact," J. Appl. Phys., vol. 31, No. 12, Dec., 1960b, pp. 2188-2195.

Bell, J. F., "Experimental Study of the Interrelation Between the Theory of Dislocations in Polycrystalline Media and Finite Amplitude Wave Propagation in Solids," J. Appl. Phys. vol. 32, No. 10, Oct., 1961a, pp. 1982-1993.

Bell, J. F., "An Experimental Study of the Unloading Phenomenon in Constant Velocity Impact," J. Mech. Phys. Solids, vol. 9, 1961b, pp. 1-15.

Bell, J. F., "Further Experimental Study of the Unloading Phenomenon in Constant Velocity Impact," J. Mech. Phys. Solids, vol. 9, 1961c, pp. 261-278.

Bell, J. F., and Stein, A., "The Incremental Loading Wave in the Pre-Stressed Plastic Field," J. de Mecanique, vol. 1, No. 4, Dec., 1962, pp. 395-412.

Bell, J. F., "An Experimental Diffraction Grating Study of the Quasi-Static Hypothesis of the Split Hopkinson Bar Experiment," J. Mech. Phys. Solids, vol. 14, 1966, p. 309.

Bell, J. F., "The Physics of Large Deformation of Crystalline Solids," Springer Tracts in Natural Philosophy, vol. 14, Springer-Verlag, Berlin, Heidelberg and New York, 1968.

Bianchi, G., "Some Experimental and Theoretical Studies on the Propagation of Longitudinal Plastic Waves in a Strain-Rate-Dependent Material," in Stress Waves in Anelastic Solids, IUTAM Symposium, Eds., Kolsky, H., and Prager, W., 1963, pp. 101-117.

Campbell, J. D., "The Yield of Mild Steel under Impact Loading," J. Mech. Phys. Solids., vol. 3, 1954, pp. 54-62.

Campbell, J. D., and Dowling, A. R., "The Behavior of Materials Subjected to Dynamic Incremental Shear Loading," J. Mech. Phys. Solids, vol. 18, 1970, pp. 43-63.

Convery, E., and Pugh, M. L. D., "Velocity of Torsional Waves in Metals Stressed Statically into the Plastic Range," J. Mech. Eng. Sci., vol. 10, No. 2, 1968, pp. 153-164.

Cristescu, N., "On the Propagation of Elastic-Plastic Waves in Metallic Rods," Bull. Acad. Polonaise Soc. Serie des Sciences Techniques, vol. 11, No. 4, 1963, pp. 129-133.

Cristescu, N., Dynamic Plasticity, North Holland, 1967.

Cristescu, N., "The Unloading in Symmetric Longitudinal Impact of Two Elastic-Plastic Bars," Int. J. Mech. Sci. vol. 12, 1970, pp. 723-738.

Cristescu, N., "A Procedure for Determining the Constitutive Equations for Materials Exhibiting Both Time-Dependent and Time-Independent Plasticity," Int. J. Solids Structures, 1972, vol. 8, pp. 511-531.

De Vault, G. P., "The Effect of Lateral Inertia on the Propagation of Plastic Strain in a Cylindrical Rod," J. Mech. Phys. Solids, vol. 13, 1965, pp. 55-68.

Donnell, L. H., "Longitudinal Wave Transmission and Impact," Trans. ASME, Appl. Mech. Div., vol. 52, No. 1, 1930, pp. 153-167.

Duwez, P. E., and Clark, D. S., "An Experimental Study of the Propagation of Plastic Deformation under Conditions of Longitudinal Impact," Proc. Amer. Soc. of Testing Materials, vol. 47, pp. 502,532.

Efron, L., Longitudinal Plastic Wave Propagation in Annealed Aluminum Bars, Ph.D. Thesis, Michigan State University, 1964.

Efron, L., and Malvern, L. E., "Electromagnetic Velocity-Transducer Studies of Plastic Waves in Aluminum Bars," Exp. Mech., June, 1969.

Eleiche, A. M., and Campbell, J. D., "The Influence of Strain-Rate History on the Shear Strength of Copper and Titanium at Large Strains," University of Oxford, Dept. of Eng. Sciences Report, Report No. 1106/74, Oct., 1974.

Frantz, R. A. Jr., and Duffy, J., "The Dynamic Stress-Strain Behavior in Torsion of 1100-0 Aluminum Subjected to a Sharp Increase in Strain Rate," J. Appl. Mech., Dec., 1972, pp. 939-945.

Hauser, F. E., Simmons, J. A., and Dorn, J. E., "Strain Rate Effects in Plastic Wave Propagation," in Response of Metals to High Velocity Deformation, Interscience Publishers, New York, 1961, pp. 93-114.

Hildebrand, F. B., Advanced Calculus for Applications, Prentice-Hall, Inc., 1962, Englewood Cliffs, New Jersey.

Holt, D. L., Babcock, S. G., Green, S. J., and Maiden, C. J., "The Strain Rate Dependence of the Flow Stress in Some Aluminum Alloys," Trans. Amer. Soc. Metals, vol. 60, 1967, p. 152.

Jeffrey, A., and Taniuti, T., Nonlinear Wave Propagation, Academic Press, New York, 1964.

Khan, A. S., "Behavior of Aluminum During the Passage of Large-Amplitude Plastic Waves," Int. J. Mech. Sci., vol. 15, 1973, pp.503-516.

Klepaczko, J., "Strain Rate History Effects for Polycrystalline Aluminum and Theory of Instersections," J. Mech. Phys. Solids, vol. 16, 1968, pp. 255-266.

Klepaczko, J., "Some Experimental Investigations of the Elastic-Plastic Wave Propagation in Bars," Proc. Conf. on Foundation of Plasticity, Warsaw, 1973.

Klepaczko, J., Frantz, R. A., and Duffy, J., "History Effects in Polycrystalline FCC Metals Subjected to Rapid Changes in Strain Rate and Temperature," Brown University Tech. Report AFML-TR-74-173, Dec., 1974.

Kolsky, H., "An Investigation of the Mechanical Properties of Materials at Very High Rates of Loading," Proceedings, Phys. Soc. of London, London, England, vol. 62, Series B, 1949, p. 676.

Kolsky, H., and Douch, L. S., "Experimental Studies in Plastic Wave Propagation," J. Mech. Phys. Solids, vol. 10, 1962, pp. 195-225.

Lawson, J. E., and Nicholas, T., "The Dynamic Mechanical Behavior of Titanium in Shear," J. Mech. Phys. Solids, vol. 20, 1972, pp. 65-76.

Lindholm, U. S., "Some Experiments with the Split Hopkinson Pressure Bar," Tech. Report No. 1, Contract No. DA-23-072-ORD-1674, Sw. R. I. Project No. 02-1102, Southwest Research Institute, San Antonio, Texas, March, 1964.

Lubliner, J., "A Generalized Theory of Strain-Rate-Dependent Plastic Wave Propagation in Bars," J. Mech. Phys. Solids, vol. 12, 1964, pp.59-65.

Lubliner, J., and Valathur, M., "Some Wave-Propagation Problems in Plastic-Viscoplastic Materials," Int. J. Solids Structures, vol. 5, 1969, pp. 1257-1298.

Malvern, L. E., The Propagation of Longitudinal Waves of Plastic Deformation in a Bar of Material Exhibiting a Strain-Rate Effect," Ph.D. Thesis, Brown University, Providence, Rhode Island, 1949.

Nicholas,T., "Strain Rate and Strain Rate History Effects in Several Metals in Torsion," Exp. Mech., vol. 11, 1971, p. 370.

Nicholas, T., "An Analysis of the Split Hopkinson Bar Technique for Strain-Rate-Dependent Material Behavior," J. Appl. Mech., March, 1973, pp. 277-282.

Papirno, R., and Gerard, G., "Dynamic Stress-Strain Phenomena and Plastic Wave Propagation in Metals," Transactions of the ASM , vol. 53, 1961, pp. 381-406.

Phillips, A., Wood, E. R., Zabinski, M. P., and Zannis, P., "On the Theory of Plastic Wave Propagation in a Bar---Unloading Waves," Int. J. Non-Linear Mechnics, vol. 8, 1973, pp. 1-16, Pergamon Press.

Ripperger, E. A., and Watson, Hal. Jr., "The Relationship Between the Constitutive Equation and One-Dimensional Wave Propagation," in Lindholm, U. S., Ed., Mechnical Behavior of Materials under Dynamic Loads, Springer, Berlin, 1968, pp. 294-313.

Ripperger, E. A., and Yeakley, L. M., "Measurement of Particle Velocities Associated with Waves Propagating in Bars," Experimental Mechanics, vol. 3, No. 2, Feb. 1963, pp. 47-56.

Rubin, R. U., "Propagation of Longitudinal Deformation Waves in a Prestressed Rod of Material Exhibiting a Strain-Rate Effect," J. Appl. Phys., vol. 25, No. 4, April, 1954, pp. 528-536.

Santosham, T. V., and Ramsey, H., "Small Plastic Strain Wave Propagation in Prestressed Soft Copper Rods," Int. J. Mech. Sci., vol. 12, 1970, pp. 447-457.

Sokolovsky, V. V., "The Propagation of Elastic-Viscoplastic Waves in Bars," Prikl. Math. Mekh., vol. 12, No. 3, 1948, pp. 216-280.

Sternglass, E. J., and Stuart, D. A., "An Experimental Study of the Propagation of Transient Longitudinal Deformations in Elastoplastic Media," J. Appl. Mech., vol. 20, 1953, pp. 427-434.

Suliciu, I., Malvern, L. E., and Cristescu, N., "Remarks Concerning the 'Plateau' in Dynamic Plasticity," Archiwum Mechaniki Stosowanej, vol. 24, 1972, pp. 999-1011.

Suliciu, I., Malvern, L. E., and Cristescu, N., "Quasi-linear Rate-Type Constitutive Equations and Incremental Stress Waves," Int. J. Solids Structures, vol. 10, 1974, pp. 21-33.

Taylor, G. I., "Propagation of Earth Waves from an Explosion," British Official Report RC 70, 1940.

Taylor, D. B. C., "Non-Uniform Yield in a Mild Steel under Dynamic Straining," in Proc. Conf. Properties of Materials at High Rates of Strain, Inst. Mech. Engrs., London, 1957, pp. 229-238.

Tietz, T. E., and Dorn, J. E., "The Effect of Strain Histories on the Work Hardening of Metals," ASME Trans, vol. 41A, 1949, p. 163.

von Kármán, T., "On the Propagation of Plastic Deformation in Solids," Nat. Defense Res. Council, Report A-29, Feb., 1942.

Wood, E. R., and Phillips, A., "On the Theory of Plastic Wave Propagation in a Bar," J. Mech. Phys. Solids, vol. 15, 1967, pp. 241-254.

Yew, C. H., and Richardson, H. A. Jr., "The Strain Rate Effect and the Incremental Plastic Wave in Copper," Exp. Mech., vol. 9, Aug., 1969, pp. 366-373.

BIOGRAPHICAL SKETCH

Chang-Sheng Ting was born in Sian, Shensi Province, China, on December 8, 1946. He was graduated from Taiwan Provincial Cheng-Kung University at Tainan, Taiwan, China, in 1967 with a major in civil engineering, following which he attended the Graduate School of National Taiwan University. He got a Master of Science degree in Engineering Mechanics on July, 1969. He taught undergraduate courses in structural mechanics at the Chinese Military Academy during the one-year R.O.T.C service. With a view to broadening his education in mechanics, he enrolled in the Graduate School at the University of Florida in September, 1970. Since then he has been working toward a Ph.D. degree with a major in engineering mechanics, which is to be awarded in August, 1975.

I certify that I have read this study and that in my opinion it conforms to acceptable standards of scholarly presentation and is fully adequate, in scope and quality, as a dissertation for the degree of Doctor of Philosophy.

Lawrence E. Malvern
Lawrence E. Malvern, Chairman
Professor of Engineering Sciences

I certify that I have read this study and that in my opinion it conforms to acceptable standards of scholarly presentation and is fully adequate, in scope and quality, as a dissertation for the degree of Doctor of Philosophy.

Martin A. Eisenberg
Professor of Engineering Sciences

I certify that I have read this study and that in my opinion it conforms to acceptable standards of scholarly presentation and is fully adequate, in scope and quality, as a dissertation for the degree of Doctor of Philosophy.

Edward K. Walsh
Edward K. Walsh
Professor of Engineering Sciences

I certify that I have read this study and that in my opinion it conforms to acceptable standards of scholarly presentation and is fully adequate, in scope and quality, as a dissertation for the degree of Doctor of Philosophy.

Robert E. Reed-Hill
Robert E. Reed-Hill
Professor of Material Sciences and Engineering

I certify that I have read this study and that in my opinion it conforms to acceptable standards of scholarly presentation and is fully adequate, in scope and quality, as a dissertation for the degree of Doctor of Philosophy.

Sung Y. Liu
Associate Professor of
Engineering Sciences

This dissertation was submitted to the Graduate Faculty of the Department of Engineering Sciences in the College of Engineering and to the Graduate Council, and was accepted as partial fulfillment of the requirements for the degree of Doctor of Philosophy.

August, 1975

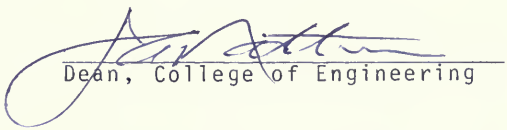

Dean, College of Engineering

Dean, Graduate School